Frontiers of Liquid Atomization

An Indo-US workshop

IUSSTF
Indo-US Science and Technology Forum

IIT Madras Research Park,
Chennai

About the sponsor:

The Indo-U.S. Science and Technology Forum (IUSSTF) was established in 2000 under an agreement between the Governments of India and United States of America with a mandate to promote, catalyze and seed bilateral collaboration in science, technology, engineering and biomedical research through substantive interaction amongst government, academia and industry.

As its mandate, IUSSTF provides an enabling platform to the scientific enterprises of the two nations by supporting an S&T program portfolio that is expected to foster sustainable interactions with a potential to forge long term collaborations. IUSSTF program manifests are largely catalytic in nature that helps to create awareness through exchange and dissemination of information and opportunities in promoting bilateral scientific and technological cooperation.

IUSSTF has an evolving program portfolio that is largely conceived and driven by scientific communities of both the countries through extending support for symposia, workshops, conferences on topical and thematic areas of interest; visiting professorships and exchange programs; travel grants; fellowships; advanced training schools; public-private networked centres and knowledge R & D networked centres. IUSSTF also works towards nurturing contacts between young and mid career scientists by convening stimulating flagship events like the Frontiers of Science and Frontiers of Engineering symposium through the U.S. National Academies model. At the same time it reaches out to industries by partnering with business associations to generate high quality events on technology opportunities for business development to foster elements of innovation and enterprise through networking between academia and industry.

IUSSTF maintains a close working relationship with the federal agencies, laboratories, government institutions, and the academia in U.S. and India, cutting across all disciplines. IUSSTF has been entrusted to administer the bi-national US-India S&T Endowment Fund (for joint research and development, innovation, entrepreneurial and commercialization activities in S&T) and the Indo-US Joint Clean Energy Research and Development Center (to support multi-institutional network projects in clean energy using public-private partnership model of funding).

As an autonomous, not-for-profit society, IUSSTF has the ability, agility and flexibility to engage and involve industry, private R&D labs; and non governmental entities in its evolving activity manifold. This operational uniqueness allows the IUSSTF to receive grants and contributions from independent sources both in India and USA, besides the assured core funding from the two governments.

IUSSTF solicits proposals for its activities thrice a year (January, May and September) and awards are made on the basis of peer reviews both in India and USA.
IUSSTF values your interactions and looks forward to work with the S&T community of both countries to implement new ideas that endeavor to promote cutting edge Indo-U.S. Science and Technology collaborations.

CONTENTS

S No.	Title	Author	Page No.
1.	(A tentative of secondary) turbulent atomization modeling from first principles.	N. Rimbert	1
2.	Challenges of Studying Primary Atomization by Simulations	M. Herrmann	5
3.	Comprehensive Modeling of Spray Formation from Gas Turbine Injectors: Recent Approaches and Open Issues	Achintya Mukhopadhyay	10
4.	Dynamics of Non-Newtonian Fluid Flow in Simplex Atomizers	Milind A. Jog	14
5.	Evaporation and Combustion of Isolated Spray Droplets	V. Raghavan	18
6.	Inner nozzle flow and Spray Modeling for Compression Ignition Engine Applications	Sibendu Som	22
7.	Internal Combustion Engine Sprays	John Abraham	26
8.	Investigations of the air and liquid velocity fields in a prefilming airblast atomizer	P Suriyanarayanan NS Vikramaditya L Venkatakrishnan	30
9.	Liquid Atomization in Gas-Centered Swirl Coaxial Atomizers	D. Sivakumar	38
10.	Manipulation of Internal Flows for Spray Creation	Steven H. Collicott	42

11.	Modelling of Primary Atomisation in Liquid Rocket Engine Injectors	T. John Tharakan	47
12.	Modelling the heat release response of premixed flames to unsteady upstream fuel-air ratio stratification in lean-premixed-prevapourised combustors	Santosh Hemchandra	52
13.	Multiphase Flow Modeling and Simulation	S. Subramaniam	59
14.	Prediction of drop size and velocity distributions in a spray for the simulation of liquid fuel combustion	Amitava Datta	65
15.	Spray impingement studies for biofuels	Anand T N C Shamit Bakshi	69
16.	Studies on Atomization and Sprays of Plant Oil Biofuels	Devendra Deshmukh R. V. Ravikrishna	73
17.	The State of the Art in Biomedical Sprays	Guillermo Aguilar	77
18.	Water Mist based Suppression of Flow Opposed Flame Spread over Thin Solid Fuels in Space and Earth Environments	K Chenthil Kumar Amit Kumar	82
19.	From Williams spray equation to multiphase population balance: a viable route to modeling dense sprays	*Mahesh V. Panchagnula*	86
20.	VOF-Lagrangian Particle Tracking Coupling to Simulate Multiscale Primary Atomization	Gaurav Tomar Daniel Fuster Stephane Popinet Stephane Zaleski	90

(A tentative of secondary) turbulent atomization modelling from first principles.

N. Rimbert
LEMTA ESSTIN, Université de Lorraine – CNRS
nicolas.rimbert@esstin.uhp-nancy.fr

Abstract :

The goal of this presentation is to show how it is possible to tentatively build a turbulent atomization model rooted on first principles. On the large scale, the mechanism of fragmentation is related to the classical instability mechanisms which are shown, though the instability threshold is far trespassed, to still echo in the turbulent flow that appears. On the small scale, turbulent intermittencies are related to a cascading mechanism with well determined properties: the model is built on the statistical properties of self-avoiding randomly stretched vortices. This leads to a log-stable distribution of vortices which act as the sinews of the re-agglomeration mechanism of the ligaments produced by the breakup of the thin sheets of liquid. This eventually leads to a mirroring log-stable distribution of droplets. Strength of the model stems from the fact that very few parameters need to fitted, actually, as in most turbulence model, the average turbulent kinetic energy and dissipation rate are the only parameters needed. Therefore this modelling may be suited as a starting point for sub-grid modelling of atomization processes in CFD.

Keywords :

Turbulent atomization, large scale instability, small scale turbulent intermittency, ligament mediated fragmentation, Smoluchowski coagulation equation

1 Introduction

Turbulent atomization models are scarce and most experimentalists still resort to empirical PDF to describe the size distribution of the droplet in the resulting mist. (Lefevre, 1989) is still a good reference on the subject. Turbulent sprays are mainly characterized by the huge range of scales that are involved. Therefore use of log-normal distribution has very early become a common practice in the community (with small adaptations when needed) since the logarithmic magnifying glass tend to make the distribution narrower. This eventually led Kolmogorov (1941) to devise a stochastic process explaining their widespread appearance. This modelling became famous when used later to describe turbulence intermittencies (between large and small vortices, see Rimbert, 2010, for more details). However when the liquid jet is flowing rather slowly, classical linear instabilities are well known to govern the mechanism of drop formation. Therefore there is a bridge to build between these two worlds. The bridge seems to be related to the ligaments that have been shown to appear once high-speed imaging became available (see Pich & Erdman, 1987 for instance). Maps of theses two worlds can be found partly in the review of Eggers and Villermaux (2008), as far as linear instabilities and ligaments re-agglomeration are concerned, and Gorokhovski and Herrmann (2008), as far as Kolmogorov theory and DNS of two-phase flows are concerned.

The goal of this paper is to show how it is possible to build this bridge on as solid a ground as possible. This will be illustrated by considering what is called the secondary atomization mechanism of a droplet but it could be extended to other configurations as far as the adequate large scale instability mechanism is considered. The gist of this work has been published in two papers (Rimbert, 2010; Rimbert and Castanet, 2011) while other parts have only be presented in international conferences (Rimbert, 2011) so far.

This paper is divided in two parts. Part one focus on the large scale modelling of the atomization process. It is therefore devoted to the study of the deformation of the bulk of the liquid and to the birth of the instability which starts the atomization. Second part focus on the small scale modelling of the droplet size distribution and relates it to turbulence intermittencies mediated re-agglomeration of the ligaments and to log-stable distributions (firstly used in spray PDF in Rimbert & Séro-Guillaume, 2004). Theses latter are generalisations of lognormal laws obtained through a cascading mechanism related to a random self-avoiding stretching of vortices scenario.

2 Large scale modelling

The non-dimensional parameters governing the stability of a droplet in an air stream are the (aerodynamic) Weber number and the Ohnesorge number as defined by:

$$We_{aero} = \frac{\rho_G U^2 d}{\gamma} \text{ and } Oh = \frac{\mu_L}{\sqrt{\gamma \rho_L d}}$$

where ρ_G and ρ_L stand respectively for the air density and the water density; γ is the air-water surface tension, μ_L is the liquid dynamic viscosity and d the droplet diameter. For not too large value of the Ohnesorge number, when the *We* number is high enough there appears a atomization mechanism known as bag-breakup. The six stages of this mechanism can be found in Fig. 1. Hsiang and Faeth (1995) presents an experimental determination of the bag-breakup range in the (*We-Oh*) domain.

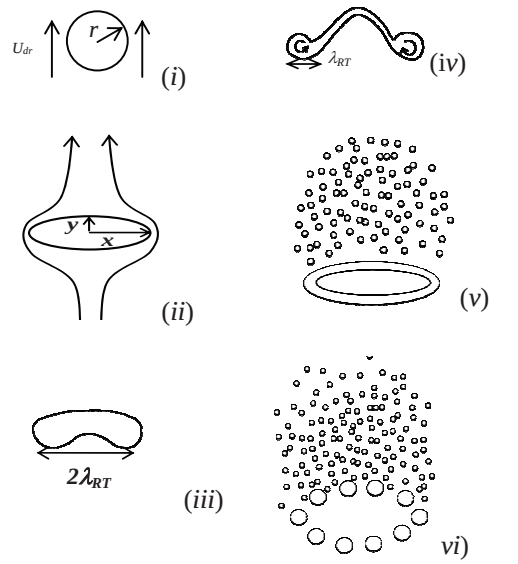

Figure 1: the six stages of the bag breakup (*i*) inception (*ii*) deformation (*iii*) RT instability (*iv*) bag formation (*v*) bag breakup (*vi*) rim breakup (Rimbert & Castanet, 2011)

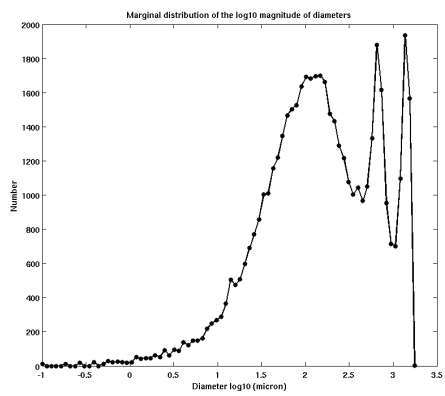

Figure 2: drop size PDF in an industrial nozzle in the bag breakup *We* number range. Notice the three separate peaks (Rimbert & Castanet, 2011).

Measurements of droplets size resulting from the bag breakup has been made in (Rimbert & Castanet, 2011) and some results are presented in Fig. 2. The three peaks can be related from right to left to the peak of the mother droplet, the peak of the daughter droplets related to the breakup of the rim and, lastly, the large peak can be related to the breakup of the bag. In this part we will mainly focus on stage (*ii*) and (*iii*) of figure 1.

2.1 Droplet deformation and breakup

Stage (*ii*) is modelled using the DDB theory of Ibrahim *et al.* (1995). The droplet is assumed to deform into a spheroid whose great axis is oscillating according to a non-linear second order differential which can be linearized around the initial spherical shape. The discriminant of the linearized equation can be written (Rimbert, 2011)

$$\Delta = \left(\frac{4\mu_l}{R^2 \rho_l}\right)^2 - 4\left(\frac{27\pi^2\gamma}{16R^3\rho_l}\right) = 4^4 t_H^{-2} - 54\pi^2 t_R^{-2}$$

Where the two characteristic times are defined by:

$$t_{Ray} = \sqrt{\frac{D^3\rho_l}{\gamma}} \text{, and } t_V = \frac{D^2\rho_l}{\mu_l},$$

The first one is the Rayleigh characteristic time of the droplet oscillation while the second one is viscous damping characteristic time. Note that $Oh = t_{Ray}/t_V$.

2.2 Large scale instabilities

Stage (*iii*) can be related to the growth of the classical Rayleigh-Taylor instability and more details can be found in (Rimbert & Castanet, 2011). The most amplified wavelength of the RT instability and its growth rate are given in the following equation:

$$\lambda_{RT,\max} = 2\pi\sqrt{\frac{3\gamma}{f\Delta\rho}}, \quad n_{RT,\max} = \left(\frac{2}{3^3}\frac{\rho_l}{\gamma}f^3\right)^{\frac{1}{4}}$$

Zhao *et al.* (2010) and concurrently Rimbert & Castanet (2011) have shown that by using the deformed droplet drag law to determine the deceleration *f* it is possible to determine the number of wavelength appearing on the drop surface and therefore to distinguish between turbulent atomization mechanism as can be found on Fig. 3. There are some discrepancies in the modelling (DDB model is replaced by correlation in the concurrent model) as well as in whether bag-breakup should be related to one-wave growth or to two-wave growth.

2.3 Secondary breakup classification

More recently, using the same kind of modelling, Rimbert (2011) has shown that by comparing the rise time of the oscillating droplet to the characteristic growth time of the instability, the classical assumption that droplet deform elliptically

before the instability do start writes $n_{RT} t_{rise} > 1$ or equally

$$4\sqrt{Oh_c^2 - Oh^2} < KWe^{3/4},$$

where K is a function of We. The corresponding domain are depicted on Fig. 3. Note also that this results in no oscillation above a given threshold Oh_c = 1.44 and therefore no instability can occur.

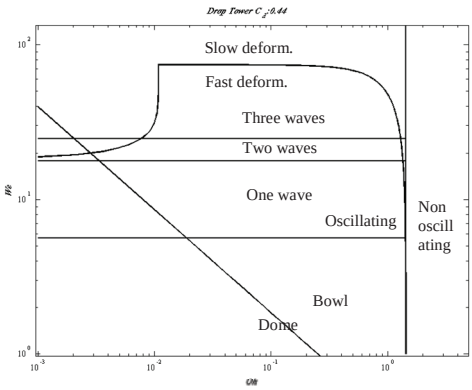

Figure 3: *We-Oh* diagram of different domains of atomization obtained by combining DDB theory and RT instability. (Rimbert, 2011)

The number of droplets obtained from these large scale instabilities which eventually results in the building up of the rim and its breakup have been studied somewhat differently in Zhao *et al.* (2010) and Rimbert & Castanet (2011).

3 Small scale modelling

Small droplets are mainly the result of the breakup of the burst of the bag. Pilch and Erdman have shown that this eventually resulted in a large production of small ligaments. Villermaux and co-workers have emphasized that these ligaments were to reorganize in a re-agglomeration mechanism. They therefore devised a non-turbulent self-convolution mechanism which involves some new parameters in a (yet) unknown manner.

3.1 Turbulent reorganisation of ligaments

Rather than resorting to this new, uncomplete and non turbulent theory, Rimbert & Castanet (2011) decided to resort to classical Smoluchowski agglomeration equation which reads:

$$\frac{\partial n(d,t)}{\partial t} = \tfrac{1}{2}\int_0^d a(d-\xi,\xi)\, n(d-\xi,t)\, n(\xi,t)\, d\xi - n(d,t)\int_0^\infty a(d,\xi)\, n(\xi,t)\, d\xi$$

Where n is the number of droplet of diameter d and a is the turbulent aggregation kernel (assumed constant for the sake of simplicity) given by

$$an_0 \sim \partial u / \partial x \sim \sqrt{\varepsilon / \nu_G},$$

where ε is the turbulence dissipation rate and ν_G is the kinematic viscosity of the gas phase.

By assuming that the aggregation characteristic time is also supposed to be much shorter than the overall aggregation time t which will be set as equal to the turbulent integral time τ_{int} i.e. aggregation can be supposed to occur inside the largest eddies, one gets:

$$d = 2d_0 \frac{L_{\text{int}}}{k^{\frac{1}{2}}}\sqrt{\frac{\varepsilon}{\nu_G}} \propto \varepsilon^{\frac{1}{2}}$$

Where L_{int} is the integral scale of turbulence and k is the turbulent kinetic energy. Therefore there is a direct relationship between log(d) and log(ε), the last term being known to show great variability called intermittencies.

3.2 Link to turbulence intermittencies

Theses intermittencies in the dissipation rate are known to be related the presence of both slowly rotating large eddies and rapidly rotating small eddies. By writing the evolution equation of such an eddy in a random environment and by taking into account that vorticity conservation ensures that vortex lines cannot be self-intersecting (cf. Fig. 4), Rimbert (2010) has shown that vortex line can be mapped into Self-Avoiding walk or SAW.

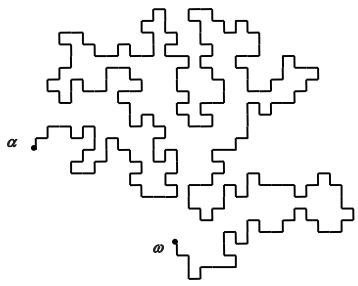

Figure 4: A sample of a self-avoiding walk (SAW). In turbulence, vortices are known to be both randomly stretched and self avoiding. Therefore ther exists a mapping between vortices and SAW.

This results in a distribution of vorticity, and henceforth, of dissipation given by a log-stable law, a generalisation of lognormal law. The main difference between the two laws being that stable laws do not have analytically closed form but only analytically closed Fourier transform given by:

$$\hat{p}_\alpha(k;\beta,\sigma,\delta) = \exp\left(ik\delta - \sigma^\alpha |k|^\alpha \left[1 + i(sign(k))\beta\omega(|k|,\alpha)\right]\right) \quad (1)$$

where the parameters $0<\alpha \le 2$, $0 < \sigma$, $-1 \le \beta \le 1$ and μ are real and

$$\omega(|k|,\alpha) = \begin{cases} \tan(\alpha\pi/2) & \text{if } \alpha \neq 1 \\ -(2/\pi)\log|k| & \text{if } \alpha = 1 \end{cases},$$

The most important parameter of these distributions is the stability index α (which is equal to 2 for Gaussian distribution and 1 for Cauchy distribution

as they are special cases, admitting an analytical form of stable distributions). As stable laws can be skewed either to the left or to the right, a skewness parameter β whose value range between -1 and 1 is the second parameter. Lastly, the scale parameter σ and the shift parameter δ are the closest to the standard deviation and the mean of normal Gaussian distribution but, they can firstly differ (when defined) and, secondly, strongly depend on the chosen form of the characteristic function. Using scaling properties of SAW, they were found to be α = 1.70 for the stability index and β = -1 for the asymmetry parameter. From experimental results, the scale parameter is given by

$$\sigma_{\ln\varepsilon}^{\alpha} = \ln\left(\frac{\lambda}{\eta}\right)$$

where λ is the Taylor micro-scale and η is the Kolmogorov scale. For turbulent intermittency, the shift parameter $\delta_{\ln\varepsilon}$ was left undetermined but has been shown to be related to the logarithm of the Taylor scale for log-stable spray PDF.

3.3 Log stable PDF in atomization

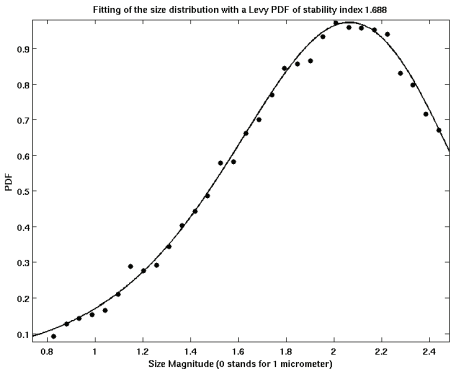

Figure 5: size distribution of the droplets related to the breakup of the bag.

Fig. 5 shows that droplet size PDF stemming from the bag can indeed be modelled using log-stable laws. Moreover width of the distribution can be related to the ratio between the Taylor and Kolmogorov scales, both of which can be determined knowing the local value of the turbulent kinetic energy k and dissipation rate ε

4 Conclusion

As can be seen in the preceding section, the strength of this model is that once k and ε are known, all the characteristic length of turbulence can be determined as well as the intermittent distribution of vorticity and dissipation. This can then be used to build a turbulent agglomeration mechanism which eventually leads to a log-stable droplet size distribution whose parameters can be each computed. Therefore it could be used to build a source term for subgrid modelling of the spray texture, such as the inclusion of an interfacial area concentration equation (Rimbert & Séro-Guillaume, 2005) for instance.

Bibliography

Eggers, J., Villermaux, E., *Physics of liquid jets*, Reports on Progress in Physics 71, pp. 036601 (2008)

Gorokhovski M., Herrmann M. *Modeling Primary Atomization* Ann. Rev. Fluid Mech., 40: 343-366 (2008)

Hsiang, L-P., Faeth G.M. *Drop Deformation and breakup due to shock wave and steady disturbance* Int. J. Multiphase Flow, 21, 545-560, (1995)

Ibrahim E.A., Yang H.Q., Przekwas A.J. *Modeling of Spray droplets deformation and breakup* AIAA J. Propulsion and Power 9, 651-654, (1993)

Kolmogorov A.N., *On the logarithmically normal law of distribution of the size of particles under pulverization* Dokl. Akad. Nauk. SSSR 31, 99 (1941).

Lefebvre H., *Atomization and Sprays* Hemisphere Publishing Corporation (1989)

Pilch M. Erdman C.A. *Use of Breakup time data and velocity history data to predict the maximum size of stable fraglments for acceleration-induced breakup of a liquid drop* Int. J. Multiphase Flow 13, 6, 741-757, (1987)

Rimbert N., Castanet G. *Crossover between Rayleigh-Taylor Instability and turbulent cascading atomization mechanism in the bag-breakup regime* Phys. Rev. E 84, 016318 (2011)

Rimbert N. *Simple model for turbulence intermittencies based on self-avoiding random vortex stretching* Phys. Rev. E 81, 056315 (2010)

Rimbert N., Séro-Guillaume O. *Log-Stable laws as asymptotic solutions to a fragmentation equation: application to the distribution of droplets in a High Weber number Spray* Phys. Rev. E. 69, (2004) 056316

Rimbert N. *On the classification of secondary atomisation mechanisms* ILASS – Europe 2011, 24th Annual Conference on Liquid Atomization and Spray Systems, Estoril, Portugal, September 2011

Séro-Guillaume O., Rimbert N. *On a thermodynamic closure for two phase flows with interfacial area concentration transport equation* Int. J. Mult. Flow, 31 (2005) 897–920

Zhao H., Liu H.F., Li W.F., and Xu J.L. *Morphological classification of low viscosity drop bag breakup in a continuous air jet stream* Phys. Fluids 22, 114103 (2010)

Challenges of Studying Primary Atomization by Simulations

M. Herrmann
School for Engineering of Matter, Transport and Energy, Arizona State University, Tempe, AZ 85287

Understanding the physical details of the initial breakup of injected liquid fuel jets remains one of the outstanding problems in multi-phase flows. While significant progress has been made in the past years to study the primary atomization region experimentally, using for example ballistic imaging [1, 2] and X-ray techniques [3, 4], such analysis cannot yet provide the full 4-D data needed for a detailed analysis. Numerical simulations, on the other hand, have the potential to generate the needed comprehensive 4-D data sets. Several studies with this goal have been published in recent years, an incomplete list contains the work of [5–18]. However, to become a tool that can be used complimentary to or even instead of experimental analysis, numerical simulations have to fulfill a list of requirements. These include governing equations ideally derived from first principle, consistent code and solution verification, and validation if modeling assumptions are introduced. Fulfilling these requirements, discussed in more detail in the following sections, remains a challenge.

Governing Equations

In single phase flows, the Navier-Stokes equations are commonly accepted to be valid from first principle. However, in liquid/gas flows, the phase interface represents a change in material properties on scales associated with the mean free path of molecules. On such length scales, the continuum hypothesis inherent in the Navier-Stokes equations is no longer valid requiring instead a statistical mechanics description. Enforcing the continuum hypothesis, i.e. limiting a mesh Knudsen number to be much smaller than unity, turns the phase interface effectively into a material discontinuity in the Navier-Stokes equations. In non-atomizing liquid/gas flows, this is not problematic, although it poses a number of numerical challenges. In atomizing flows, however, the length scale associated with the actual break-up event goes to zero at the instant of topology change. The associated Knudsen number thus becomes large and the Navier-Stokes equations are no longer valid. From a first principle point of view, the dynamics at the moment of topology change and for a short time before and after thus have to be treated using a statistical mechanics approach which includes the then dominant van-der Waals forces. In the absence of a statistical mechanics treatment a model has to be introduced for the details of the topology change. The use of such a model implies that the governing equations are no longer derived from first principle.

It remains an open question, of whether a treatment of the phase interface as a material discontinuity using the Navier-Stokes equations is a valid approximation for atomization of liquid jets. If the final stages of individual breakup events are dominated by instabilities represented by the Navier-Stokes equations, e.g. shear layer, Rayleigh-Taylor, or capillary instabilities, the solutions to the Navier-Stokes equations can be expected to capture the correct atomization physics. If the breakup mechanism occurs via the formation and breakup of thin liquid sheets, the incorporation of a statistical mechanics treatment to describe the sheet rupture is likely required.

Numerical Methods

For an overview of available numerical methods to solve for liquid/gas flows in the continuum limit the reader is referred to available overview articles in the literature [19, 20]. This section is intended to point out some of the numerical challenges a chosen method has to address to be viable for predictive atomization simulations.

The guiding principle for choosing or designing a numerical method should be that numerical discretization errors must be clearly differentiable from modeling errors inherent in the governing equations. Any mixing of the two is unacceptable from a fundamental point of view, since it

precludes solution verification and thus cannot give a fair evaluation of the error and applicability of the model itself. Unfortunately, it remains common practice to violate this principle and either couple physical modeling parameters directly to numerical parameters like grid spacing, or accept modeling restrictions that limit how small grid spacings can become. An example of the former is the topology change model inherent in fixed grid methods. The topology change model, which is a necessity for simulations based on the continuum Navier-Stokes equations, typically consists of a breakup length scale, such that if two opposing interface segments approach each other closer, topology change is introduced. In fixed grid methods like the level set method or volume of fluid, the breakup length scale is equal to the local grid spacing and thus is a numerical and not a modeling parameter. An example of the latter are standard Lagrangian point particle spray models.

From a theoretical point of view, a chosen numerical method has to fulfill three requirements: it has to be consistent, i.e. the numerical approximation approaches the governing PDEs under grid and time step refinement, it has to be stable, i.e. the numerical solution remains bounded, and it has to converge, i.e. the numerical solution approaches the solution of the governing PDEs under grid and time step refinement. For linear, well posed initial value problems, convergence is guaranteed if the method is both consistent and stable, however, in how far this is true for the non-linear Navier-Stokes equations is a not fully answered question.

In fact for many numerical methods currently in use for liquid/gas flows, the formal proof of consistency, stability, and convergence has not been achieved and thus requires further research. For example, finite difference methods unavoidably incur a zeroth-order error in the infinity norm at the phase interface, since even the smallest error in the position of the interface causes an intermittent O(1) error in material properties due to their discontinuous nature. Similarly, finite volume methods incur at least a first-order error in cells containing the phase interface. Even though it is common practice to blend out errors at discontinuities when analyzing the convergence behavior of numerical methods, whether this is appropriate for atomizing flows, where the atomization process is dominated by the dynamics at the phase interface is an open question.

Code Verification

Code verification is an often overlooked key requirement for a predictive simulation tool. Its goal is to ensure that the consistent, stable, and convergent numerical solution techniques of the governing equations are implemented in the software correctly. To check this, the obtained numerical solution has to follow the theoretical error convergence behavior that can be derived from the theoretical proof of convergence of the numerical method. However, to define the error, an exact solution is required. Exact solutions to the Navier-Stokes equations exist, however they are inadequate for multiphase flows, since they require the introduction of simplifications and thus deactivate some terms in the governing equations.

An alternative to using exact solutions to the Navier-Stokes equations is to use the method of manufactured solution [21–23]. The key idea is to allow an extension of the governing equations by adding source terms. Then, instead of trying to find an exact solution to the governing equations, one reverses the process and chooses an exact solution and derives the source terms that would result in the chosen exact solution. Because the exact solution is chosen, it can be arbitrarily complex and have each term in the governing equations non-zero, i.e. active. Since code verification is a mere mathematical exercise, the chosen exact solution need not be physical. It in fact is often beneficial to choose exact solutions that are unphysical to thoroughly test all implementation terms.

The method of manufactured solution has proven very successful in code verification of single phase solvers, however extension of the technique to liquid/gas flows with discontinuous phase interfaces are areas of active research with some promising initial results [24].

Solution Verification

Solution verification refers to the exercise that ensures that an obtained numerical solution to the governing equations is not unduly impacted by numerical discretization errors both in space and time. It can be done by performing a series of simulations using varying grid and time step sizes. Since an exact solution is typically not available to define the error, one needs to demonstrate that the numerical solution is in the asymptotic convergence region. Note that the achievable, so-called observed order of accuracy is usually smaller than the formal order of accuracy that Taylor series expansions of the employed numerical method can provide.

Roache [25] established a formal method of reporting solution verification results by introducing the so-called grid convergence index (GCI). It is based on Richardson-extrapolation and includes a formal quantitative measure of whether a solution is in the asymptotic range. Although the GCI in principle can establish whether a solution is verified, its application to liquid/gas flows with phase interfaces is complicated by the fact that the phase interface is a discontinuity in the continuum limit. Further research is needed of how to consistently incorporate the phase interface discontinuity in the GCI analysis. Among the open questions is if and how errors introduced at the phase interface influence the simulation results away from the phase interface. As mentioned above, some numerical methods are by definition prone to zeroth- or first-order errors at the phase interface. While it is believed that such methods are not dominated by these errors away from the interface, it remains to be conclusively proven for the case of atomizing flows.

Solution verification ought to be performed for each reported simulation result, even if initial and boundary conditions do not significantly change. The common practice of establishing a required resolution either by physical arguments or by solution verification of a single operating condition is understandable from a simulation cost perspective, but not sufficient. Such arguments can only be made to give guidance on the likely necessary resolution, which then still has to be verified. Using the guidance, this can then be done in a cost effective manner by performing grid/time step coarsening instead of refinement.

As for code verification, a major complication for solution verification is the typical inherent mixing of modeling and numerical parameters. It is a crucial prerequisite for both code and solution verification, that modeling parameters are independent of mesh parameters it otherwise becomes impossible to differentiate between modeling errors and numerical errors. Examples of models for atomizing flows that are typically coupled to local mesh scales and thus would require further improvements include the treatment of the delta function in the surface tension term of the Navier-Stokes equation [26, 27], the Lagrangian point particle approximation in spray models, and topology change models in fixed grid methods.

Validation

The purpose of validation is to ensure that the correct governing equations for the analyzed physical problem are solved. It can only be performed after successful code verification and only using numerical results that have undergone solution verification.

One challenge for validating simulation tools for atomizing flows lies in the limited available experimental validation data. With few exceptions, experimental data is available only in regions far away from the injector, consists of integral quantities, and does not fully define all boundary or initial conditions. There is in fact a severe lack of quality experimental data useable for validation and significant efforts should be made to establish these data sets in the near future.

Furthermore, although simulations are deterministic in nature, small changes in boundary and initial conditions can have different outcomes. As such a validation simulation has to be performed for an ensemble of boundary and initial conditions that represent the experimental conditions and it is the ensemble averages that have to be compared.

It must be stressed that reproducing experimentally obtained results while adjusting model parameters is not validation. Validation simulations should be performed without any knowledge of the experimental results, except for the boundary and initial conditions. Only after solution verification should the numerical results be quantitatively compared to the experimental results. If at that stage, a discrepancy is found and the model is adjusted, the simulation is no longer a validation and a new validation case has to be performed.

Prediction

Prediction is the generation of solution verified simulation results for which no experimental data is available. A code verified and validated simulation tool generating solution verified predicted data sets of the atomization process will be the ideal tool to study atomization and help derive lower order models for engineering applications. However, the requirement of code verification, the need for ensemble average solution verified validation, and ensemble averaged solution verified prediction drastically increases computational cost. Although, using todays computational resources, single non-verified simulations of the atomization process are possible, following the outlined procedure adds orders of magnitude more cost. However, with the continued fast paced growth of supercomputers, the required computational power will become available in the next one to two decades. At that point, and perhaps significantly earlier, simulations will be able to enhance and perhaps replace experiments as the preeminent scientific discovery tool for atomizing flows.

References

[1] M. Linne, M. Paciaroni, J. Gord, and T. Meyer. *Applied Optics*, 44(31):6627–6634, 2005.

[2] M. Linne, M. Paciaroni, T. Hall, and T. Parker. *Experiments in Fluids*, 40(6):836–846, 2006.

[3] Y. J. Wang, K.-S. Im, K. Fezzaa, W. K. Lee, Jin Wang, P. Micheli, and C. Laub. *Applied Physics Letters*, 89(15):151913–151913, 2006.

[4] Y. Wang, X. Liu, K.-S. Im, W.-K. Lee, J. Wang, K. Fezzaa, D. L. S. Hung, and J. R. Winkelman. *Nat Phys*, 4(4):305–309, 2008.

[5] G. M. Bianchi, P. Pelloni, S. Toninel, R. Scardovelli, A. Leboissetier, and S. Zaleski. *SAE Tech. Pap.*, (2007-01-0244), 2007.

[6] W. Bo, X. Liu, J. Glimm, and X. Li. *SIAM J. Sci. Comput.*, 33:1505–1524, 2011.

[7] O. Desjardins, V. Moureau, and H. Pitsch. *J. Comput. Phys.*, 227(18):8395–8416, 2008.

[8] O. Desjardins and H. Pitsch. *Atom. Sprays*, 20(4):311–336, 2010.

[9] D. Fuster, A. Bague, T. Boeck, L. Le Moyne, A. Leboissetier, S. Popinet, P. Ray, R. Scardovelli, and S. Zaleski. *Int. J. Multiphase Flow*, 35(6):550–565, 6 2009.

[10] M. Herrmann. *Journal of Engineering for Gas Turbines and Power*, 132(6):061506–10, 2010.

[11] M. Herrmann. *Proceedings of the Combustion Institute*, 33(2):2079–2088, 2011.

[12] M. Herrmann. *Atom. Sprays*, 21(4), 2011.

[13] D. Kim, O. Desjardins, M. Herrmann, and P. Moin. In *ILASS Americas*, Chicago, IL, 2007.

[14] R. Lebas, T. Menard, P. A. Beau, A. Berlemont, and F. X. Demoulin. *Int. J. Multiphase Flow*, 35(3):247–260, 2009.

[15] X. Li, M. Arienti, M. C. Soteriou, and M. Sussman. AIAA 2010-210, pp. 1–16, 2010.

[16] T. Menard, S. Tanguy, and A. Berlemont. *Int. J. Multiphase Flow*, 33(5):510–524, 2007.

[17] J. Shinjo and A. Umemura. *Int. J. Multiphase Flow*, 36(7):513–532, 7 2010.

[18] J. Shinjo and A. Umemura. *Int. J. Multiphase Flow*, 37(10):1294–1304, 12 2011.

[19] M. Gorokhovski and M. Herrmann. *Annual Review of Fluid Mechanics*, 40(1):343–366, 2008.

[20] R. Scardovelli and S. Zaleski. *Annu. Rev. Fluid Mech.*, 31:567–603, 1999.

[21] W. L. Oberkampf and F. G. Blottner. *AIAA J.*, 36(5):687–695, 1998.

[22] P. J. Roache. *J. Fluids Eng.*, 124(1):4–10, 2002.

[23] C. J. Roy. *J. Comput. Phys.*, 205(1):131–156, 2005.
[24] P. Brady, M. Herrmann, and J. Lopez. In *ILASS Americas*, Ventura Beach, CA, 2011.
[25] P. J. Roache. *J. Fluids Eng.*, 116(3):405, 1994.
[26] J. U. Brackbill, D. B. Kothe, and C. Zemach. *J. Comput. Phys.*, 100:335–354, 1992.
[27] M. Sussman, P. Smereka, and S. Osher. *J. Comput. Phys.*, 114:146, 1994.

Comprehensive Modeling of Spray Formation from Gas Turbine Injectors: Recent Approaches and Open Issues

Achintya Mukhopadhyay*
Department of Mechanical Engineering
Jadavpur University Kolkata – 700032 India

Motivation

Performance and emission characteristics of gas turbine combustors are crucially dependent on the spray characteristics, especially the droplet size distribution. The increasing demands of higher efficiency and stringent emission regulations require design of combustors with reduced factors of safety in performance and emission issues. The availability of powerful computing platforms has made CFD with improved prediction capabilities a viable tool for design of combustors and reduced the requirement of expensive experimental studies in the design process. However, in the CFD modeling of spray combustors, a major area of uncertainty is the initial size and velocity distribution of droplets in the spray at the combustor inlet. The capability of the CFD code to predict crucial phenomena like cold start-up, ignition, flame stability, and emission of soot, hydrocarbons and NO_x depends on the correct prescription of the initial spray condition. The present state of the art approach relies on experimental observations and/or empirical correlations, both of which depend on the injector geometry and operating conditions. However, the demands of efficiency and emission often require design of not only the combustor but innovative design of the injector as well. Modern gas turbine combustors use innovative injector designs like hybrid atomizers, which combine the benefits of both pressure-swirl and airblast injectors [1].Depending on the liquid injection pressure and air flow rates, these injectors can behave like pressure-swirl or airblast atomizers. Since the atomization mechanisms for pressure-swirl and airblast atomizers are fundamentally different [2], design of these injectors require detailed investigation of the atomization process. In such cases, comprehensive predictive models, with minimum dependence on empiricism, are necessary at the design stage. Moreover, the experimental studies for determining spray characteristics mostly concentrate on behavior at ambient pressure and cold conditions. Reliable experiments at high pressure and high temperature are difficult and relatively scarce. Comprehensive predictive models can be very useful in such situations also.

Basic Steps in Modeling

The objective of the comprehensive model is to predict droplet size and velocity distribution in the spray from input data of the geometry and operating conditions of the atomizer. The basic steps in the modeling are: (i) modeling of the internal hydrodynamics of the injector leading to prediction of the liquid sheet velocity and thickness and spray cone angle (ii) modeling of the primary and secondary breakup of the liquid sheet with inputs from the internal hydrodynamics model leading to the prediction of breakup length and mean droplet diameter and (iii) prediction of the droplet size and velocity distribution of the polydisperse spray using the predicted mean droplet diameter and primary breakup length. The overall structure of the model can be represented as shown in Fig. 1.

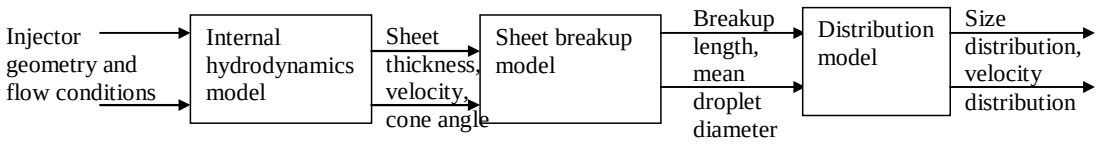

Fig.1: Schematic of the comprehensive model

* E-mail: achintya.mukho@gmail.com

A full comprehensive model incorporating all the three modules is rare. However, comprehensive models incorporating some of the above sub-models have been reported. Liao et al. [3] and Ibrahim and Jog [4] incorporated the first two modules in their analysis of pressure-swirl atomizers while Kim et al. [5], Movahednejad et al. [6] and Nath et al. [7, 8] combined the last two modules in their analyses. Liao et al. [3] and Movahednejad et al. [6] used linear analysis in their breakup model while nonlinear breakup models were used in [4, 5, 7, 8].

Modeling of Internal Hydrodynamics of Injectors

The simulation of the flowfield inside the injector has been probably the mostly widely studied component of the above model. Most of these studies, e.g., Dash et al. [9] and Ibrahim and Jog [4] used fixed grid Eulerian approaches like Volume of Fluid (VOF) to locate the interface profile for the liquid sheet. Datta and Som [10] used a thermodynamic criterion for the same purpose. An alternative approach for modeling the two phase flow in the atomizer is the Arbitrary Eulerian Lagrangian (ALE) method used by Sakman et al. [11] and Jeng et al. [12]. However, these works investigated only pressure-swirl atomizers. On the other hand, Chin et al. [13] modeled the internal hydrodynamics of a hybrid atomizer. But they did not focus on the interface profile. Very recently, Chatterjee et al. [14] and Mahapatra et al. [15] simulated the hydrodynamics of a hybrid atomizer using a VOF-based model. Their work investigated the effect of variation of different geometrical parameters and inlet positions on the flowfield. They also explored the impact of providing recession in the inner air and liquid conduits. Of the three modules of the comprehensive modeling mentioned in the previous paragraph, this part is the most well-established and widely accepted. Experimental validation of the predicted flowfield using optical techniques like PIV has added further credence to the results.

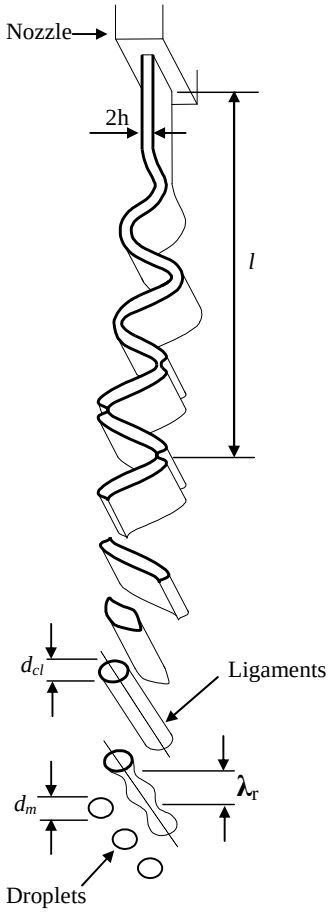

Fig. 2: Schematic of sheet breakup leading to spray formation

Modeling of Breakup of Liquid Sheets

This module is the most complicated and controversial part of the comprehensive model. The popular approach [5, 16, 8] is to assume that the longitudinal waves corresponding to the wave number giving highest growth rate grows and eventually leads to breakup of the liquid sheet into ligaments. The breakup, occurs when the waves on the two interfaces touch each other. After the sheet breaks up, ligaments are formed. The ligaments so formed undergo further breakup according to Rayleigh theory to form drops of equal size. The spray formation process is schematically represented in Fig. 2. Traditionally, linear analysis is used for the breakup of the sheets into ligaments. In the linear analysis, the breakup is said to occur when the amplitude of the disturbance reaches a critical value (generally based on the analysis of Clark and Dombrowski [17] for planar liquid sheets). However, more accurate nonlinear analysis has also been done to determine the breakup length [18, 19, 7]. In all these analyses, temporal instability has been used to determine the dimensionless breakup time, which is equated to the dimensionless breakup length, using Gaster transformation. An alternative approach is to combine the linear analysis with experiments using high speed visualization to determine the amplitude at breakup [20] as shown in Fig. 3. In addition to the stability analysis, nonlinear analysis has also been done using vortex dynamics methods [21, 22] and approximate numerical

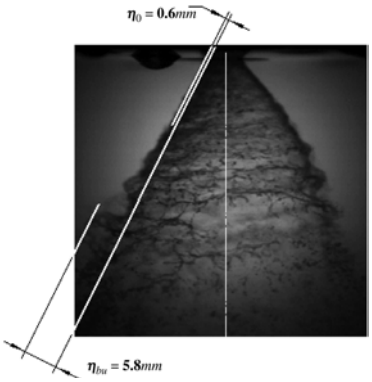

Fig. 3: Schematic of amplitude of disturbance on liquid sheet [20]

techniques [23]. However, there is some lack of consensus on the exact mechanism of the primary breakup of liquid sheets at different conditions. Especially, some authors have questioned the breakup due to longitudinal mode of instability alone. This is an area which requires more investigations. High speed visualization, as in [24, 25, 16] can add to the present level of understanding. Detailed numerical simulations have also been attempted. Park and Heister [26] used BEM-based solution for breakup of liquid sheets, assumed inviscid, in pressure-swirl atomizers. Their simulation predicted the droplet size distribution from first principles. Siamas et al. [27] used DNS for determining the near-field dynamics of annular liquid sheets in presence of coflowing gases. Although these approaches [26, 27] give very detailed picture of the fluid dynamics of liquid sheet breakup, they are too expensive for use as design tools. Consequently, more work is needed to develop predictive models for liquid sheet breakup at reasonable computational cost. In addition, there is scope of significant amount of work for the breakup of ligament into drops.

Prediction of Droplet Size and Distribution

This module of the predictive model accounts for the stochastic nature of the spray formation process and leads to prediction of probability distribution functions (pdf) for droplet size and velocity in the spray. The traditional approach of using empirical distribution functions is of limited use in the design of new classes of injectors for which sufficient data may not be available. Although the approach of Heister and coworkers (e.g., [26]) directly lead to the development of the pdf for droplet size, such approach, as mentioned before, is too expensive for use as a design tool. The common approaches [28] for predicting the size and velocity pdf are based on use of either maximum entropy formulation (MEF) or discrete probability function (DPF). Of the two, the maximum entropy formulation has been used more commonly. The method is based on the concept of maximizing information entropy subject to certain constraints posed by different conservation equations. Different variants of this method have been developed by Li, Tankin and coworkers (e.g., [29, 30]), Sellens, Brzustowski and coworkers (e.g., [31, 32) and Domouchel and coworkers (e.g., [33, 34]). The distribution functions can be expressed in terms of both droplet number based distribution and droplet volume based distribution. Similarly, prior distribution functions may or may not be necessary depending on whether Bayesian entropy or Shannon entropy is used. In the context of the comprehensive model, the drop diameter predicted by the breakup model is considered as the mass mean diameter of the distribution. In addition, the breakup length predicted by the breakup model, is used to calculate the loss of momentum and energy of the liquid sheet due to drag [35, 5, 8]. The MEF models can be fine-tuned through comparison with the experimental predictions from Phase Doppler Particle Analyzer (PDPA).

Summary

Although the individual sub-modules of the comprehensive model have been developed to a reasonable extent, their coupling is still in a nascent stage. However the importance of comprehensive predictive models in CFD-based design of gas turbine combustion systems is obvious. This is especially true for new classes of injectors with widely different working principles like hybrid atomizers and effervescent atomizers.

Acknowledgement
Much of my present understanding in the above subject has evolved during research in this area supported by Indian Space Research Organisation (ISRO) and Gas Turbine Research Establishment (GTRE) under the GATET programme. I also gratefully acknowledge the contribution of our students, Sujit Nath, Souvick Chatterjee, Samiran Samanta and Soumik Mahapatra and my colleagues, Profs. Amitava Datta, Swarnendu Sen and Koushik Ghosh.

References

1 Rizk, N.K., Chin, J.S. and Razdan, M.K., ASME J. Eng. Gas Turbines Power, 119, 34 – 44, 1997.
2 Benjamin, M.A., Jensen, R.J. and Arienti, M., Atomization Sprays, 20, 485 – 512, 2010.
3 Liao, Y., Sakman, A. T., Jeng, S. M., Jog, M. A., and Benjamin, M. A., ASME J. Eng. Gas Turbines Power, 121, 285–294, 1999.
4 Ibrahim, A.A. and Jog, M.A., ASME J. Eng. Gas Turbines Power, 129, 945–953, 2007.
5 Kim, W. T., Mitra, S. K.,Li, X.,Prociw, L.A. and Hu, T. C. J., Part. Part. Syst. Charact., 20, 135-149, 2003.
6 Movahednejad, E., Ommi, F., Hosseinalipour, S.M., Chen, C.P., Mahdavi, S.A., Heat Mass Transfer, 2011.
7 Nath, S., Datta, A., Mukhopadhyay, A., Sen, S. and Tharakan, T.J., Atomization Sprays, 20, 983 – 1003, 2010.
8 Nath, S., Mukhopadhyay, A., Datta, A., Sen, S. and Tharakan, T.J., Prediction of size and velocity distributions in sprays formed by the break up of planar liquid sheets using maximum entropy formalism Atomization Sprays, 20, under review, 2011.
9 Dash, S.K., Halder, M.R., Peric, M. and Som, S.K., ASME J. Fluids Engg., 123, 829 – 835, 2001.
10 Datta, A. and Som, S.K., Int. J. Heat Fluid Flow, 21, 412 – 419, 2000.
11 Sakman, A. T., Jog, M. A., Jeng, S. M., and Benjamin, M. A., AIAA J., 38, 1214–1218, 2000.
12 Jeng, S. M., Jog, M. A., and Benjamin, M. A., AIAA J., 36, 201–207, 1998.
13 Chin, J.S., Rizk, N.K. and Razdan, M.K., J. Propuls. Power, 16, 297 – 301, 2000
14 Chatterjee, S., Mahapatra, S., Mukhopadhyay, A. and Sen, S., Computational Modeling and Parameteric Study of Internal Hydrodynamics of Hybrid Atomizer, Proc. 22nd National Conference on IC Engines and Combustion, NIT Calicut, December 2011.
15 Mahapatra, S., Chatterjee, S., Mukhopadhyay, A. and Sen, S., Geometric Optimization of Hybrid Atomizer, Proc. 22nd National Conference on IC Engines and Combustion, NIT Calicut, December 2011.
16 Negeed, E.R., Hidaka, S., Kohno, M. and Takata, Y., Int. J. Heat Fluid Flow, 32, 95 - 106, 2011.
17 Clark, C. J. and Dombrowski, N., Proc. Royal Society, London A,. 329, 467–478, 1972.
18 Jazayeri, S. A. and Li, X., J. Fluid Mech., 6, 281–308, 1999.
19 Ibrahim, A. A. and Jog, M. A., Int. J. Multiphase Flow, 34, 647–664, 2008.
20 Fu, Q.-F., Yang, L.-J., Qu, Y.-Y. And Gu, B., J. Propuls. Power, 26, 955 – 968, 2010
21 Rangel, R.H. and Sirignano, W.A., Phys. Fluids A, 3, 2392 – 2400, 1991.
22 Lozano, A., Garcia-Olivarez, A. and Dopazo, C., Phys. Fluids, 10, 2188 – 2197, 1998.
23 Tharakan, T. J., Ramamurthi, K., and Balakrishnan, M., Acta Mech., 156, 29–46, 2002.
24 Park, J., Huh, K.Y., Li, X. And Renksizbulut, M., Phys. Fluids, 16, 625 – 632, 2004.
25 Wahono, S., Honnery, D., Soria, J. and Ghojel, J., Exp. Fluids, 44, 451 – 459, 2008.
26 Park, K.S. and Heister, S.D., Int. J. Multiphase Flow, 36, 1 – 12, 2010.
27 Siamas, G.A., Jiang, X. and Wrobel, L.C., Phys. Fluids, 21, 042103, 2009.
28 Babinsky, E. and Sojka, P.E., Prog. Energy Combust. Sci., 28, 303-329, 2002.
29 Li , X. and Tankin, R. S., *Combust.Sci.Technol.*, 68, 147-155, 1989.
30 Li, X. and Tankin, R. S., *Part.Part.Syst. Charact.*, 9, 195-201, 1992.
31 Sellens, R. W. and Brzustowski, T. A., *Atomization Spray Technol.*, 1, 195-201, 1985.
32 Sellens, R.W., Part.Part.Syst. Charact., 6, 17-27, 1989.
33 Dumouchel, C.; Malot, H., Part. Part. Syst. Charact., 16, 220-228, 1999.
34 Dumouchel, C., Part. Part. Syst. Charact., 23, 468-479, 2006.
35 Cousin, J.; Yoon, S.J.; Dumouchel, C. *Atomiz. Spray*, 6, 601-622, 1996.

Dynamics of Non-Newtonian Fluid Flow in Simplex Atomizers

Milind A. Jog
Mechanical Engineering, Thermal-Fluids and Thermal Processing Laboratory,
University of Cincinnati, Cincinnati, OH 45221-0072
Email: Milind.Jog@uc.edu

Abstract

Simplex or pressure swirl atomizers are used to produce liquid sprays in a variety of applications that cover a wide range of flow conditions. The geometry of a pressure swirl atomizer is fairly simple but the flow through the atomizer is quite complex as it involves two phases, regions of recirculation, unsteady and turbulent flow. In many applications the liquid exhibits non-Newtonian rheology and time varying surface tension which adds further complexities to computationally model the flow in the atomizer. The ability to accurately predict the two-phase flow of such complex fluids in pressure swirl atomizers and to evaluate the effects of nozzle geometry, flow conditions, and liquid properties on the atomizer performance is critical to improve nozzle designs. An overview of the work in this area is presented along with opportunities for Indo-US research collaborations.

Introduction

Simplex atomizers have many desirable characteristics that include simplicity of construction, ease of manufacture even in small size, reliability, good atomization quality, low clogging tendencies, and low pumping power requirements [1]. These advantages have made it a versatile atomizer. A commonly used geometry of a simplex atomizer is shown in Figure 1. The tangential inlet slots result in imparting a swirling motion to the liquid as it enters the swirl (or spin) chamber. A convergent section accelerates the flow as it enters the exit orifice. The swirl motion of the liquid pushes it close to the wall and creates a zone of low pressure along the center line which results in back flow of air in the nozzle creating an air-cored vortex. The liquid emanates from the orifice as a conical sheet that becomes unstable and undergoes a complex process of breakup to form a spray.

The important performance parameters are: the liquid film thickness which governs the mean spray droplet size (typically Sauter Mean Diameter), the spray cone angle, and the discharge coefficient [2].

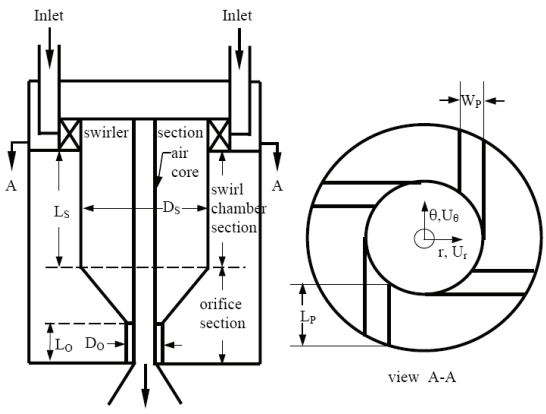

Figure 1: A schematic of a pressure swirl atomizer

The performance of the atomizer is governed by the liquid properties, injection flow conditions and nozzle geometry. For Newtonian fluids, as the mass flow rate through the nozzle is increased from zero, the performance parameters change significantly at first, but eventually at high mass flow rate the discharge coefficient, the film thickness, and the spray cone angle become insensitive to the variations in flow Reynolds number [3]. Simplex atomizers are typically designed to operate in this range as a consistent performance can be expected irrespective of small changes in the inlet pressure. As such, in this regime, inlet flow conditions tend to have only a small effect on the atomizer performance. Hence most of the work on simplex atomizers has generally focused on investigation of the effect of nozzle geometry and liquid properties on atomizer performance [4-10]. Moreover, if the liquid properties are fixed for a given application, change in nozzle geometry becomes an effective method to achieve desired atomizer performance.

Many applications involve fluids that exhibit non-Newtonian flow behavior, which include, among others, atomization of aqueous polymeric solutions in manufacturing of pharmaceutical products, paint sprays, spray drying of food and detergents, consumer product sprays in household products, medical drug delivery for respiratory system, and agricultural sprays [11-13]. In spite of these applications, the vast majority of studies on liquid atomization using a simplex atomizer have been carried out with Newtonian fluids. Atomizers are typically designed for, and tested with, Newtonian fluids. As such investigation of non-Newtonian fluid flow through simplex atomizers is crucial to understand how they will perform while atomizing non-Newtonian fluids in a variety of applications.

Often the non-Newtonian atomizing liquids are solutions of polymers and surfactants. The apparent viscosity of the polymeric solutions tends to have a strong dependence of shear rate [14]. For example, measurements of the apparent viscosity of aqueous solutions of Hydroxyethylcellulose (HEC) for three different concentrations are shown in Fig. 2 [15]. HEC is a purely-viscous water soluble polymer. At very low shear rate the solution behaves as a high viscosity Newtonian liquid with its apparent viscosity close to the zero-shear value. This is followed by a power-law behavior with increasing shear rate. Such behavior is often represented by Carreau model [14]. Other polymers may have visco-elastic properties and may require nonlinear visco-elastic models [16].

Surfactants have a long chain molecular structure with a hydrophilic head and a hydrophobic tail. Their adsorption at the liquid-air interface results in reduction of the surface tension of the solution. This time-dependent phenomenon lends to a dynamic surface tension variation as depicted in Fig. 3 [17]. Once a new air-liquid surface is created, the interfacial tension is initially close to that of the solvent and then decreases with time as the surfactant molecules diffuse and are adsorbed at the interface. Once the interface is repopulated with surfactant molecules, the surface tension reaches an equilibrium value. The equilibrium surface tension is a function of surfactant concentration. With increasing surfactant concentration, σ decreases until the critical micelle concentration (or CMC) and remains constant thereafter [17] as shown in Fig. 4. The CMC of a surfactant is the concentration at which micelles (colloid-sized clusters or aggregates of monomers) start to form [18]. Both shear-rate dependent viscous behavior and dynamic surface tension variation alters the flow inside the atomizer compared to a Newtonian fluid flow.

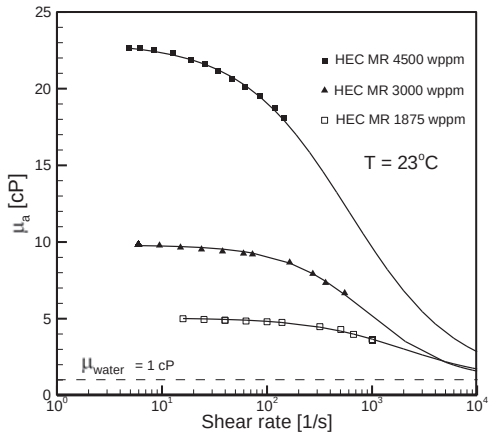

Figure 2. Apparent viscosity variation with shear rate for aqueous solutions of HEC MR [15]

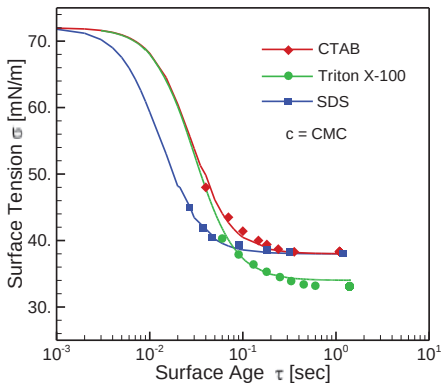

Fig. 3. Variation of surface tension with surface age for three aqueous surfactant solutions [17]

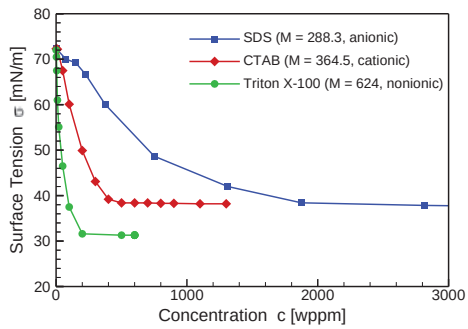

Fig. 4. Equilibrium surface tension variation with concentration [17]

Computational Modeling

To computationally model the flow, one must be able to track the liquid/gas interface accurately. The location of the interface is not known a-priori and must be determined as part of the solution. Advanced computational methods to track the phase interface include Arbitrary-Lagrangian-Eulerian (ALE), Volume-of-Fluid (VOF), and level-set method. The ALE method [19] is divided in two steps. The first step is the Lagrangian step where the grid points move with the local velocity. The points on the interface always remain on the interface tracking a sharp, accurate interface. The second step is the Eulerian step where a new grid is created by moving points back in the axial direction. Jog and co-workers [2, 8-10] have developed a computational code based on the ALE method to determine the flow in a simplex atomizer and predict the effects of atomizer geometry on its performance.

In the VOF method [20], in addition to the governing equations for mass and momentum conservation, an equation for the volume fraction of each phase is solved. When the volume fraction is between zero and one, there exists a fluid interface within the computational cell. One shortcoming of this method is that the sharp variations in the properties (density and viscosity) are spread over three to four cells. Das et al. [21], Donjat et al. [22], Hansen et al. [23], and Ibrahim and Jog [24] have employed the VOF method to simulate the flow in a simplex atomizer.

Compared to the large number of studies on the experimental/analytical investigations of Newtonian fluid sprays, very few studies are available in the literature that consider flow of non-Newtonian fluids through simplex atomizers [25-27]. Som and co-workers [25-26] have determined experimentally as well as through an approximate analysis the discharge coefficient and spray cone angle for flow of time-independent, purely viscous, power-law non-Newtonian fluid through a simplex atomizer with purely tangential entry. Mandal et al. [28] have computationally modeled the flow of a power-law fluid in a simplex atomizer. Their predictions of film thickness (made dimensionless by orifice radius), spray cone half angle, and the discharge coefficient with atomizer constant are shown for power-law index of 0.4 (pseudoplastic), 1 (Newtonian), and 1.2 (dilatant). Atomizer constant (K) is the ratio of the inlet area to the product of swirl chamber diameter and the exit orifice diameter. Increase in K corresponds to an increase in the inlet area which reduces the angular momentum of the fluid and results in an increase in the film thickness and the discharge coefficient and a decrease in the cone angle. There is significant difference in the values of these performance parameters for different values of n.

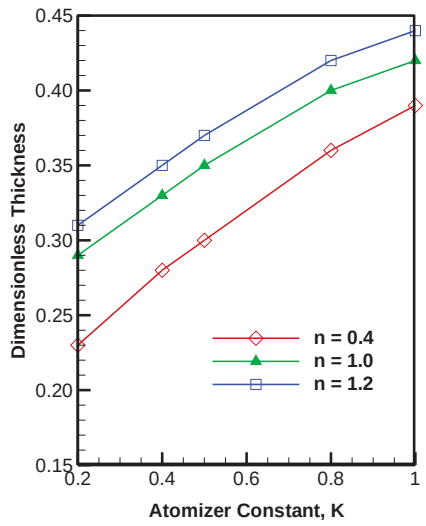

Fig. 5. Variation of dimensionless thickness with atomizer constant

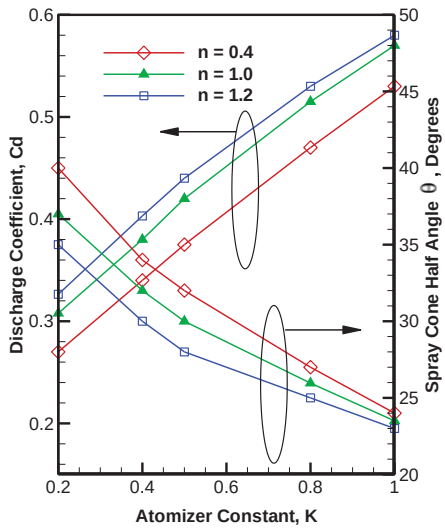

Fig. 6. Variation of discharge coefficient and spray angle with atomizer constant

Atomizer performance with visco-elastic and/or surfactant laden liquids is likely to be more complicated than that shown in Figs. 5 and 6.

Direction of Future Work and Opportunities for Indo-US Collaboration

To develop a predictive model for the atomization process, a comprehensive approach must be adopted that includes a computational treatment of the flow in the atomizer and a model for the non-linear breakup process of the liquid sheet exiting from the atomizer. There has been considerable work on the liquid sheet and jet instability and breakup with Newtonian (for example, [29-32]) as well as non-Newtonian fluids (for example, [12-13, 33]). However, developing a comprehensive model that combines both the internal flow computations and the nonlinear breakup process external to the atomizer remain a challenge for non-Newtonian and surfactant laden fluids. Development of such a comprehensive model to study the dynamics of the flow and spray formation for complex fluids would lend to opportunities for Indo-US research collaborations.

References:

[1] Lefebvre, A.H., 1989. Atomization and Spray. Hemisphere Publishing, New York.

[2] Jeng, S.M., Jog, M. A., and Benjamin, M. A., 1998. AIAA Journal 36 (2), 201-207.

[3] Ibrahim, A.A., and Jog, M. A., 2006. Recent Research Developments in Applied Physics Vol. 9, 1-20.

[4] Giffen, E., and Muraszew, A., 1953. The Atomisation of Liquid Fuels. John Wiley, New York.

[5] Rizk, N.K., and Lefebvre, A. H., 1984. Progress in Aeronautics and Astronautics 95, 563-580.

[6] Rizk, N.K., and Lefebvre, A. H., 1985. Journal of Propulsion and Power 1, 193-199.

[7] Rizk, N.K., and Lefebvre, A. H., 1986. Atomization and Spray Technology 2, 219-233.

[8] Sakman, A.T., Jog, M. A., Jeng, S. M., and Benjamin, M. A., 2000. AIAA J. 38, 1214-1218.

[9] Liao, Y., Sakman, A. T., Jeng, S. M., Jog, M. A., and Benjamin, M. A., 1999. J. Engineering for Gas Turbine and Power 121, 285-294.

[10] Xue, J., Jog, M. A., Jeng, S. M., and Benjamin, M. A., 2004. AIAA Journal 42 (12), 2408-2415.

[11] Hecht, J.P., 2005. Proc. of 18th Annunal Conference of ILASS, Irvine, CA.

[12] Petersen, F. J., Worts, O. F. and Schaefer, T., Sojka, P. E., 2001. Pharmaceutical Development and Technology, 6(2), 201-210.

[13] Geckler, S. C., and Sojka, P. E. 2008. Journal of Fluids Engineering, 130(6), 061303.

[14] Bird, R.B., Stewart, W. E., and Lightfoot, E. N., 2002. Transport Phenomena. Wiley, New York.

[15] V. Ravi, M. A. Jog, and R. M. Manglik, Paper Number ILASS2011-181, Proc. of the 23rd Annual Meeting of ILASS, Ventura, CA, May 15 – 18, 2011.

[16] Holmberg, K., Jönsson, B., Kronberg, B., and Lindman, B., Surfactants and Polymers in Aqueous Solution, Wiley, New York, 2003.

[17] K. P. Gatne, M. A. Jog, and R. M. Manglik, Langmuir, Vol. 25 (14), 8122-8130, 2009.

[18] Rosen, M.J., Surfactants and Interfacial Phenomena, Wiley, New York, NY, 1989.

[19] Hirt, C.W., Amsden, A. A., and Cook, J. L., 1974. Journal of Computational Physics 14, 227-253.

[20] Hirt, C.W., and Nichols, B. D., 1981. Journal of Computational Physics 39, 221-225.

[21] Dash, S.K., Halder, M. R., Peric, M., and Som, S. K., 2001. J. Fluids Engineering 123 (4), 829-835.

[22] Donjat, D., Estivalezes, J. L., and Michau, M., 2002. Proc. of 15th Annual ILASS Conference, Madison, WI.

[23] Hansen, K.G., Madsen, J., Trinh, C. M., Ibsen, C. H., Solberg, T. and Hjertager, B. H., 2002. Proc. of ILASS-Europe, Zargoza.

[24] Ibrahim, A.A., and Jog, M. A., 2006. Proc. of 19th Annual Conference of ILASS, Toronto, Canada.

[25] Som, S.K., 1983. Journal of non-Newtonian Fluid Mechanics 12, 39-68.

[26] Som, S.K., and Biswas, G., 1986. Applied Scientific Research 43, 3-22.

[27] Schutz, S., Breitling, M., and Piesche, M., 2004. Chem. Eng. Technology 27 (6), 619-624.

[28] A. Mandal, M. A. Jog, J. Xue, and A. A. Ibrahim, International Journal of Heat and Fluid Flow, Vol. 29 (5), pp.1494-1503, 2008

[29] A. A. Ibrahim and M. A. Jog, 2008. Int. J. Multiphase Flow, Vol. 34(7), 647-664, 2008

[30] A. A. Ibrahim and M. A. Jog, 2006. Acta Mechanica, Vol. 186, 113-133, 2006.

[31] T. John Tharakan, K. Ramamurthi, 2002. Acta Mechanica 156, 29 – 46

[32] Sirignano, W. A., and Mehring, C., 2000. Progress in Energy and Combustion Science, 26: 609-655.

[33] Kongara, S. S. V.V. and Jog, M. A., 2006. Proceedings of the 19th Annual Meeting of ILASS, Toronto, Canada.

Evaporation and Combustion of Isolated Spray Droplets

Dr. V. Raghavan
Assistant Professor, Department of Mechanical Engineering, IIT Madras, Email: raghavan@iitm.ac.in

Introduction

Liquid fuel sprays are employed in several practical devices such as liquid-fuel rocket engines, diesel engines, gas turbines, industrial furnaces and many others. Reaction zones are formed either in regions surrounding these droplets (diffusion flames) or in regions where fuel-air ratios are within the flammability limits (premixed flames). In most practical systems, such as in diesel engines, the combustion process is very complicated. After the formation of a spray (disperse liquid-phase in the gas-phase), evaporation and mixing leads to formation of combustible mixtures. Spray structure with regard to its spatial distribution, drop size distribution and density, is very complex. The process of combustion taking place in a spray has been presented by Chiu et al. [1]. To understand each and every process involved in spray combustion, it is necessary to have a complete knowledge of the mechanism of vaporization and combustion of individual droplets, effects of interaction between the droplets, and the statistical description of the droplets with regard to their size and spatial distribution. It is very difficult to obtain detailed information on the mechanism or the burning rate, by direct studies of spray combustion. The research works on isolated droplets fall into studies on single- and multi-component droplets under normal, micro and zero gravity environments, under high temperature, and high pressure environments. Numerous experimental and numerical studies are available in literature.

Experimental Studies

Droplet evaporation and combustion studies have been undertaken by several researchers. Godsave [2] and Spalding [3] carried out the earliest studies on liquid fuel droplet combustion. Several researchers have conducted isolated droplet combustion studies [4-9]; they considered both suspended droplets as well as free droplets in a drop chamber facility. The steady-state experimental setup of Godsave [2] and Spalding [3] has been quite useful to measure instantaneous burning rates of renewable fuels and their blends as reported in recent experimental studies [10-11]. A similar porous sphere setup has been used to measure the steady vaporization rates of alternative fuels such as alcohols and biodiesels under hot convective flow conditions. Experiments in microgravity environments [12-14] using either drop tower facilities or in space stations have proven to be quite useful in understanding the spherically symmetric evaporation and combustion features. Since several devices use high pressure environment, isolated suspended droplet evaporation and combustion studies in high pressure and high temperature environments have been studied by several researchers [15-18]. Evaporation of a suspended binary fuel droplet at elevated temperatures and pressures has been studied by Ghassemi et al. [19]. At low pressures, bubble formation within the liquid binary droplet has been observed.

Numerical Studies

Starting from simplified analytical models, comprehensive and predictive numerical models, having several levels of complexities, have been reported by several researchers to simulate the evaporation and combustion processes of an isolated spray droplet and droplet arrays under several environmental conditions [20-33]. The complexities in handling real gas effects and gas solubility effects in high pressure environments, water absorption in alcohol droplets, need for solving liquid-phase, differences in suspended and moving droplets and many more have been discussed in detail in these studies.

Overview of Experimental and Numerical Results

Figures 1 to 8 present various experimental and numerical results. Results from porous sphere experimental results, numerical simulation of moving and suspended droplet combustion, special feature in modeling alcohol combustion, results of moving n-dodecane droplet in high pressure nitrogen environment and droplet interaction effects are presented. Research has revealed that neighboring droplets exert a strong influence and therefore, a typical spray droplet will not have burning characteristics of an isolated droplet except when the separation distance between the droplets is large. In this case, a separate flame exists around each droplet. On the other hand, when the separation distance between the droplets is very small, they collectively burn with a single merged flame, in which case the mode of burning is termed as group burning. For intermediate values of separation distance, interference effects such as starvation for oxygen and enhancement of heat transfer from the flame of the neighboring droplet, become important.

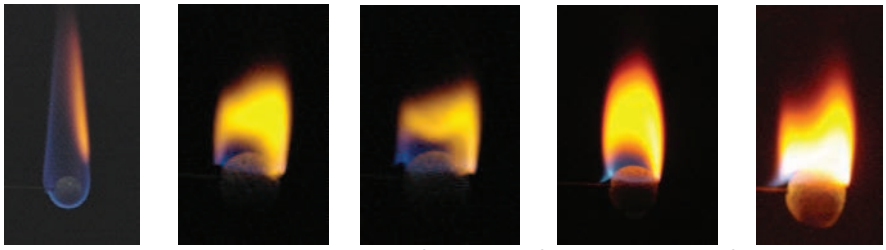

Figure 1: Flame photographs of methanol fed porous sphere flames

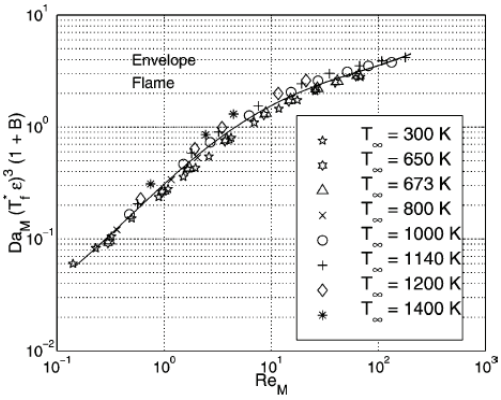

Figure 2: Scaled Damkohler number vs. Reynolds number – demarcation of envelope and wake flames

Figure 3: Instantaneous flame photographs of ethanol-gasoline blends: (a) 0% gasoline and (b) 30% gasoline

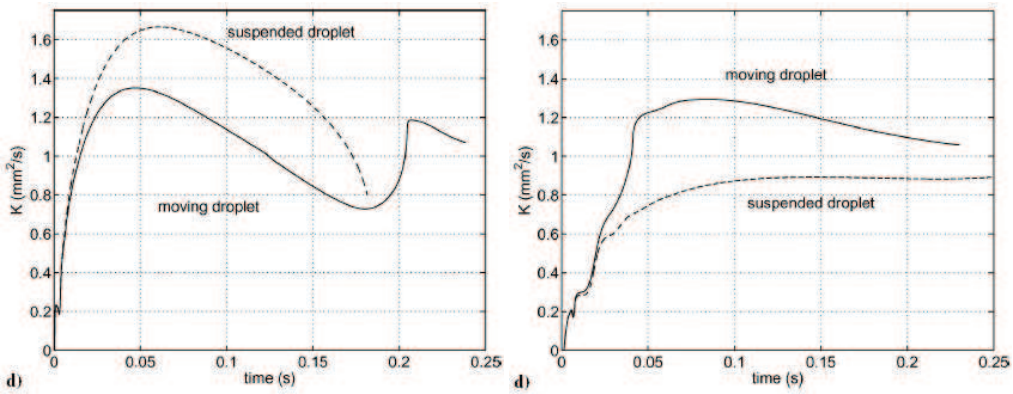

Figure 4: Comparison between the burning features of suspended and moving droplets: Re_0=50 (left), Re_0=8 (right)

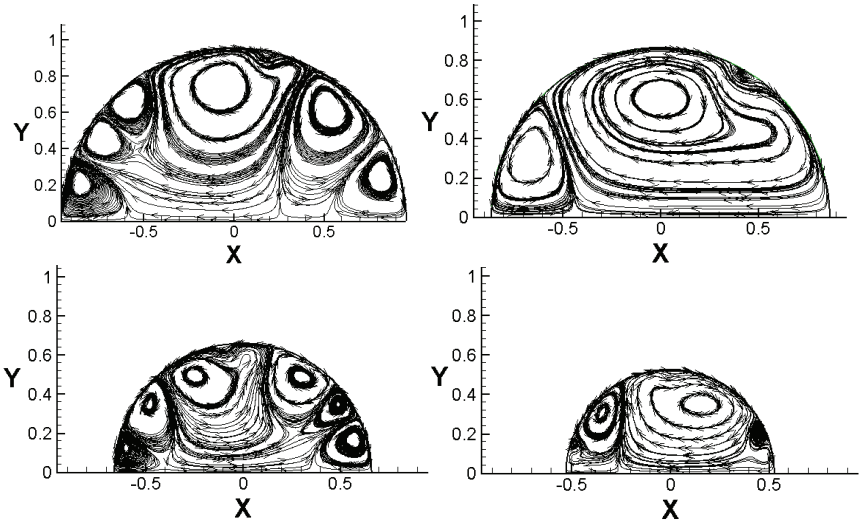

Figure 5: Liquid-phase streamlines at various times during the active combustion phase of methanol droplet in quiescent environment; d_0=430 microns, Re_0=0.01

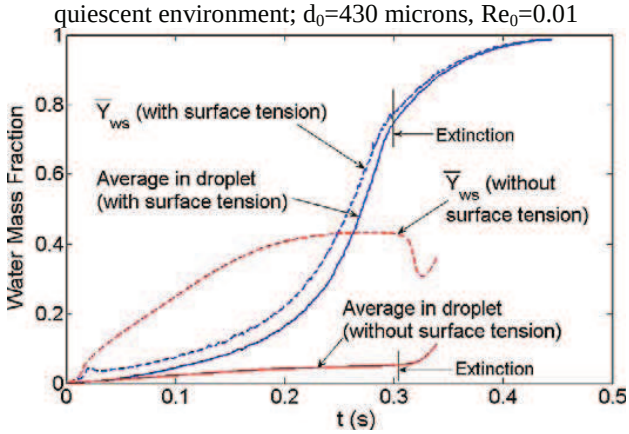

Figure 6: Prediction of water absorption in methanol droplet combustion

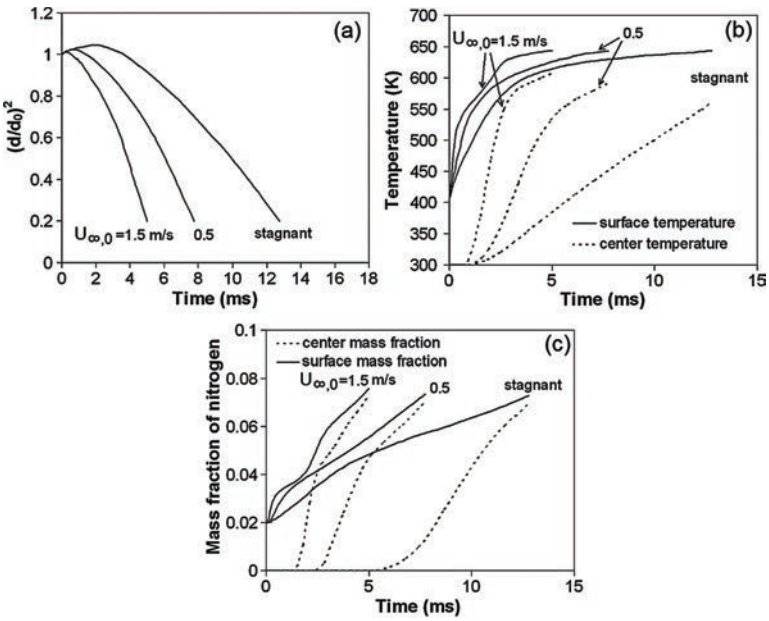

Figure 7: Evaporation of moving n-dodecane droplets in high pressure ($p = 4p_c$; $T=2T_c$) nitrogen environment

Figure 8: Experimental investigation of interference effects between two burning methanol spheres

References

1. Chiu HH, Kin HY, Croke EJ, *Proc. Combust. Inst.* 19 (1982) 97-110.
2. Godsave, G. A. E., *Proc. Combust. Inst.* 4 (1953) 818-830.
3. Spalding, D. B., *Proc. Combust. Inst.* 4 (1953) 847-864.
4. H. Isoda and S. Kumagai, *Proc. Combust. Inst.* 7 (1959) 523-530.
5. S. Kumagai, T. Sakai and S. Okajima, *Proc. Combust. Inst.* 13 (1971) 779-785.
6. S. Okajima and S. Kumagai, *Proc. Combust. Inst.* 15 (1974) 401-407.
7. S. Okajima and S. Kumagai, *Proc. Combust. Inst.* 19 (1982) 1021-1027.
8. H. Hara and S. Kumagai, *Proc. Combust. Inst.* 23 (1990) 1605-1610.
9. H. Hara and S. Kumagai, *Proc. Combust. Inst.* 25 (1994) 423-430.
10. S. Parag and V. Raghavan, *Combustion Flame* 156 (2009) 997-1005
11. V. Raghavan, S. Rajesh, S. Parag and V. Avinash, *Comb. Sci. Tech.* 181 (2009) 877-891.
12. Cho, S. Y., Choi, M. Y. and Dryer, F. L., *Proc. Combust. Inst.* 23 (1990) 1611-1617.
13. Nayagam, V., *Combustion Flame* 157 (2010) 204-205.
14. Hicks, M. C., Nayagam, V. and F. A. Williams, *Combustion Flame* 157 (2010) 1439-1445.
15. Chung, S.S. and Kawaguchi, O. KSME J. (1990) 172–177.
16. Nomura, H., Ujiie, Y., Rath, H.J., Sato, J. and Kono, M., *Proc. Combust. Inst.* 26 (1996) 1267–1273.
17. Ghassemi, H., Baek, S.W. and Khan, Q.S., *Comb. Sci. Tech.* 178 (2006) 1669–1684.
18. Khan, Q.S., Baek, S.W. and Ghassemi, H., *Comb. Sci. Tech.* 179 (2007) 2437–2451.
19. Ghassemi, H., Baek, S.W. and Khan, Q.S., *Comb. Sci. Tech.* 178 (2006) 1031–1053.
20. Law, C. K. and H. K. Law, *Combustion Flame* 29 (1977) 269-275.
21. Chigier, N. A., *Prog. Energy Combust. Sci.* 2 (1977) 97-114.
22. Sirignano, W. A. *Prog. Energy Combust. Sci.* 9 (1983) 291-322.
23. Sirignano, W. A. *Prog. J. Heat Transfer (ASME)* 108 (1986) 633-639.
24. Megaridis, C.M. and Sirignano, W.A., *Proc. Combust. Institute* 23 (1990) 1413–1421.
25. Jia, H. and Gogos, G., *J. Thermophys. Heat Transfer* 6 (1992) 738–745.
26. Jia, H. and Gogos, G., *Int. J. Heat Mass Transfer* 36 (1993) 4419–4431.
27. Marchese, A.J., Dryer, F.L., and Nayagam, V. , *Combustion Flame* 116 (1999) 432-440.
28. Zhu, G.S. and Aggarwal, S.K., *ASME J. Eng. Gas Turbines and Power* (2002) 762–770.
29. Pope, D. N. and G. Gogos, Combustion and Flame 142 (2005) 89–106.
30. Raghavan, V., Gogos, G., Babu, V. and Sundararajan, T., Int. J. Thermal Sciences 46(6) (2007) 589-604.
31. Raghavan, V., Pope, D. N., D. Howard and G. Gogos, Combustion and Flame 145 (2006) 791–801.
32. Zhang, H., Raghavan, V. and Gogos, G., *Int. J. Spray Combust. Dyn.* 1 (2009) 317–338.
33. Balaji, B., V. Raghavan, K. Ramamurthi and G. Gogos, *Physics Fluids* 23 (2011) 063601-1-14.

Inner nozzle flow and Spray Modeling for Compression Ignition Engine Applications

Dr. Sibendu Som
Transportation Technology Research and Development Center
Argonne National Laboratory
Argonne, IL-60439, USA

Introduction

Liquid fuel injection and atomization processes in an internal combustion engine are extremely complex involving transient, two-phase, turbulent flows at high pressures, with a wide range of temporal and spatial scales [1]. Consequently, the experimental, theoretical, and computational studies of these flows have been very challenging. It is also strongly influenced by flow dynamics inside the injector which is in turn governed by fuel properties, geometrical factors, and needle-movement. Inner nozzle flows are characterized by the generation of cavitation and turbulence [2]. Cavitation refers to the formation of bubbles in a liquid flow leading to a two-phase mixture of liquid and vapor/gas, when the local pressure drops below the vapor pressure of the fluid. Turbulence is generated inside the injector due to high pressures and abrupt geometrical changes.

Cavitation and turbulence generated inside an injector are beneficial for the development of fuel spray, since the primary break-up and subsequent atomization of the liquid fuel jet can be enhanced. In addition, cavitation increases the liquid velocity at the nozzle exit due to the reduced exit area available for the liquid. Cavitation patterns extend from their starting point around the nozzle orifice inlet to the exit where they influence the formation of the emerging spray. The improved spray development is believed to lead to more complete combustion process, lower fuel consumption, and reduced particulate emissions. However, cavitation can also decrease the flow efficiency due to its affect on the exiting jet. Imploding cavitation bubbles inside the orifice can cause material erosion thus decreasing the life and performance of the injector.

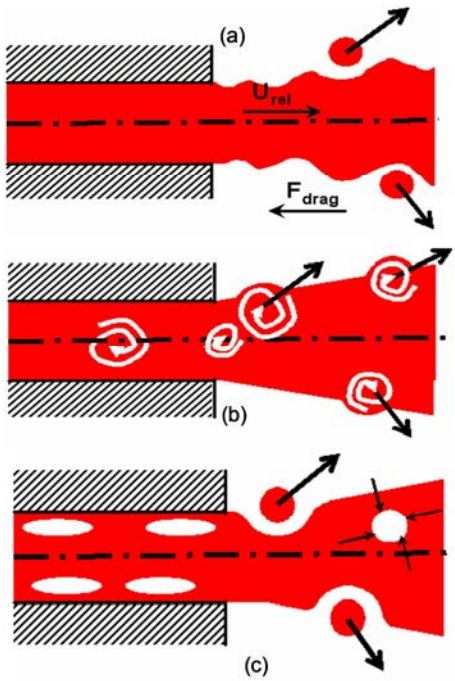

Figure 1: Schematic representation of KH-ACT primary breakup mechanism which is (a) aerodynamically, (b) turbulence, and (c) cavitation induced.

Primary breakup refers to the formation of ligaments and droplets from the ensuing fuel jet and occurs in a highly dense spray region within a short distance from the nozzle exit. They have been modeled assuming that the aerodynamic disturbances [3] play the most dominant role in breakup. Liquid jet breakup is known to be caused by the Kelvin-Helmholtz (KH) [3] and Rayleigh Taylor (RT) instabilities [4] at the interface of the two fluids. Kelvin-Helmholtz instability is a consequence of disturbances of the relative motion or high shear at the interface between the two phases. The Rayleigh-Taylor instability is caused by the inertia of the denser fluid when the system experiences an acceleration transverse to the interface in the direction of the denser fluid. Accordingly, the most commonly used atomization models, namely the KH and RT models are based on a linear

analysis of these instabilities. As discussed above, while the effects of cavitation and turbulence on the primary breakup are well established, most of the atomization models used in CFD-based engine simulations only consider aerodynamic jet breakup based on the KH and RT instabilities. Recent studies by Som et al. [5] identified the scope of improvements in KH and RT (aerodynamic) breakup models. It was observed that due to the absence of cavitation and turbulence effects in the primary breakup model, some experimental trends regarding the effects of nozzle orifice geometry could not be captured. Validation against the x-ray radiography data and optical spray measurements revealed certain short comings of the models. While the macroscopic spray characteristics were generally well predicted by aerodynamic breakup model, spray dispersion or spreading was underpredicted. These inadequacies of aerodynamic breakup models formed the major motivation for the development of Kelvin Helmholtz Aerodynamic Cavitation Turbulence (KH-ACT) induced primary breakup model (cf. Fig. 1).

This extended abstract briefly describes the development, implementation, and validation of the KH-ACT model focused towards compression ignition engine applications [6]. The abstract is organized in the following way: First the physical and computation model section briefly describes the nozzle flow and spray modeling formulations. Some KH-ACT model details and coupling (with the nozzle flow) strategy is also provided (cf. Fig. 2). The results and discussion section begins with a brief validation of the KH-ACT model. The improvements in primary breakup modeling due to the advent of KH-ACT model is demonstrated by simulating diesel and biodiesel nozzle flow and sprays. The future work section briefly mentions the planned extensions to this model for efficient design of compression ignition engine injection systems.

Physical-Computational Model

A mixture-based approach [7] comprising liquid fuel, vapor, and a non-condensable gas is considered for inner nozzle flow modeling. The mixture properties are computed by using the Reynolds-Averaged continuity and momentum equations. In order to account for large pressure gradients, the RNG $k-\in$ turbulence model is incorporated along with the non-equilibrium wall functions. Vapor generation and condensation are calculated by using the simplified solution of the Rayleigh-Plesset equation [8]. Further details of the physical model and governing equations can be found in Som et al. [7,9].

The physical-numerical model for spray simulations is based on an Eulerian-Lagrangian description of the two-phase flow. The gas-phase flow field is described using the Favre-Averaged Navier-Stokes equations in conjunction with the RNG k-ε turbulence model. The length and time scales for the spray are too small to be resolved computationally, necessitating the use of sub-grid scale models to describe the spray physics. The spray is represented by a stochastic system of a discrete number of parcels, which are tracked computationally using a Lagrangian scheme. The two phases are coupled through the mass, momentum, and energy exchange terms, which are present in both the liquid- and gas-phase equations. Further details can be found in Refs. [1,2,6,10]. Figure 1 shows different primary breakup mechanisms modeled [1,2,6]. High relative velocities between the liquid and the gas phase induce aerodynamic shear force at the liquid-gas interphase

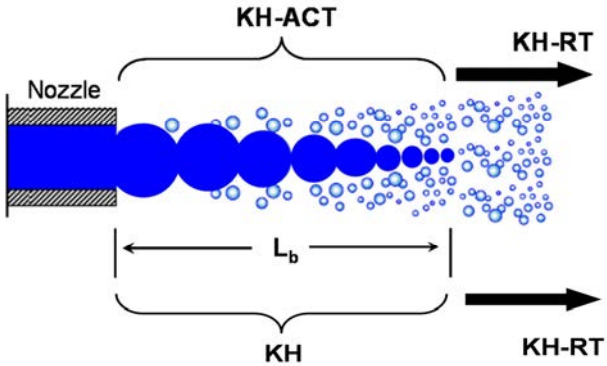

Figure 2: Coupling of the primary breakup models with inner nozzle flow simulations. The breakup length shows regime of operation for primary and secondary breakup models.

causing aerodynamic breakup. Cavitation patterns generated inside the injector nozzle can reach the nozzle exit, and their implosion enhances jet atomization as depicted in Fig. 1c. The underlying assumption is that cavitation patterns are transported to the jet periphery by the turbulence velocity inside the liquid, and either burst at the periphery or collapse before reaching it. The turbulent fluctuations in the jet are responsible for the initial perturbations on the jet surface. These waves grow according to KH instabilities until they breakup from the surface (cf. Fig. 1b).

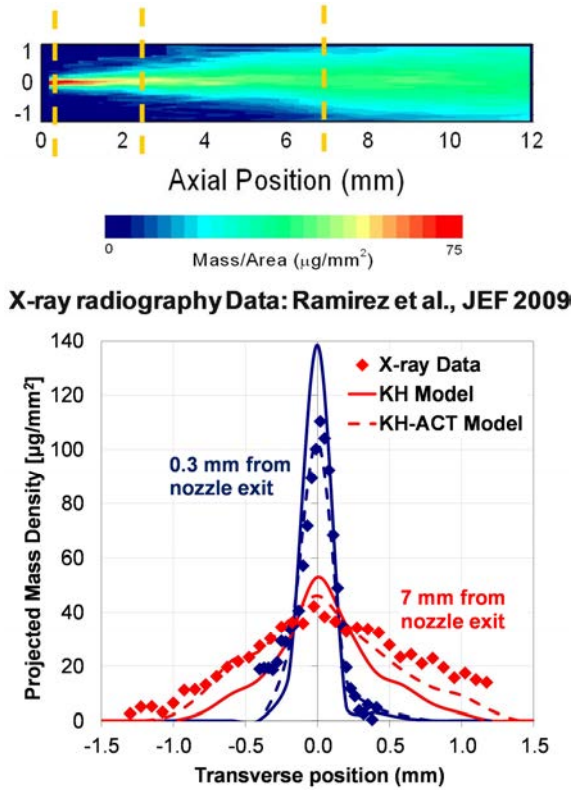

Figure 3: Comparison of KH-ACT against KH model vs. experimental data [12] at different axial locations from the injector.

Results

Optical methods have generally been used to characterize the atomization and vaporization processes in diesel engines and to validate the spray models. These methods have intrinsic limitations in the near nozzle region, where the light is scattered by the dense spray. In recent years, new techniques, such as x-ray radiography [11,12] have been developed at Argonne National Laboratory, which are capable of characterizing flows in the primary breakup region. Since the main interaction between the spray and x-rays is absorption, rather than scattering, the technique can provide temporally and spatially resolved fuel mass distribution in the near nozzle region, permitting analysis that cannot be performed using optical spray data. Figure 3 presents x-ray data [12] and comparison between the standard KH model and the new primary breakup KH-ACT model in terms of transverse distributions of projected density (i.e., fuel dispersion). The projected mass density profiles exhibit Gaussian distribution for both the measurements and simulations. In general, it is seen that the KH model over-predicts mass density and underpredicts spray dispersion. With the KH-ACT model, results improve both in terms of peak values and spray dispersion. Since the new model predicts faster breakup than the standard model, more child droplets are produced which spread more thus improving spray dispersion. In general, it is seen that the KH-ACT model agrees closer to experimental data. The KH-ACT model is then implemented for capturing the nozzle flow and spray characteristics of biodiesel fuel.

The possibility of using pure biodiesel in a diesel engine is a lucrative option. The influence of differences in properties on inner nozzle flow and spray behavior needs to be established in order to achieve optimal use of biodiesel. Figure 4 presents the vapor volume fraction contours for diesel and biodiesel which indicate that vapor generation occurs at the orifice inlet for both the fuels. For

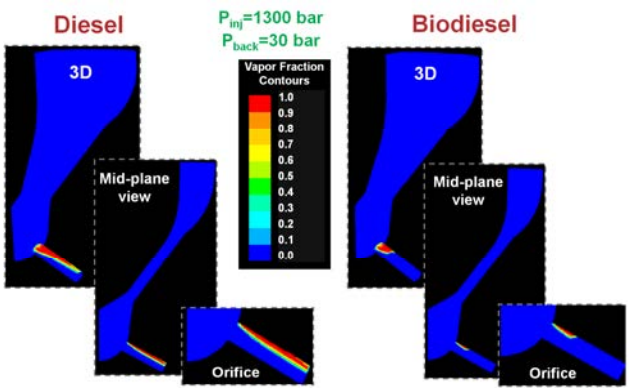

Figure 4: Vapor fraction contours for diesel and biodiesel inside the injector, at the mid-plane and orifice. The simulations were performed at full needle open position with P_{inj} = 1300 bar and P_{back} = 30 bar.

diesel, these cavitation contours, generated at the upper side of the orifice, reach the orifice exit. In contrast, for biodiesel, the cavitation contours only extend a few microns into the orifice and do not reach the injector exit. The other two views also indicate that the amount of cavitation is significantly reduced for biodiesel compared to diesel. This can primarily be attributed to the low vapor pressure and high viscosity of biodiesel compared with that of diesel [6]. Since cavitation plays a significant role in primary breakup, the atomization and spray behavior of these fuels is expected to be different.

Figure 5 presents the predicted and measured [13] liquid lengths versus ambient temperature for diesel and biodiesel fuels. As the ambient temperature is increased, the liquid length decreases due to the enhanced vaporization rate. The liquid length for biodiesel is noticeably higher than that for diesel. This could have important implications for running the same diesel engine with biodiesel, since the use of biodiesel may require changes in the piston bowl design or in the injection and/or ambient conditions in order to ensure similar liquid lengths for the two fuels. The liquid length is higher for biodiesel due to slower breakup resulting from reduced cavitation and turbulence at the nozzle exit, higher fuel density, and higher heat of vaporization compared to diesel fuel.

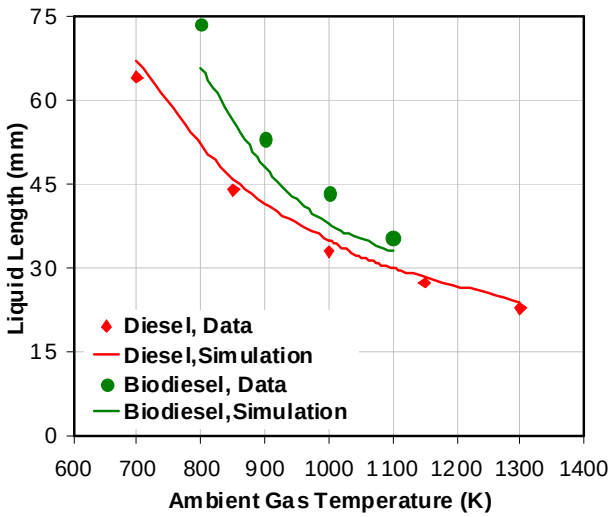

Figure 5: Measured [13] and predicted liquid lengths versus ambient gas temperature.

Future studies will focus on dynamic-coupling of nozzle flow and spray processes. Current set of simulations were performed with quasi-dynamic coupling i.e., nozzle flow results influenced the spray-combustion development only. Dynamic-coupling will enable a two-way coupling thus changes in combustion characteristics will influence the development of flow inside the injector nozzle and vice-versa. This will eventually results in a predictive tool for designing compression ignition engines for engine manufacturers.

References

1. S. Som, S.K. Aggarwal, *Combustion and Flame* 157: 1179-1193, 2010.
2. S. Som, A.I. Ramirez, D.E. Longman, S.K. Aggarwal, *Fuel* 90: 1267-1276, 2011.
3. R.D. Reitz, *Atomization and Spray Technology* 3: 309-337, 1987.
4. M.A. Patterson, R.D. Reitz, *SAE Paper No*. 980131, 1998.
5. S. Som, S.K. Aggarwal, *Atomization and Sprays* 19(9): 885-903, 2009.
6. S. Som, D.E. Longman, A.I. Ramirez, S.K. Aggarwal, *Fuel* 89: 4014-4024, 2010.
7. S. Som, et al., *Journal of Engineering for Gas Turbine and Power* 132: 1-1 to 1-12, 2009.
8. E.C. Brennen, Cavitation and bubble dynamics. Oxford University Press; 1995.
9. S. Som, PhD thesis, University of Illinois at Chicago; 2009.
10. S. Som, D.E. Longman, *Energy and Fuels* 25: 1373-1386, 2011.
11. J. Wang, *Journal of Synchrotron Radiation* 12: 197-207, 2005.
12. A.I. Ramirez, S. Som, S.K. Aggarwal, et al., *Experiments in Fluids* 47: 119-134, 2009.
13. B.S. Higgins, C.J. Mueller, D.L. Siebers, *SAE Paper No*. 1999-01-0519, 1999.

ABSTRACT: INTERNAL COMBUSTION ENGINE SPRAYS

John Abraham
School of Mechanical Engineering, Purdue University
Indiana 47907-2088, USA

Modern internal combustion engines running on liquid fuels employ injection of the liquid as the primary means of supplying the fuel to the engine. In spark-ignition (SI) engines, this may be achieved through port fuel injection (PFI), throttle-body injection (TBI), or direct-injection (DI) into the combustion chamber. In compression-ignition (CI) engines, injection may be into the port or, more likely, early during the intake cycle, as in homogeneous-charge compression-ignition (HCCI) engines, or into the chamber late in the compression cycle as in conventional diesel engines. Indirect injection into a secondary chamber has been employed in the past but is not considered an attractive option in modern engines. Injection pressures can vary from 2-3 bar in PFI engines to 2000 bar or higher in conventional direct-injection diesel engines. Injection systems may be electronically controlled as in PFI and common-rail systems or mechanically controlled.

At the lower end of injection pressures (2-3 bar), e.g. in PFI and TBI engines, the injection momentum is relatively small and injection is employed primarily as a means of fuel delivery and not to induce fuel/air mixing. The air motion is responsible for the mixing. Injection is usually into air which is at or below atmospheric pressure. Temperature of the air can vary from ambient during cold start to as high as 350 K in warm operating engines. Drop sizes are generally large (100 -200 μm SMD) and impingement with surfaces (for example, the backside of the intake valve and port runners) is common. During cold-start, this impingement can lead to difficulty in controlling the fuel/air mixture composition and to high exhaust emissions. Direct-injection into the cylinder at lower injection pressures during the intake and compression strokes are with higher injection momentum relative to those in PFI engines. They induce some level of mixing which is then enhanced by in-cylinder air motion. Interaction with piston and cylinder surfaces is common. In early-injection compression-ignition engines, this interaction is not desired. It can generate fuel distribution in the chamber that may lead to lower efficiencies and high levels of UHC and CO emissions. If the objective is to generate a homogeneous charge, interaction with the surface can lead to compositional stratification which may not be desirable. In direct-injection spark-ignition (DISI) engines, the interaction with walls can be exploited, as discussed below.

Typical injection pressures in DISI engines are lower than 200 bar. Injection may be through single or multiple holes. Injection may take place into the chamber when the pressure is close to atmospheric (during intake stroke) or 20-30 bar as when injection is closer to top-dead center. When the fuel is injected during the intake stroke, at high loads, the engine operates like a homogenous-charge engine. At lighter loads, the fuel is injected during the compression stroke and the mixture is overall lean and stratified. The vaporization of the fuel within the cylinder results in a decrease in mixture temperature. This reduces the tendency to knock – hence, DISI engines can run at higher compression ratios than PFI engines. It is important to inject the fuel so that the fuel is accessible at the spark-plug during ignition. Various strategies are adopted to achieve this. Figure 1 shows

a schematic of three of the more common approaches: (a) wall-guided spray systems in which the spray is guided by the geometry of the wall towards the spark-plug, (b) air-guided spray system in which the air-motion, e.g. tumble, swirl, squish, within the chamber is exploited to advect the spray to the spark-plug, and (c) spray-guided systems in which the spray orientation is such that the spray, or one spray in a multi-hole nozzle, is directed towards the vicinity of the spark-plug.

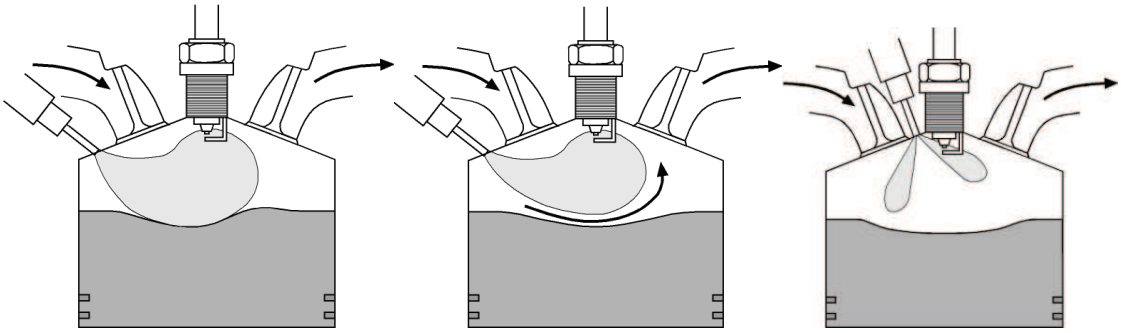

(a) Wall-guided. (b) Air-guided. (c) Spray-guided.

Figure 1. DISI combustion chamber designs.

Several types of injectors have been investigated for delivering the fuel in DISI engines. These include pressure-swirl atomizers, air-assist atomizers, and single-hole and multi-hole injectors delivering solid-cone sprays. *In DISI engines and variations of the HCCI engine concept, the development of improved engines can be accelerated by improved understanding of atomization and spray structure and interaction of the spray with the wall. This is especially important when employing multidimensional spray models to aid in the development process (Abraham, 2011).*

Injection in DI diesel engines is at high pressure, e.g. 2000 bar or higher, into a chamber where the temperature is in the range of 800-1200 K and the pressure is 50 to 100 bar prior to combustion. Solid-cone sprays are the norm in diesel engines. The liquid is atomized to drops whose SMD lie in the range of 1-10 microns. *Measurements in the atomizing region of the spray are difficult and so drop sizes in this region have to be deduced through theoretical arguments from measurements at the periphery of the spray or from measurements in the dilute spray at several hundred diameters downstream of the orifice.* This deduction often involves the use of multidimensional models in which drop sizes are estimated from models in the atomization region and then matched to those measured downstream. This is a difficult task prone to errors because of numerical inaccuracies in such models, and inadequate understanding of atomization and drop-interaction submodels. *The atomization mechanism in diesel sprays is not well understood. From a practical point of view, this lack of understanding does not appear to be of much consequence in high-temperature high-pressure operation for reasons explained in the next paragraph, but under cold-start conditions, it can be consequential. From the point of view of spray modeling, the lack of understanding of atomization and the near-field of the dense sprays poses difficulties in specifying initial and boundary conditions with any certainty. As a result, several atomization models (for example, Bracco, 1985; Reitz, 1987; O'Rourke and Amsden, 1987; Andrews, 1993) with tunable*

constants have been proposed and the constants may be adjusted to achieve desired results. These results are often highly sensitive to numerical resolution when employing Lagrangian models for the liquid phase (Abraham, 1997; Iyer and Abraham, 1997; Aneja and Abraham, 1998), lending another dimension of uncertainty to modeling sprays. Grid independent results can be obtained with Eulerian models but they are computationally intensive (Iyer et al., 2003; Iyer and Abraham, 2005).

The drops generated through atomization transfer momentum to the chamber gas, entrain the gas, and undergo rapid vaporization. The jet penetrates as a vapor jet beyond the maximum length to which the drops penetrate, i.e. the liquid-phase length – this length can extend up to 2-3 cm (Naber and Siebers, 1996; Siebers, 1998; Siebers, 1999; Iyer *et al*., 2000; Abraham and Pickett, 2010; Bajaj *et al*., 2011). In fact, this vaporization is entrainment controlled. In other words, the drop sizes are sufficiently small that if hot air is available, they vaporize rapidly. The important point to note about diesel sprays is that because the liquid phase penetrates only to a short distance relative to the overall vapor penetration, precise details about atomization and drop size distribution are not required to characterize the overall features of the jet. The near-field of the spray where the liquid-phase length reaches its maximum length achieves a statistical steady-state in a relatively short period of time (0.1-0.3 ms). The quasi-steady structure downstream of the maximum liquid-phase length has been fairly well-characterized through extensive experimental studies (Naber and Siebers, 1996; Siebers, 1998; Huang, 2000). In fact, vapor jets can characterize the diesel jet well (Abraham, 1997; Iyer and Abraham, 1997; Abraham and Pickett, 2010; Bajaj *et al*., 2012). The suggestion has recently been made that since the chamber pressure and temperature conditions may be supercritical with respect to the liquid fuel, liquid drops may not exist at all (Dahms *et al*., 2011). Figure 2 shows a schematic of the structure of high-pressure diesel sprays. The spray angle in the near-field of the jet is generally smaller than in the far-field (Reitz and Bracco, 1979; Bracco, 1985; Wu et al., 1983; Naber and Siebers, 1996). In the far-field these angles tend to approach that of the turbulent gas jet. Identified in Figure 2 are a possible (conflicting views exist on this) intact liquid core (L_1), the liquid-phase penetration length (L_2), a quasi-steady region of the jet (L_3), and the transient head-vortex (L_4).

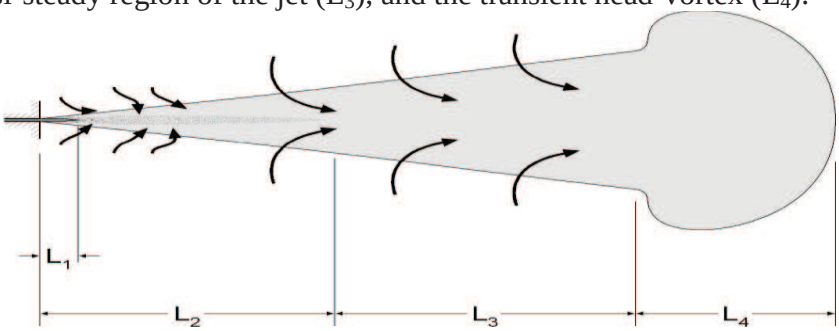

Figure 2: Schematic of a full-cone diesel spray

In the case of engine sprays, where the injection is intermittent, it is important to consider the transient nature of the spray in trying to understand mixing. In figure 2, this transient behavior is predominant in the head-vortex. Note, however, that for a period of time after start of injection the part of the spray where transient mixing and development are important constitutes a significant fraction of the spray. When injection ends, the

behavior of the jets is again influenced strongly by transients. In fact, these transients can influence the mixing behavior in diesel engines and impact pollutant emissions (Musculus *et al*., 2007; Musculus, 2011). With the increasing use of common-rail injectors to deliver the fuel, there is the opportunity of using multiple injections during one engine cycle. Pulse injection, or the special case where two pulses are employed – split injection, has been shown to result in decreased emissions of soot and nitrogen oxides.

References

1. Abraham, J., What is adequate resolution in the numerical computations of transient jets? SAE Paper 970051 (1997).
2. Abraham, J. and Pickett, L.M., Computed and measured fuel vapor distribution in a diesel spray, *Atomization and Sprays*, 20(3):241-250 (2010).
3. Abraham, J., Computational study of charge stratification in early-injection SCCI engines under light-load conditions, *International Journal of Automotive Technology*, 12(5):721-732 (2011).
4. Andrews, M.J., The large-scale fragmentation of the intact liquid core of a spray jet, *Atomization and Sprays*, 3:29-54 (1993).
5. Aneja, R. and Abraham, J., How far does the liquid penetrate in a diesel engine: computed results vs measurements? *Combustion Science and Technology*, 138:233-255 (1998).
6. Bajaj, C., Pickett, L.M., and Abraham, J. Vaporization effects on transient diesel spray structure, *Atomization and Sprays*, to appear (2012).
7. Bracco, F.V., Modeling of engine sprays, SAE Paper 850394 (1985).
8. Dahms, R.N., Pickett, L.M., and Oefelein, J.C., A dense fluid approximation for the simulation of diesel injection process, ILASS-Americas 23rd Annual Conference, Ventura, CA, May 2011.
9. Huang, Y., *Experimental studies of impulsively started liquid-into-gas and gas-into-gas turbulent jets*, Ph.D. Thesis, Princeton University, Princeton, NJ (2000).
10. Iyer, V. and Abraham, J., Penetration and dispersion of transient gas jets and sprays, *Combustion Science and Technology*, 130:315-335 (1997).
11. Iyer, V. and Abraham, J., An evaluation of a two-fluid Eulerian-liquid Eulerian-gas model for diesel sprays, *ASME Journal of Fluids Engineering*, 125:660-669 (2003).
12. Iyer, V., Post, S.L., and Abraham, J., Is the liquid penetration in diesel sprays mixing controlled? *Proceedings of the Combustion Institute*, 28:1111-1118 (2000).
13. Iyer, V. and Abraham, J., Two-fluid modeling of spray penetration and dispersion under diesel engine conditions, *Atomization and Sprays*, 15(3):249-269 (2005).
14. Musculus, M.P.B., Lachaux, T., Pickett, L.M., and Idicheria, C.A., End-of-injection over-mixing and unburned hydrocarbon emissions in low-temperature-combustion diesel engines, SAE Paper 2007-01-0907 (2007).
15. Musculus, M., Entrainment waves in decelerating transient turbulent jets, *Journal of Fluid Mechanics*, 638:117-140 (2009).
16. Naber, J.D. and Siebers, D.L., Effects of gas density and vaporization on penetration and dispersion of diesel sprays, SAE Paper 960034 (1996).
17. O'Rourke, P.J. and Amsden, A.A., The TAB method for numerical calculation of spray droplet breakup, SAE Paper 872089 (1987).
18. Reitz, R.D., Mechanisms of atomization processes in high-pressure vaporizing sprays, *Atomization and Spray Technology*, 3:309-337 (1987).
19. Reitz, R.D. and Bracco, F.V., On the dependence of spray angle and other spray parameters on nozzle design and operating conditions, SAE Paper 790494 (1979).
20. Siebers, D.L., Liquid-phase fuel penetration in diesel sprays, SAE Paper 980809 (1998).
21. Siebers, D.L., Scaling liquid-phase fuel penetration in diesel sprays based on mixing-limited vaporization, SAE Paper 1999-01-0528 (1999).
22. Wu, K.-J., Su, C.-C., Steinberger, R.L., Santavicca, D.A., and Bracco, F.V., Measurements of the spray angle of atomizing jets, *ASME Journal of Fluids Engineering*, 105:406-413 (1983).

Investigations of the air and liquid velocity fields in a prefilming airblast atomizer

P SURIYANARAYANAN, N S VIKRAMADITYA AND L VENKATAKRISHNAN

Council for Scientific and Industrial Research
National Aerospace Laboratories Bangalore
Experimental Aerodynamics Division

1. Introduction

Atomization in a liquid fuelled injection system is of more importance in many industrial combustion processes especially in aircraft engines due to increasingly stricter norms in emission levels. The interest is partly due to improving fuel efficiency and one many fuel atomization methods commonly used in air breathing aircraft engines is by using a blast of air[1]. Several studies have been conducted to characterize prefilming airblast atomizers and the effect of various operating parameters on the spray behavior. Characterization of the spray helps in better understanding of the mixing process and in reducing the emission levels.

Lefebrve and Miller[2] proposed a pre-filming concept for airblast atomization. They showed that the smaller droplets are formed by maximizing physical contact between the air and the liquid being injected. Smaller sized droplet formation helps in increasing the surface area thereby reducing the liquid vaporization time, hence providing better fuel efficiency. Rizk and Lefebrve[3] studied the influence of the air velocity and liquid properties on the drop size distribution in an airblast atomizer. Han et al.[4] investigated the effects of the fuel nozzle displacement on the spray characteristics and found that there was significant variation in cone angle, droplet number density and recirculation pattern of the spray. They showed that flows with high degree of swirl are characterized by the presence of a cetral toroidal recirculation zone (CTRZ) in addition to high turbulence and combustion intensity. Gurubaran et.al[5] who studied prefilming atomizers, concluded that the dispersion of the liquid phase moves downstream with increase in liquid flow rate and that the SMD decreases with increase in air-liquid mass flow ratio (ALR). Gurubaran et.al [6] who carried out 2D PIV and PDPA studies showed that droplets of smaller SMD cluster around the core while the larger droplets spread towards the periphery.

Zheng et.al[7] investigated the structure of a contra-swirling, prefilming atomizer and concluded that the effects of ambient pressure on SMD distribution is small as it is highly dependent on the liquid sheet break up mechanism. Carvalho & Nestor [8] showed that increasing the velocity of the inner air causes instability and produces smaller break-up lengths and better atomization. In the presence of the swirl, the outer atomising air leads to a faster decrease of the break-up length and is highly effective in obtaining a high quality atomization. Rosa et. al [9] studied the influence of swirl on the droplet behavior and velocity and turbulent fields. They show that spatial distribution of size, velocity and particle number density is a strong function of swirl. Investigations on the effect of swirl in a simplified airblast atomizer were carried out by Lavergne et.al [10] who concluded that the SMD and velocity distribution are greatly affected by the swirl. LDV measurements to quantify the effect on swirl on turbulence quantities were carried out Mocikat et al[11]. They concluded that swirl (up to a swirl number of 0.5) does not significantly affect the turbulence quantities in a steady case while for an unsteady case it increases the turbulence quantities by order of magnitude. Miller et al [12] showed the control of swirl in a modified GE CFM56 gas turbine engine fuel atomizer through coanda blowing. This type of blowing increased the uniformity of the spray spread rate and improved flame holding.

Feras et.al[13] studied the influence of chamber pressure, liquid flow rate and gaseous phase flow rate on the spray fluctuating frequency. And showed that the dynamics of the flow through the atomizer is dependent on the Strouhal number and is valid for a wide range of ambient pressure and airflow rates. Zhu et al [14] studied a combustor coupled with spray atomizer during unsteady combustion process. And showed that the process undergoes self-excited oscillations and is a strong function of atomization which itself depends on air flow rate.

While earlier studies have made use of multiple diagnostic techniques like PSPA, LDV and 2D PIV, there has been no effort to document the three component velocity field of the air alone and air-liquid flows through such atomizers. The advantage of making such stereo PIV measurements is the capability to capture the *uv*, *uw* and *vw* stresses which can shed light on the air-liquid turbulent mixing in the atomizer. Further, most studies have been at high ALRs due to the challenge of making measurements at large liquid flow rates. In the present study, Stereo PIV has been used to characterize the flow behavior of a prefilming airblast atomizer operating at an ALR of unity and a swirl

number of 1.09 in order to quantify the effect of the swirling air flow on the liquid field. The PIV measurements are carried out at several axial locations and validated against LDV data. Limited PDPA measurements are made to obtain the radial variation of droplet sizes.

2. Experimental procedure

Figure 1 shows the schematic of the prefilming airblast atomizer used in the present study. The atomizer has a central pintle with six wire-cut grooves and incorporates 12 vanes set in a frontal adaptor at an angle of 50° to the freestream. This yields a swirl number of 1.09. The design of the atomizer is the same as was used in Gurubaran et. al [5, 6].Water was used as the liquid medium in the present study. It was required to maintain an air-liquid mass ratio of unity. The corresponding liquid flow rate was 3.5l/min.

2.1 Laser Doppler Velocimetry setup

A 2-component TSI LDV system was used with an Isel XYZ traverse system to measure the 2D velocity field at an axial location of 45 mm from the atomizer exit. An FSA 4000-P signal processor and FLOWSIZER™ software were used to analyze the data. Data rates between 1 and 0.8 kHz were achieved. Flow measurement area was 150 x 150 mm at 5 mm interval. 15,000 data sample were captured in the coincidence mode.

2.2 Phase Doppler Particle Analyzer setup

The 1-D PDPA system was used with an Isel XYZ traverse system to measure the radial variation of particle diameter at axial locations in steps of 5mm. The focal length of the receiving optics is 500 mm and with a slit aperture of 150 microns. The measurements were carried out in the refraction mode scattering mechanism with an off-axis angle of 60° for the receiver. Nukiyama-Tanasawa routine was used for diameter fitting and 15,000 samples were captured in the coincidence mode.

2.3 PIV Setup

The flow-field with water droplets was illuminated by a Spectra Physics dual cavity Nd:YAG, PIV 400 laser. The flow is imaged using 2 IDT MotionPro Y5 PIV cameras

having a sensor resolution of 2336(H) x 1728(V) pixels using Nikon 85 mm tilt/shift schiemflug lenses. The air is seeded using a modified Wright nebulizer which generates fog particles having a size of 0.5 microns. For the air-liquid field, it is to be noted that the velocity field measured is that of the water and not that of the air flow. It was not possible to simultaneously measure the air flow field velocity due to the signal from the water being much more than that of any seeding in the air. The PIV acquisition and processing was carried out using the *ProVISION XS™* software from IDT, USA. For each case 6000 images were acquired and processed to yield 3000 velocity fields. This ensured statistically significant numbers for the mean and fluctuating quantities.

The optimal interrogation size was arrived at by means of using the adaptive sizing method provided in the processing software. This turned out to be 24 x 24 pixels with overlap of 50%, which corresponds to 2.5mm x 2.5mm in physical resolution. The flow was imaged up to an axial distance of 85 mm.

3. Results and discussion

3.1 Droplet size distributions

Figure 2 shows the radial variation of droplet sizes at seven axial locations between 15 mm to 85 mm from the exit. The figure shows that in the central region, the droplet sizes are quite large (up to 100 microns) near the exit and there is not much radial variation of sizes. With increasing downstream distance the droplet sizes in the central core increase to a maximum of 130 microns before reducing monotonically to a minimum of 20 microns at the last station of 85mm. This is in contrast to the monotonic decrease observed by Gurubaran et al [5] who measured radial profiles of droplet diameter between 12 mm and 50 mm from the exit at ALR of 5.43 and 7.0. The existance of SMD maxima in the central core till 35 mm implies that at the current ALR of unity, the centrifugal force caused by the swirl is not large enough to carry the bigger droplets to the periphery.

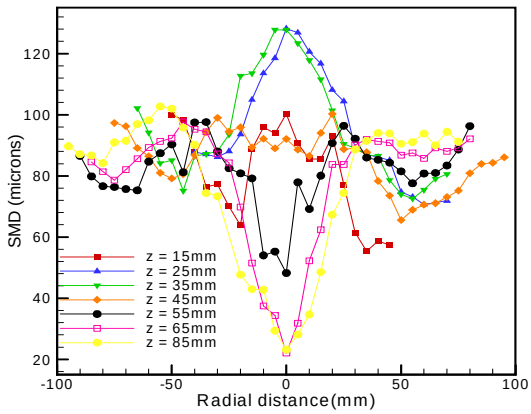

Figure 2. Radial variation of droplet diameter with downstream distance.

3.2 Mean and turbulent Velocity fields from LDV data

LDV measurements were made on both air-alone and air-water flow fields. The mean streamwise velocity field for the the air-alone case at an axial distance of 45mm is presented as a contour plot in Figure 3a and the air-water field in Figure 3b. The contour

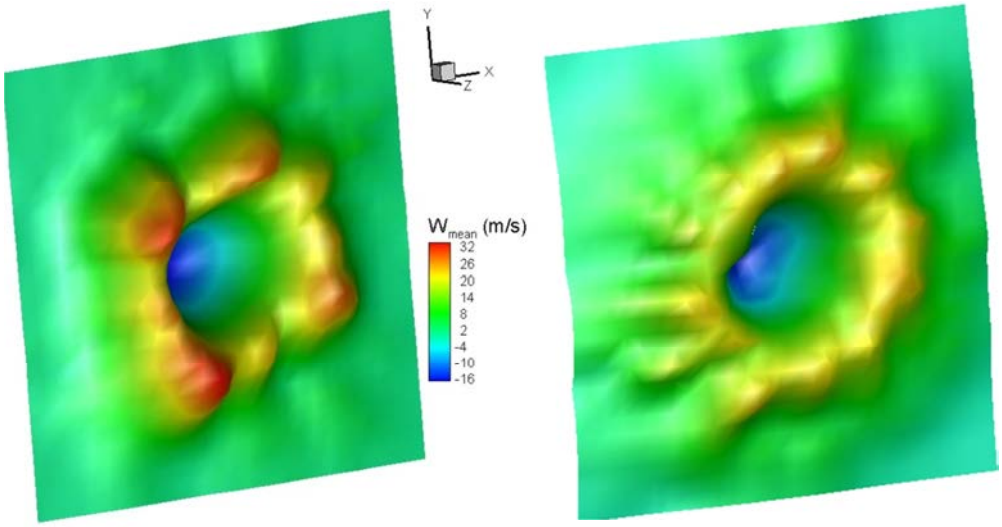

Figure 3. Streamwise mean velocity field at 45mm from exit for (a) air-alone and (b) air-water cases.

is presented as raised heights (equivalent to the streamwise velocity) above a plane in order to have a better appreciation of the velocity field. The data immediately show that the mean field is not symmetric and has significant circumferential variation of streamwise velocity towards the periphery. The velocity in the central core is strongly negative due to the strong toroidal recirculation produced by the swirl. Further the air-water field as expected has lower magnitudes of positive and negative velocity. This can be attributed to two reasons. Firstly, the breakup of the liquid sheet absorbs some of the energy of the air flow. Secondly, unlike the sub-micron sized seeding of the air flow, the droplets are large (> 20μm) and hence may not follow the flow with fidelity. Larger sized droplets however, were filtered out of the LDV data by using an appropriate cut-off for the pedestal.

Figures 4a,b present the distribution of streamwise turbulence intensity at the same axial location. The streamwise turbulent velocities have been non-diemnsionalized using the maximum streamwise velocity (which is that of air) of 33m/s. The plots show that the turbulence intensity is significantly reduced in the air-water case and a lesser asymmetry seen in its distribution.

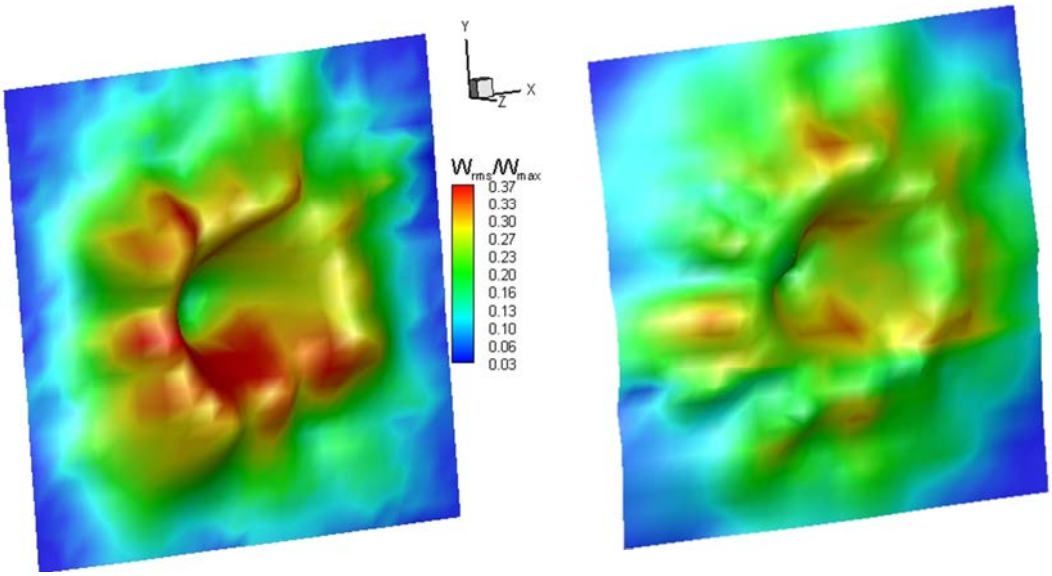

Figure 4. Streamwise turbulence field at 45mm from exit for (a) air-alone and (b) air-water cases.

3.3 Velocity and turbulence fields from PIV data

Figure 5a,b present the data from PIV for the same operating conditions and locations as

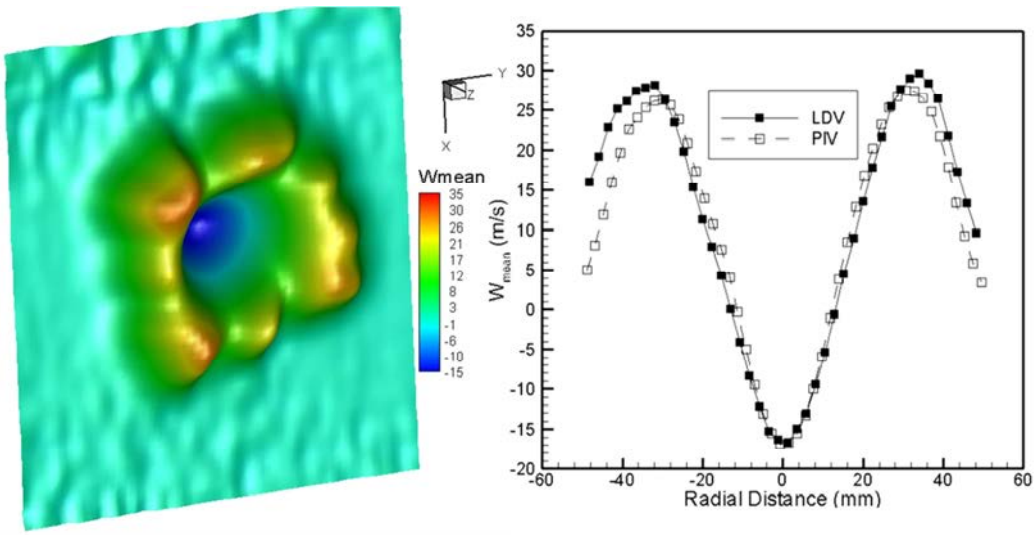

Figure 3. Streamwise mean velocity field at 45mm from exit for (a) air-alone and (b) comparison against LDV data.

for the LDV data. Figures 3a, b show the coparisons between the two measurements. Figure 3b which is the comparison of mean velocity along a particular diamter, shows that there is quite a good agreement in the mean velocities.

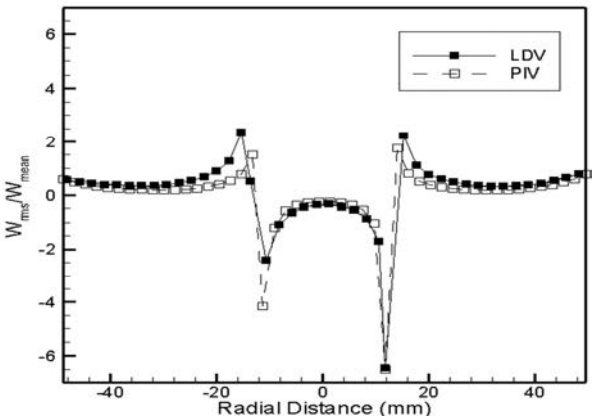

Figure 3c presents the comparison of normalized turbulent streamwise velocities as measured using LDV and PIV. The close agreement of the turbulent velocities show that the stereo PIV data can be used for interpreting the turbulence field of the atomizer flow. Having validated the stereo PIV measuremnts, the air and air-liquid flow field at several axial stations will subsequently be mapped.

4. Summary

The air-liquid velocity field have been the subject of several earlier investigations. However, most studies have been carried out with either single point measurements like LDV or in 2-D planes using PIV. Usage of stereo PIV for mapping the three-component field enables the calculation of turbulent stresses of all three components which would help in better understanding of liquid sheet breakup and atomization.

5. Acknowledgement

The authors acknowledge the Gas Turbine Research Establishment, Bangalore for support of this work through project GTRE/MMG/KVIP/9152/04/LPO/A/05.

References

1. Liu, Huimin, “Science and Engineering of Droplets, Fundamentals and Applications”, Noyes Publications, Park Ridge, New Jersey, U.S.A., William Andrew Publishing, LLC, Norwich, New York, U.S.A.
2. Lefebrve, A.H., and Miller, D., ‘The development of an Air Blast Atomizer for Gas Turbine Apllication’, COAReport- Aero-193,College of Aeronautics, Cranfield, England, 1996.
3. Rizk, N. K., and Lefebrve, A. H., “ Influence of Air and Liquid Properties on Airblast Atomization,” ASME J. Eng. Gas Turbine Power, 102, pp. 706-710, 1980.
4. Han, Y. M., Seol, W. S., Lee, D. S., Yagodkin, V, I., and Jeungm, I. S., “Effects of Fuel Nozzle Displacement on Pre-Fliming Airblast Atomization,” ASME J. Eng. Gas Turbine Power, 123, pp. 33-40, 2001.
5. Gurubaran, K. R., Sujith, R.I, and Chakravarthy, S.R., “Characterization of a Prefilming Airblast Atomizer in a Strong Swirl Flowfield”, Journal of Propulsion and Power, Vol. 24, No. 5, 2008.
6. Gurubaran, K. R., Sujith, R.I, and Chakravarthy, S.R., “Flow field measurements of a prefilming airblast atomizer”, AIAA 2005-4148, 41st AIAA/ASME/SAE/ASEE Joint Propulsion Conference & Exhibit 10-13 July 2005, Tucson, Arizona.
7. Zheng, Q.P., Jasuja, A.K., Lefebvre, A. H., “Structure of Airblast Sprays Under High Ambient Pressure Conditions”, Journal of Engineering for Gas Turbines and Power, Vol. 119, JULY 1997.
8. Carvalho, I.S., Heitor, M.V., "Liquid film break-up in a model of a prefilming airblast nozzle." Experiments in Fluids, Vol. 24, 1998.
9. Rosa, A, B., de, la, Bachalo, W.D., Rudolf, R.C., "Spray Characterisation and Turbulence Properties in an Isothermal spray with swirl." Journal of Engineering for Gas Turbines and Power, Vol. 112, 1990.

10. Lavergne, G., P., Trichet; P., Hebrard; Y., Biscos, "Liquid sheet disintegration and atomisation process on a simplified airblast atomiser." Journal of Engineering for Gas Turbines and Power, Vol. 115, 1993.
11. Mocikat, H., T. Gurtler, D. Petrak, H. Herwig, “LDV measurements in complex swirling flows, their physics and a database for CFD evaluations”, Experiment in Fluids, Vol. 46, 2009.
12. Miller, M.F., McManus, K.R., and Allen, M.G., “An Aerodynamic Control System for Modifying Fuel Spray Distributions”, AIAA 2000-0192.
13. Feras, Z., Batarseh; Markus, Gnirb; Ilia, V., Roisman; Cameron, Tropea, "Fluctuations of a spray generated by an airblast atomiser." Experiments in Fluids, Vol. 46, 2009.
14. Zhu, M., Dowling, A.P., Bray, K.N.C., “Self-Excited Oscillations in Combustors with Spray Atomizers”, Journal of Engineering for Gas Turbines and Power, Vol. 123, 2001.

Liquid Atomization in Gas-Centered Swirl Coaxial Atomizers

D. Sivakumar
Assistant Professor, Department of Aerospace Engineering
Indian Institute of Science (IISc), Bangalore 560012, India
E-mail: dskumar@aero.iisc.ernet.in

Gas-centered swirl coaxial atomizers have been employed in liquid propellant rocket engines operating under a staged combustion cycle with an oxygen rich pre-burner [1,2]. The atomizer discharges an annular swirling liquid sheet and a central gas jet from the coaxially arranged outer and inner orifices respectively. The central gas jet is analogous to the gaseous oxygen (GOX) and the annular swirling liquid sheet to the liquid kerosene (RP-1). Knowledge of the liquid sheet atomization and spray dynamics are essential for the design and optimization of these atomizers. Gas-centered swirl atomizers have been studied under two major configurations: premixing type and coaxial type. In the premixing type, the liquid flows over the inner wall of the gaseous orifice by passing it through tangential ports and a mixing process between the liquid and the gas occurs inside the gaseous orifice. In the coaxial type, the liquid and the gas flow via two different orifices arranged coaxially. Figure 1 shows a schematic of a coaxial type gas-centered swirl atomizer. Soller et al. [2] observed that the coaxial type atomizers exhibit superior combustor wall compatibilities compared to that of the premixing type atomizers in the context of wall thermal stress levels.

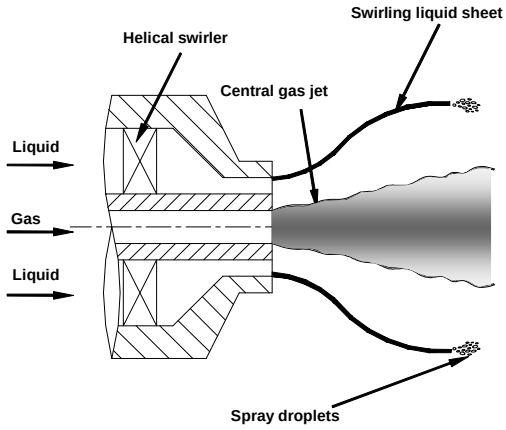

Fig. 1. A schematic of jets discharging from a gas-centered swirl coaxial atomizer.

The spray formation occurs in gas-centered swirl coaxial atomizer by means of an interaction process between the swirling liquid sheet and the gas jet. The influence of coflowing air on the breakup behavior of liquid sheets, particularly for planar liquid sheets, has been studied extensively [3-6]. Limited studies have been reported on the role of an inner gas stream on the stability of an axisymmetric liquid sheet [7-8]. A systematic experimental investigation on the role of central gas jet on the breakup of outer liquid sheet in gas-centered swirl coaxial atomizers has been carried out at IISc with water and air as simulants [9]. Different gas-centered

swirl coaxial atomizer configurations with different geometrical parameters (inner and outer orifice diameters and swirler geometry parameters) were examined in the study. The characteristics of liquid sheet breakup were obtained by capturing images of sprays using a Nikon D1X digital camera with diffused backlighting system. For a given liquid sheet condition, with increasing air jet Reynolds number, Re_g the liquid sheet continuously shrinks along with a decrease in the sheet breakup length. The sheet atomizes into a spray of droplets in the very near region of the orifice exit at very high Re_g. Figure 2 shows the variation of sheet breakup length with Re_g for liquid sheets discharging from a gas-centered swirl coaxial atomizer. The variation of breakup length with Re_g given in Fig. 2 shows that the breakup length remains unaltered in the lower values of Re_g and drastic changes in L_b are seen at higher Re_g. The study further revealed that the sheet breakup region is marked by features such as ejection of ligaments from the sheet surface, droplet clusters, increased surface corrugations on the liquid sheet, and cellular structures on the liquid sheet [10].

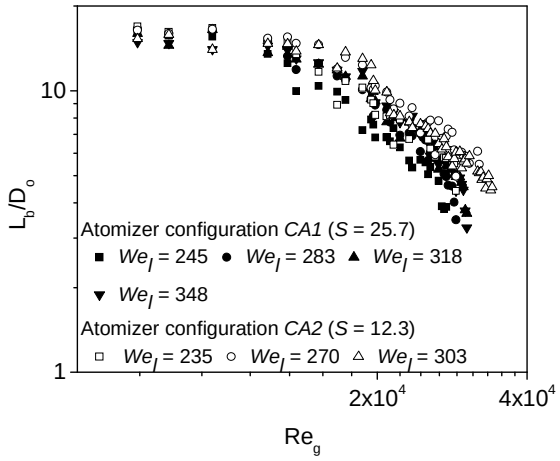

Fig. 2. The variation of breakup length of liquid sheet with Re_g.

Classification of atomization regimes in the spray formation process assumes importance in atomization modeling. The work of Adzic et al. [8] on the breakup of an axisymmetric liquid sheet by an inner gas stream identified three major sheet breakup regimes: Kelvin–Helmholtz regime, cellular regime and atomization regime. Recently, a detailed experimental study [11] of sprays discharging from gas-centered swirl coaxial atomizers showed that the spray exhibits different regimes: wave-assisted sheet breakup, perforated sheet breakup, segmented sheet

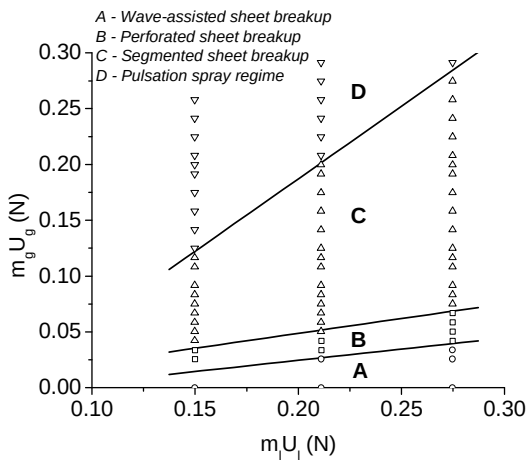

Fig. 3. Atomization regimes for sprays from gas-centered swirl coaxial atomizers.

breakup, and pulsating spray regime. For this purpose, a high speed camera system (Redlake Y4L) along with a backlighting source was operated with different combinations of camera frame speed and image resolution. For a typical gas-centered swirl coaxial atomizer, Fig. 3 identifies these regimes in the plot of $m_g U_g$ (central air jet momentum) versus $m_l U_l$ (liquid momentum). With increasing velocity of central air jet, U_g, the nature of fluid dynamic interaction process between the liquid sheet and the air jet gets changed and hence the mechanism of spray formation.

The pulsating sprays are marked by an intermittent, periodic ejection of liquid masses in the near region of the orifice exit. Such unsteady spray oscillations could result in potentially catastrophic combustion instability in liquid propellant rocket engines. Several studies [12-17] have been devoted to understand the behavior of unsteady spray oscillations in coaxial atomizers. The central orifice lip is one of the major injector geometrical parameters influencing the spray pulsation [13]. The work of Im et al. [14] on sprays from gas (outer)–liquid (inner) swirl coaxial injector showed that the recess length of the central orifice increases the frequency of self-pulsation due to the enhanced flow interaction between the liquid and gas streams. The work by Lightfoot and Danczyk [15] revealed that the interaction between the central gas flow and the annular film flow in the near region of central orifice lip develops several non-uniformities in the spray. Some of these non-uniformities, axisymmetric and asymmetric pulsing in the spray, affect the temporal mass-distribution. For recessed gas-centered coaxial injectors, Canino et al. [16] showed that Strouhal number increases with the gas-to-liquid jet momentum ratio, J (for J>1) and in the range 0.2 to 0.45. Experimental studies have been conducted at IISc [17] on the dynamics of pulsating sprays discharging from gas-centered swirl coaxial atomizers. Unsteady sprays bursts were tracked

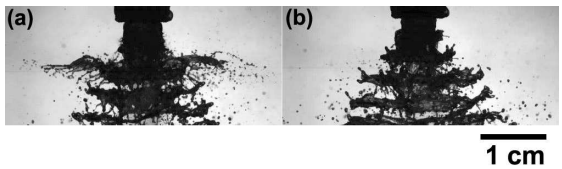

Fig. 4. (a) Big burst, and (b) regular bursts seen in pulsating sprays from the gas-centered swirl coaxial atomizer.

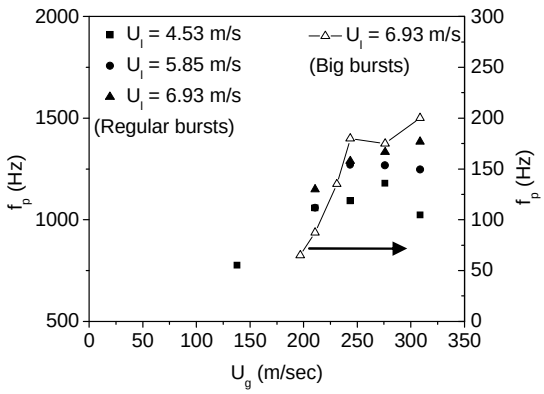

Fig. 5. The variation of pulsation frequency, f_p with U_g for the pulsating sprays from the gas-centered swirl coaxial atomizer.

with the aid of high speed video recordings of sprays. The study revealed that the burst phenomenon in the pulsating spray is not 100% periodic. It also highlights different bursting structures. Two types of bursting are dominantly seen in a typical pulsating spray discharging from gas-centered swirl coaxial atomizers: big bursts and regular bursts. Figure 4 shows typical images of big burst and regular bursts in a pulsating spray condition. As seen in Fig. 4(a), the big burst is marked by a rapid radial spreading of liquid masses along with a cloud of micron-sized ligaments/droplets. The regular bursts are marked with a radial spreading liquid mass without any dominant presence of micron-sized ligaments/droplets clouds as seen in Fig. 4(b). Analysis shows that the frequency of big bursts is much smaller than that of the regular bursts as shown in Fig. 5. Further studies have been pursued at IISc to understand the atomization process and spray characteristics of sprays discharging from recessed-type gas-centered swirl coaxial atomizers.

References

[1] R.K. Cohn, P.A. Strakey, R.W. Bates, D.G. Talley, J.A. Muss, and C.W. Johnson, AIAA 2003-0124 (2003).
[2] S. Soller, R. Wagner, H.-P. Kau, P. Martin, and C. Maeding, AIAA 2005-3750 (2005).
[3] A. Mansour and N. Chigier, N., Phys. Fluids A, 2 (1990) pp. 706-719.
[4] B.E. Stapper, W.A. Sowa, and G.S. Samuelsen, J. Engg. Gas turbines and Power, 114 (1992) pp. 39-45.
[5] J. Park, K.Y. Huh, X. Li, and M. Renksizbulut, Phys. Fluids, 16 (1994) pp. 625-632.
[6] A. Lozano, F. Barreras, C. Siegler, and D. Löw, Exp Fluids 39 (2005) pp. 127-139.
[7] I.S. Carvalho and M.V. Heitor, Exp Fluids 24 (1998) pp. 408-415.
[8] M. Adzic, I.S. Carvalho, and M.V. Heitor, Optical Diagnostics Engg 5 (2001) pp. 27-38.
[9] V. Kulkarni, D. Sivakumar, C. Oommen, and T.J. Tharakan, J. Fluids Engg. 132 (2010) 011303.
[10] V. Kulkarni, M.Sc. (Engg) thesis, Indian Institute of Science, June, 2009.
[11] D. Sivakumar and V. Kulkarni, Exp. Fluids 51 (2011) pp. 587-596.
[12] V.G. Bazarov and V. Yang, J. Prop. Power 14 (1998) pp. 797-806.
[13] J. Tsohas, and S.D. Heister, J. Prop. Power 27 (2011) pp. 793-810.
[14] J.-H. Im, D. Kim, P. Han, Y. Yoon, Atomization and Sprays 19 (2009) pp. 57-74.
[15] M.D.A. Lightfoot, and S.A. Danczyk, ICLASS2009, Vail, Colorado, USA.
[16] J.V. Canino, S.D. Heister, V. Sankaran, and S.I. Zakharov, AIAA 2005-4297 (2005).
[17] D. Sivakumar, V. Rout, U. Satish Babu, and J. Tharakan, ICFD2011, Sendai, Japan (2011).

Manipulation of Internal Flows for Spray Creation

Steven H. Collicott, Professor
School of Aeronautics and Astronautics
Purdue University

Introduction

We all know spray production to be a fluid process which is either rich with or fraught with complexity and nonlinearity. Models for wave growth on a liquid jet are one approach to predicting and understanding the early stages of the spray production process. Experiments to test such models show agreement in some cases and room for improvement in other cases and always show the additional complexity that exists nearby in the downstream sense.

Figure 1 shows example images from two Purdue experiments on measuring wave growth. Both led to quantitative results for amplification. The low-speed jet compares to theory over a half-dozen wavelengths whereas the high speed jet is noticeably more complex. The high speed jet has the most upstream waves becoming visible at several origins around the circumference of the jet. These waves grow in amplitude and in extent in the circumferential sense around the jet. The wave regions merge. The waves interact, even creating a node-like streamwise line near the lower part of the image beginning about one jet diameter downstream. As interactions continue downstream from *5D/4*, the jet begins to spread and the first droplets appear.

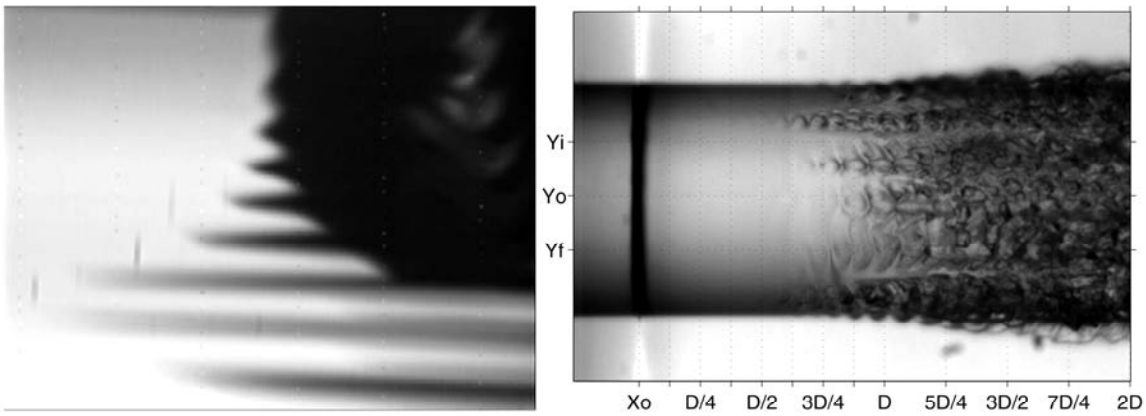

Figure 1. Two examples from Purdue from wave-growth measurement experiments. Left is from [1] showing a low-speed jet (gravity and flow are top to bottom) with 40:1 imaging compression in the streamwise direction. Right is from [2] showing a high-speed liquid jet with several wave phenomena growing in the streamwise direction. Downstream shows a turbulent –like complexity in the flow. Flow is left to right, gravity is top to bottom

It is the complexity of this near-exit wave interaction that gives rise to droplet production in many flows. What causes the waves to begin? Certainly the simple but vague answer is: a perturbation and a slowly-

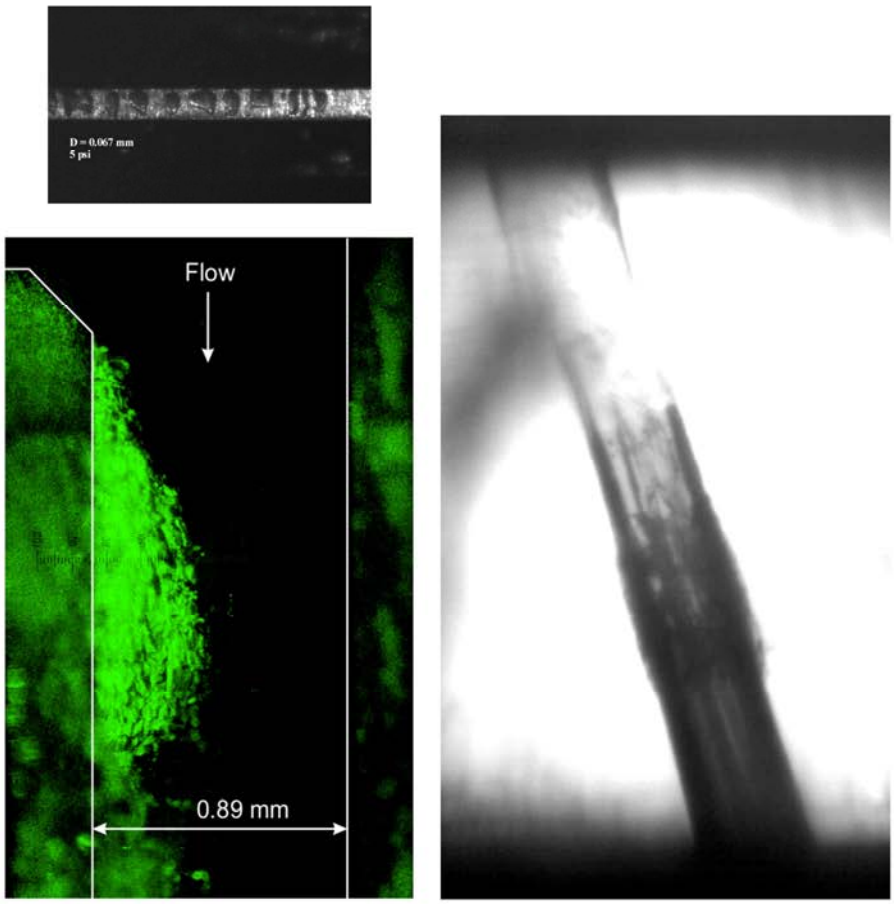

Figure 2. Cavitation examples. Upper left, 30kPa driving pressure difference in a slot flow[4]. Lower left, side view of cavitation at the chamfered entrance of a slot flow[5] at several atmospheres pressure. Right, 200MPa driving pressure in a tilted 209 micron diameter orifice[6] typical of Diesel injectors. In all images, flow is from top down, the liquid is water, and the back pressure is

growing instability. But the early waves are only the start of the overall process. What type of perturbations are most effective at creating unsteadiness that leads to desired spray properties? How do wave groups interact? How do they cause the jet to begin to spread? How does the chaotic-appearing surface flow begin to affect the flow in the core of the jet? How do these vary with fluid properties and speeds? Answers to these questions from modeling are very distant.

Perturbations likely originate at or upstream of where they are first visible. Thus perturbations visible near the exit may originate within the orifice. A number of researchers have shown that perturbations in the internal flow definitely affect the jet. Hiroyasu showed that turbulent flow in the nozzle affects the jet[3]. Cavitation in the orifice has been shown to be common over a wide range of pressures[4, 5, 6], as shown in Figure 2. Swirling internal flows, such as counter-rotating streamwise vortices in a tilted orifice or a normal orifice with cross flow over the inlet[6,7] are another form of perturbation if one pictures parallel flow through the orifice as the baseline case.

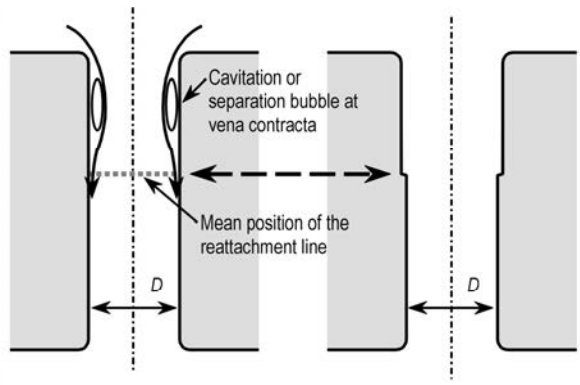

Figure 3. Step orifice design (right) of Ong[9].

Even when spray prevention is the goal – such as for using liquid jets for the hydro-entanglement of fibers in production of non-woven textiles, the internal flow has been found to be important[8]. In this case, avoiding partial cavitation has produced the persistent liquid jets that are necessary for production of these materials. The popular polyester "fleece" fabric is apparently the most common of these textiles, at least in the cooler climates.

In our group in the 1990s, the focus was on the effect of the seemingly ubiquitous inlet cavitation of jets and sprays. This cavitation was found to be present and to be unsteady in various orifice flows for driving pressure differences from as low as 1/3 atmosphere up to 2,000 atmospheres. In all cases the cavitation was unsteady. The mechanisms through which this cavitation can affect the spray spear to include both a low-frequency "chugging" of the larger scale flow and the shedding of sub-diameter length scale unsteady flow structures into the boundary layer, which flow downstream and apparently act as large perturbations to the flow processes seen, for example, in the right-hand image in Figure 1.

Control by Manipulating Cavitation

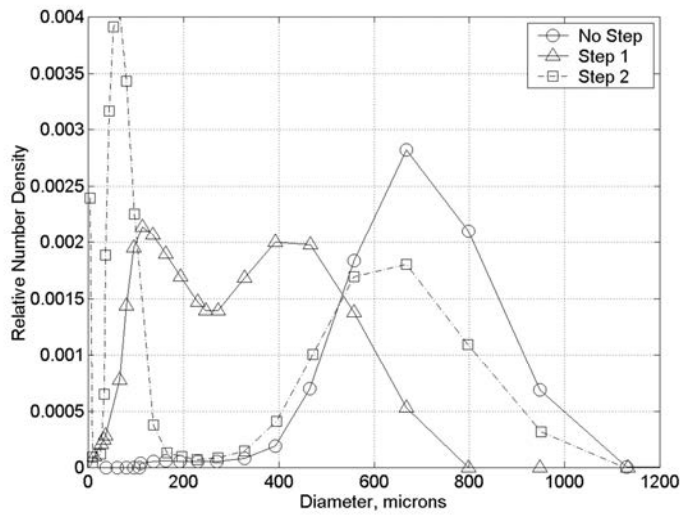

Figure 4. Droplet size distributions for plain orifice ("No Step") and two step orifices[9].

Experiments in the 1990s focused on manipulating inlet cavitation to effect changes in droplet production. This was motivated by the fact that the cavitation was an easily-visualized naturally occurring unsteady flow structure with substantial sub-diameter length scale structure.

First an up-stream facing step was used to try to increase the natural unsteadiness of the reattachment process of the liquid flow at the downstream end of the cavitation bubble. This approach was successful. Figure 3 shows this arrangement, taken from [9]. This system created substantial numbers of minute droplets compared to the smooth orifice jet, see Figure 4, also from [9].

Next a fluidic device was created to attempt modulate the effect of the step, as shown in Figure 5, from Ref. [10]. This system worked, could be turned on and off and modulated. But small droplet production was not as effective as with the original step orifice. Computations of the internal flow field, including the unsteady cavitation, were made to attempt to correlate certain flow structures with the production of smaller droplets[11]. Optimizing such a device remains an open question, along with extending it to higher speeds.

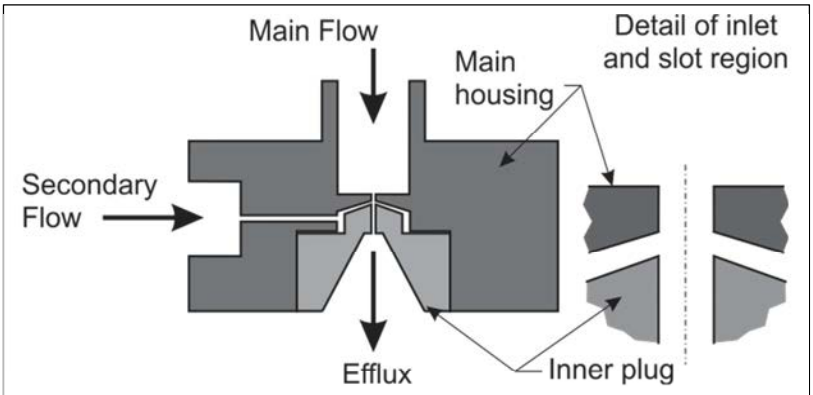

Figure 5. Diagram of the internal flow geometry for the fluidic spray control work of Tseng[10,11].

Goals of the Current Work

Current work uses the recent results of Portillo et al.[2] as a baseline. Modifications to the orifice to permit the introduction of perturbations are being made. This is exploratory work that seeks to apply the lessons from Hiroyasu and others to create perturbations to cause the jet to respond immediately in large-amplitude non-linear manners. This moves beyond wave growth models and besides identifying practical tools to use for manipulating sprays we hope to motivate others to advance CFD and modeling. The range of possible perturbations appears unbounded, just like the design of internal flow geometries in practical devices has been for many decades. Exploring an unbounded frontier with experiments complements the analytical and computational approaches to identifying fluid instabilities that lead to desirable droplet production.

Acknowledgements

An NSF CAREER award in 1995 funded much of the early cavitation work. Cummins Co. provided with additional support. Computational codes from Purdue colleague Steve Heister have been a big part of our program.

References

1. S. H. Collicott, S. Zhang, S. P. Schneider , “Quantitative liquid jet instability measurement system using asymmetric magnification and digital image processing,” *Experiments in Fluids*, **16**, No. 5, pp. 345-348, April, 1994.
2. E. Portillo, S. H. Collicott, G. A. Blaisdell, “Measurements of Axial Instability Waves in the Near Exit Region of a High Speed Liquid Jet,” In press, *Physics of Fluids*, 2012.
3. N. Tamaki, M. Shimizu, K. Nishida, and H. Hiroyasu, “Effects of Cavitation and Internal Flow On Atomization of A Liquid Jet,” *Atomization and Sprays*, vol. 8, pp. 179-197, 1998.
4. H. Li, P, K. Sanchez, and S. H. Collicott, “Visualization of Cavitation in Low-Pressure Miniature Slot Flows,” *Institute for Liquid Atomization and Sprays-Americas 98*, Sacramento, CA, May 1998.

5. M. Henry, and S. H. Collicott, “Internal Structure of Cavitating Slot Flow”, *Atomization and Sprays,* vol. 10, no. 6, pp. 545-563, November/December 2000
6. H. Li and S. H. Collicott, “Visualization of Cavitation in High Pressure Diesel Fuel Injector Orifices,” *Atomization and Sprays*, **16**, No. 8, pp. 875-886, December 2006.
7. R. A. Bunnell and S. D. Heister, ``Three-Dimensional Unsteady Simulation of Cavitating Flows in Injector Passages'', *Journal of Fluids Engineering*, V 122, No. 4, pp. 791-797, 2000.
8. A. Begenir, H. V. Tafreshi, B, Pourdeyhimi, “Effect of nozzle geometry on hydroentangling water jets: experimental observations,” *Textile Research Journal*, February 2004.
9. D. Ong, C-P Yeh, T. J. Hoverman, and S. H. Collicott, “Effects of a Small Step in an Orifice on Liquid Jet Breakup,” *Atomization and Sprays*, **13**, No. 2/3, pp. 297-307. 2003.
10. K. Tseng and S. H. Collicott, “Demonstration of a Fluidic Spray Control Orifice,” *Journal of Propulsion and Power,* **27**, No. 3, May-June, 2011.
11. K. Tseng, *Fluidic Spray Control*, Ph.D. Thesis, School of Aeronautics and Astronautics, Purdue University, May 2006.

Modelling of Primary Atomisation in Liquid Rocket Engine Injectors

T. John Tharakan
Flow and Acoustics Division, Liquid Propulsion Systems Centre
Trivandrum -695547, Kerala, India

Liquid rocket engines extensively use impinging and swirl coaxial injectors for propellant atomisation and mixing. In these injectors, a liquid sheet is created which moves relative to the surrounding gaseous medium. In liquid rocket injectors, the liquid sheet formed is invariably sandwiched between two gas layers. The gaseous phase may be either quiescent or moving. In impinging injectors, the liquid sheet formed is perpendicular to the plane of two jets while in swirl injectors the liquid sheet is an annular cone. The relative motion between the liquid and gas promotes the growth of disturbances which ultimately cause the liquid sheet to disintegrate into fragments. The fragments rapidly contract into unstable ligaments under the effect of surface tension. Finally, the ligaments are broken into a multitude of droplets. This process is referred to as primary atomisation. The modelling of the primary atomisation process will benefit not only injector design and improvement but also numerical simulation of spray combustion. Disintegration of a liquid sheet between two gas layers is a problem of hydrodynamic instability and has been extensively studied. Excellent reviews on the subject are available in Lasheras and Hopfinger (2000), Ibrahim and Jog (2006), Benjamin et. al. (2010) and Lin (2003).

Numerical solutions have been obtained using both linear and nonlinear models. These solutions reveal the existence of two types of waves viz. antisymmetric (Fig. 1) and symmetric (Fig. 2). Linear analysis of a planar liquid sheet shows that these two modes are uncoupled whereas for annular or conical sheets this is not the case. Nonlinear analysis of a planar liquid sheet indicates that a purely symmetric wave can exist but antisymmetric wave has a superimposed and coupled symmetric character.

In swirl injectors, the liquid sheet is annular in shape. This configuration can be reasonably represented by a planar liquid sheet when the sheet thickness is much smaller than the mean radius of the annulus.

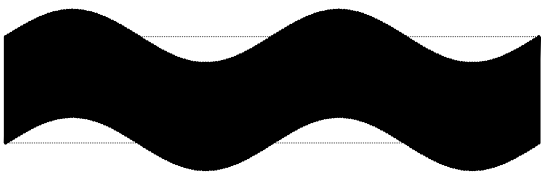

Fig. 1 Antisysmmetric Wave

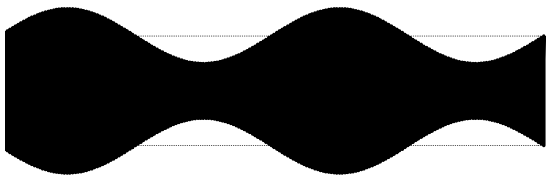

Fig. 2 Symmetric Wave

The linear theory has been extensively used in literature to predict the growth rate and wave number of the most unstable wave. The influence of viscosity of the liquid on wave growth was investigated using the linear theory by Li and Tankin (1991). Teng et al. (1997) determined the effect of ambient gas viscosity on the stability of viscous liquid curtain. Heislbetz et al. (2007) have carried out linear stability analysis of a highly viscous incompressible planar liquid sheet for this configuration and validated the predictions. Cao and Li (2000) investigated the effect of compressibility in the gas medium when the lateral wave modes were not present. Tharakan and Ramamurthi (2005) investigated the effect of the simultaneous presence of longitudinal and lateral waves on the instability of a planar liquid sheet exposed to unequal gas velocities.

Tharakan and Ramamurthi (2010) also investigated the effect of compressibility of liquid and gas on instability of a planar liquid sheet exposed to unequal gas velocities. Rao and Ramamurthi (2009) investigated the effect of base velocity profile of the liquid sheet on the instability of a planar liquid sheet in a stationary gas.

Although the breakup of planar liquid sheets has been extensively modelled, breakup of annular sheets is not yet fully understood and further investigations are required. Shen and Li (1996a and 1996b) carried out the instability analysis of a viscous annular liquid sheet moving in two gas streams with different velocities. Panchagnula et al. (1996) developed a linear model describing the instability behaviour of annular, swirling, inviscid sheets subject to inner and outer gas flows of differing velocities. Liao et al. (2001) developed a dispersion relation for swirling annular liquid sheet sandwiched by swirling air streams, including the effects of viscosity. Du and Li (2005) carried out a linear instability analysis for a viscous annular liquid jet moving in two gas streams with unequal swirls and velocities.

The conventional linear analysis cannot predict the breakup of liquid sheets as the distance between the two sheet surfaces is preserved. Mitra et. al (2001) carried out a dual mode linear stability analysis under the combined influence of antisymmetric and symmetric modes of disturbance at the two liquid-gas interfaces, which could predict the liquid sheet breakup. Fu et. al (2010) predicted the breakup length of the conical liquid sheet (Fig. 3) using the dual mode linear stability analysis and validated the predictions with experiments. Dual mode analysis and its variations represent the state-of-the-art in the area of linear analysis and more work has to be done to develop this type of formulation. This would enable rapid estimation of breakup length and droplet size for planar and annular liquid sheets.

All the above investigations focused on the linear instability of the gas-liquid interface. Moreover, linear theory assumes infinitesimal perturbations. Such an assumption is not valid at sheet break up when amplitude of the disturbance becomes of the same order as the liquid sheet thickness itself. Also, it is supposed that the wavelengths of the instabilities obtained by linear analysis remain prominent in the nonlinear deformation leading to break up, which need not be the case. Nonlinear modelling is required, particularly near the break up region, for a more accurate determination of break up length and droplet size that would be useful for the simulation of spray combustion.

Mehring and Sirignano (2000) analyzed linear and nonlinear waves on inviscid planar liquid sheets in a gas of negligible density. Kim and Sirignano (2000) studied three-dimensional effects on thin inviscid planar liquid sheets by a similar approach to Mehring and Sirignano. Jazayeri and Li (2000) carried out a nonlinear stability analysis of planar liquid sheets considering initial disturbance amplitude as the perturbation parameter. They retained terms upto third order in their analysis. Mitra (2001) extended the analysis of Jazayeri and Li to include the effects of gas velocity. Tharakan et. al (2002) numerically solved a set of nonlinear differential equations for determining the breakup of inviscid liquid sheets (Fig. 4). Nath et.al (2010) studied the effects of gas velocity on the nonlinear breakup of a planar liquid sheet. Rao and Ramamurthi (2010) determined the nonlinear growth of disturbance waves on thin inviscid liquid sheets with a velocity profile across their thickness.

Nonlinear analysis has also been carried out by Rangel and Hess (1990), Rangel and Sirignano (1991) and Lozano et al. (1998). Here the evolution of liquid sheets is

determined using a vortex discretisation method. Numerical errors in the vortex discretisation method are, however, relatively large as it involves a number of interpolations to arrive at a solution. Vortex discretisation is a promising approach that needs to be pursued further to attain its full potential.

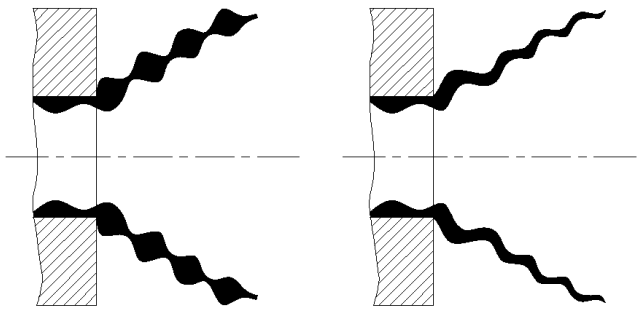

Fig. 3 Growth of disturbance wave on conical liquid sheets

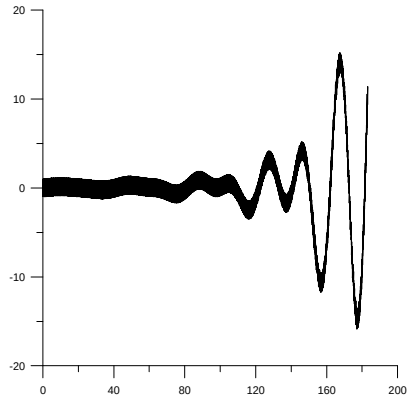

Fig. 4 Growth of disturbance wave on planar liquid sheet

Nonlinear analyses of thin annular liquid sheet break up were carried out by Mehring and Sirignano (1999a, b) and Parker and Heister (2006) in a stationary gaseous medium. Ibrahim and Jog (2008) developed a nonlinear instability model for an annular liquid sheet subjected to unequal inner and outer gas velocities and including outer gas swirl. Extension of nonlinear models of both planar and annular sheets to a wider range of configurations is an area of further research.

All the previous models of the primary instability have been based on Kelvin-Helmholtz instability growth mechanism. For the case of an annular liquid sheet in a liquid rocket engine swirl injector, this instability mechanism predicts that the sheet will break up into axisymmetric toroidal rings. However, preliminary experimental results have shown that this is not always the case. This indicates that there is a nonaxisymmetric instability mode which cannot be predicted by the Kelvin-Helmholtz mechanism. Further theoretical studies are necessary to investigate alternative mechanism like the Rayleigh-Taylor-Kelvin-Helmholtz instability growth model for annular liquid sheets.

References

1. Lasheras, J.C., and E.J. Hopfinger., ‘Liquid jet instability and atomization in a coaxial gas stream,’ Annual review of fluid mechanics, vol. 32, pp. 275-308, 2000.
2. Ibrahim, A.A. and M.A. Jog, ‘Effect of liquid and air swirl strength and relative rotational direction on the instability on the instability of an annular liquid sheet,’ Acta Mechanica., vol. 186, pp. 113-133, 2006.
3. Benjamin, M.A., R. J. Jenson, and M. Arienti, ‘Review of atomization: Current knowledge and future requirements for propulsion combustors,’ Atomisation and Sprays, vol. 20, No. 6, pp. 485-512, 2010.
4. Lin, S.P.,’ Breakup of liquid sheets and jets,’ Cambridge university press, Cambridge, UK, 2003.
5. X. Li and R.S. Tankin, ‘On the Temporal Instability of a Two-dimensional Viscous Liquid Sheet, J. Fluid Mech.,’ vol. 226, pp. 425-443, 1991.

6. Teng, C. H., S.P. Lin, and J. N Chen, Absolute and convective instability of a viscous liquid curtain in a viscous gas, J. Fluid Mechanics, vol. 332, pp.105-120, 1997.
7. Heislbetz, B., K. Madlener and H.K. Ciezki, 'Breakup characteristics of a Newtonian liquid sheet formed by a doublet impinging jet injector, AIAA paper 5694, 43rd AIAA/ASME/SAE/ASEE Joint Propulsion Conference, 2007.
8. Cao, J. and X. Li, 'Stability of plane liquid sheets in compressible gas streams,' J. Prop. Power, vol. 16, pp. 623-627, 2000.
9. Tharakan, T.J. and K. Ramamurthi,. 'Growth of longitudinal waves in plane liquid sheets having lateral wave modes when exposed to two gas Streams of unequal velocities. Atomization and Sprays, vol..15, pp. 181-200, 2005.
10. Tharakan, T.J. and K. Ramamurthi, 'Influence of liquid and gas compressibility on growth of thin liquid sheets,' Fluid Dynamics Research, vol. 42, pp. 1-22, 2010.
11. Rao, V.N and K. Ramamurthi, 'Internal instability of thin liquid sheets,' Physics Fluids, vol. 21, pp. 092106-1-092106-10, 2009.
12. Mitra, S.K., X. Li and M. Renksizbulut, 'On the breakup of viscous liquid sheets by dual-mode linear analysis,' J. Propulsion Power, 17, pp. 728-735, 2001.
13. Shen, J., and X. Li., 'Instability of an annular viscous liquid jet,' Acta Mechanica., vol. 14, pp. 167-183, 1996.
14. Shen, J. and X. Li., 'Breakup of annular liquid jets in two gas streams,' J. Propulsion Power, vol. 12, pp..752-759, 1996.
15. Panchagnula, M.V., P.E. Sojka and P.J. Santangelo., 'On the three-dimensional instability of a swirling, annular, inviscid, liquid sheet subject to unequal gas velocities,' Physics Fluids, vol.8, pp. 3300-3312, 1996.
16. Liao., Y, S.M. Jeng, M.A. Jog and M.A. Benjamin, 'On the mechanism of pressure-swirl airblast atomization,' AIAA paper 2001-3571, 2001.
17. Du, Q and X. Li, 'Effect of gas stream swirls on the instability of viscous annular jets,' Acta Mechanica, vol. 176, pp. 61-81, 2005.
18. Fu, Q., L. Yang, Y. Qu, and B. Gu, 'Linear stability analysis of a conical liquid sheet,' J. Propulsion and Power, Vol. 26, No. 5, 2010.
19. Mehring, C. and W.A. Sirignano, 'Nonlinear capillary wave distortion and disintegration of plane liquid sheet,' J. Fluid Mechanics. Vol. 388, pp. 69-113, 2000.
20. Kim, I and W.A. Sirignano, 'Three-dimensional wave distortion and disintegration of planar liquid sheet,' J. Fluid Mechanics, vol. 410, pp. 147-183, 2000.
21. Jazayeri, S.A. and X. Li, 'Nonlinear instability of plane liquid sheet,' J. Fluid Mechanics, vol. 406, pp. 281-308, 2000.
22. Mitra, S.K., 'Breakup process of plane liquid sheets and prediction of initial droplet size and velocity distribution in sprays,' PhD thesis, University of Waterloo, 2001.
23. Tharakan, T.J., and K. Ramamurthi and M. Balakrishnan, 'Nonlinear breakup of thin liquid sheets, Acta Mechanica., vol. 156, pp. 29-46, 2002.
24. Nath, S, M. Mukhopadhyay, A. Datta, S. Sen, and T.J. Tharakan, 'Influence of gas velocity on breakup of planar liquid sheets sandwiched between two gas streams,' Atomisation Sprays, vol. 20, no. 11, pp. 983-1003, 2010.
25. Rao, V.N., and K. Ramamurthi, 'Role of axisymmetric axial velocity gradients on nonlinear disintegration of liquid sheets,' Fluid Dynamics Research, vol. 42, 065505, no. 6, 2010.

26. Rangel, R.H. and C. Hess, Nonlinear spatial instability of a fluid sheet. AIAA Paper 90-0118, 28th Aerospace Sciences Meeting, Reno, Neveda, 1990.
27. Rangel, R.H. and W.A. Sirignano, The linear and nonlinear shear instability of a fluid sheet. Physics of Fluids A3, pp. 2392-2400, 1991.
28. Lozano, A., A.G. Olivares and C. Dopazo, 'The instability growth leading to a liquid sheet breakup,' Physics Fluids, 10, pp. 2188-2197, 1998.
29. Mehring, C. and W.A. Sirignano, 'Axisymmetric capillary waves on thin annular liquid sheets part I: temporal instability: Physics of Fluids, vol. 12, 1417-1439, 1999a.
30. Mehring, C. and W.A. Sirignano, 'Axisymmetric capillary waves on thin annular liquid sheets part II: spatial instability: Physics of Fluids, vol. 12, 1440-1460, 1999b.
31. Part, H. and S.D. Heistor, 'Nonlinear simulation of free surfaces and atomisation in pressure swirl atomisers,' Physics Fluids, vol. 18, 052103, 2006.
32. Ibrahim, A.A. and M.A. Jog, 'Nonlinear instability of an annular liquid sheet exposed to gas flow,' Int. J. Multiphase Flow, vol. 34, pp. 647-664, 2008.

Modelling the heat release response of premixed flames to unsteady upstream fuel-air ratio stratification in lean-premixed-prevapourised combustors

*Santosh Hemchandra**

Institute of Aerodynamics, RWTH Aachen
Aachen 52062, Germany

Introduction

Acoustic pressure fluctuations during combustion instability events can cause unsteady pressure drops across fuel injectors and air inlets, potentially resulting in mass flow-rate oscillations at these locations. In the case of liquid fueled combustors, this unsteady forcing of the fuel jet can result in unsteady atomization causing spatio-temporal variation in spray characteristics such as droplet size and velocity distributions, ambient air entrainment, group combustion number etc. [1, 2]. In lean premixed, pre-vaporized combustors, the combustion process occurs after the liquid fuel jet has vapourised and is premixed with air, in the interest of mitigating pollutant emissions. In these situations, unsteady fuel spray atomization characteristics can result in unsteady stratification in the equivalence ratio (ϕ), upstream of the flame which then causes the heat release rate to oscillate. Thus combustion instability can then be sustained due to coupling between these heat release oscillations and combustor acoustic modes [3, 4]. Evidence supporting this unsteady ϕ stratification mechanism has been shown in several studies, from measurement of oscillations in ϕ during combustion instability events [5–8] or by comparing the dependence of instability characteristics on geometry and operating conditions with correlations from theoretical analyses [9–11]. Several groups have reported experimental [5, 8, 12–18] and computational [19–25] studies of premixed flame response to ϕ fluctuations.

The instantaneous heat release rate from a flame, $q(t)$, can be written as an integral of local heat release rate contributions over the flame surface as follows,

$$q(t) = \int_{flame} \rho s_L(\phi) h_R(\phi) dA \tag{1}$$

Where, ϕ is the local equivalence ratio, s_L is the local laminar flame speed, h_R is the local heat of reaction per unit mass of the mixture and ρ is the local mixture density. Two broad groups of mechanisms causing heat release rate fluctuations can be identified as follows [26, 27]. The direct mechanism - spatio temporal ϕ fluctuations result in spatio-temporal variations in s_L and h_R of the reactant mixture along the flame surface, causing the heat release rate to oscillate. The indirect mechanism - spatio-temporal variations in s_L cause the flame surface to wrinkle resulting in burning area oscillations which cause heat release rate oscillations. Shreekrishna et al [27] have extended the linear analysis of Cho and Lieuwen [26] to the non-linear limit using a G-equation (level-set) based Reduced Order Modelling (ROM) approach which can be used

*Corresponding author: s.hemchandra@aia.rwth-aachen.de

to predict the above describing functions for convectively non-compact flames. This approach can track geometrically complex and even multiply connected flames.

A key simplifying assumption made in the above ROM approaches, however, is that the effect of gas expansion across the flame surface on the approach flow is neglected. The present work performs a quantitative comparison between heat release response characteristics of a nominally lean, two dimensional, slot stabilized, premixed methane-air flame forced by ϕ fluctuations using fully compressible reacting flow simulations, with corresponding predictions from a generalization of the reduced order model (ROM) analyzed in Shreekrishna et al [27], for the same configuration. The impact of neglecting gas expansion at the flame surface, as well as, the influence of the shape of the nominally steady flame on heat release response characteristics are assessed.

Formulation

The Reduced Order Model (ROM) for flame response prediction used in this paper generalizes previous level-set method based ROM formulations for premixed flame response to fuel-air ratio perturbations [26, 27]. The principal simplifying assumptions are that the flame is a thin surface separating unburnt reactants from products and that he influence of gas expansion across the flame front is neglected. The first assumption allows for the instantaneous evolution of the flame surface to be tracked using the G-equation as follows,

$$\frac{\partial G}{\partial t} + \vec{u} \cdot \nabla G = s_L(\phi)|\nabla G| \tag{2}$$

where, $\vec{u}$ and s_L are the local flow velocity and laminar flame speed [28]. All lengths in the above have been normalized by a burner dimension (R) and velocities by a characteristic upstream flow velocity (U_o). The zero level-set of the function G is identified with the upstream (unburnt) boundary of the flame surface being tracked. The second assumption allows for $\vec{u}$ to be specified without having to solve the Navier-Stokes equations in conjunction with eq. 2 and is commonly made in the development of reduced order models [26, 27, 29–31]. The spatio-temporal variation of ϕ is determined from spatio-temporal variations of fuel (Y_F) and oxidizer (Y_O) mass fractions respectively, determined by solving corresponding species transport equations for each mass fraction. Flame response predictions from the above model are compared with results from detailed numerical computations of harmonically forced slot stabilized, two-dimensional, methane-air premixed flame ($\phi_o = 0.85$), described in Hemchandra [32]. The nominally steady flames used in the forced computations are shown for reference in fig. 1. The characteristics of the unsteady upstream ϕ field and flame attachment boundary conditions in the ROM formulations are quantitatively matched to their corresponding characteristics in the latter detailed computations in the present work (these results are not shown here in the interest of brevity).

Describing functions corresponding to the total heat release rate and burning area responses at a given excitation frequency f_{exc} are then defined as follows, Total heat release rate:

$$F(St, \epsilon_\phi) = \frac{\hat{q}'(St, \epsilon_\phi)/Q_o}{\phi_b'(St)/\phi_o} \tag{3}$$

Burning area (indirect response):

$$F_A(St, \epsilon_\phi) = \frac{\hat{A}'(St, \epsilon_\phi)/A_o}{\phi_b'(St)/\phi_o} \tag{4}$$

where, $St = 2\pi f_{exc} L_f/U_o$, $\hat{\phi}_b'$ is the ϕ fluctuation amplitude along the slot exit plane and $\epsilon_\phi = |\hat{\phi}_b'/\phi_o|$ determined at the origin (i.e. the center of the slot exit plane). The '$\hat{}$' denotes

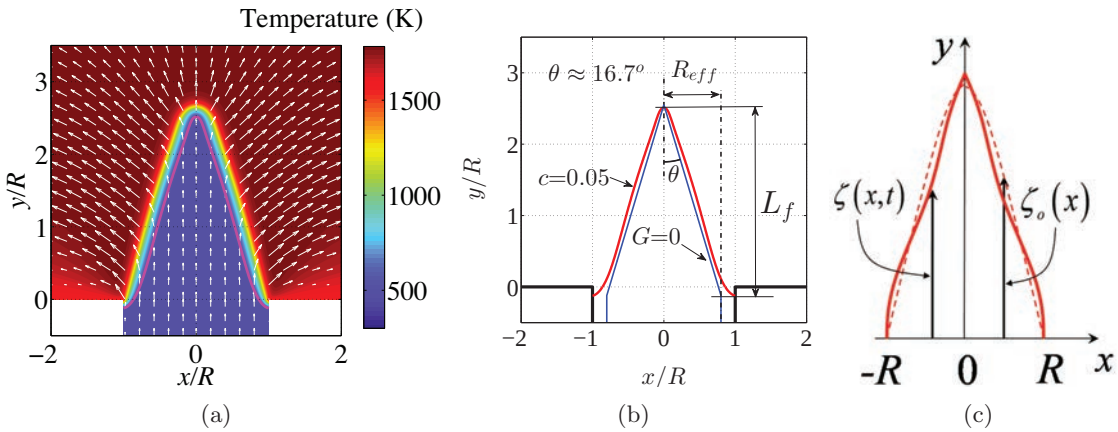

Figure 1: (a)Temperature and velocity fields around the steady flame. The magenta curve shows the flame contour ($T = 390$ K) and (b) The zero level-set used in the ROM computations - the flame contour has been overlaid for reference and (c) Schematic of perturbed flame surface in the present computations at low nominal forcing amplitude, ϵ (solid curve) and the unperturbed flame surface (broken curve) ($\phi_o = 0.85$, $v_o = 1.0$ m s^{-1}).

the FFT of the respective quantities determined at f_{exc}. Quantities (e.g.: describing functions, eqs. 3 and 4) determined from the ROM computations will be denoted by the superscript 'ROM' and quantities determined from detailed computations will be denoted using the superscript, 'Det' in the rest of this abstract.

The instantaneous flame surface shape in the present computations can be approximated as a single valued function $\zeta(x,t)$ as shown schematically in fig. 1c, in the limit of small forcing amplitudes (ϵ). Assuming that $d\zeta_o/dx \sim -\beta$ is nearly constant and that the flame is attached at $x = R$ the linearized burning area response can be written as,

$$\frac{\hat{A}'(t)}{A_o} = \frac{\beta}{1+\beta^2}\frac{\hat{\zeta}'(0)}{R} \tag{5}$$

which suggests that, the characteristics of the linearized $\hat{A}'/A_o$ are determined, to leading order, by the corresponding characteristics of the flame tip perturbation, $\hat{\zeta}_{tip} = \hat{\zeta}'(0)$.

Results

Figures 2a and b show the predicted magnitude and phase of the describing functions for total heat release rate response and burning area response determined from ROM and detailed computations (see eqs. 3 and 4) for small amplitude forcing ($\epsilon = 0.015$). First, note that the agreement between the predicted phase of the describing functions from ROM and detailed computations is excellent for all frequencies at this forcing amplitude. Next, notice that for $St < 3$ and $St > 10$ both $|F^{ROM}|$ and $|F_A^{ROM}|$ approach the corresponding predictions from detailed computations while showing smaller quantitative differences, when compared to the the predictions for $3 < St < 10$. From eq. 5, the agreement in phase is due to the excellent agreement seen in fig. 3a which shows the phase of $\hat{\zeta}_{tip}^{\prime Det}$ and $\hat{\zeta}_{tip}^{\prime ROM}$ relative to ϕ_b' at the origin. However, small differences between the predicted phases of F^{ROM} and F^{Det} (see fig. 2a) can be attributed to the mismatch in of the predicted direct response components from the two approaches due to geometric differences between the respective nominally steady flame shapes

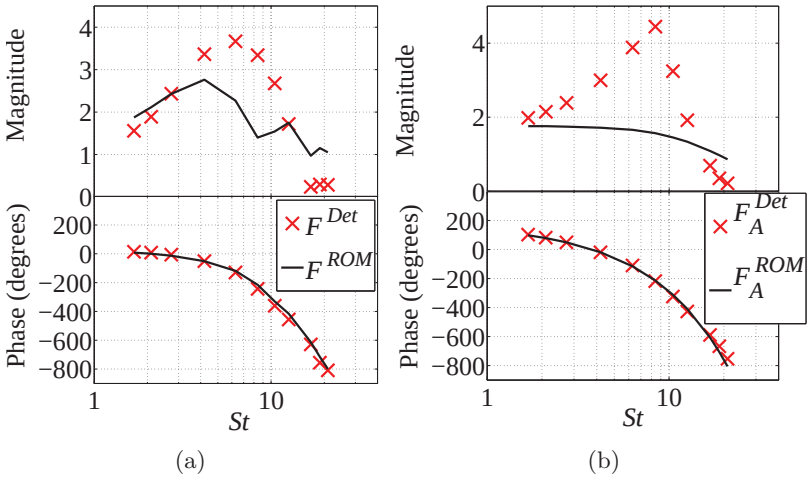

Figure 2: Comparison between the predicted characteristics of describing functions for (a) total heat release and (b) burning area as a function of Strouhal number, St. The top half of each figure shows the magnitude and the bottom half shows the phase ($\phi_o = 0.85$, $v_o = 1$ m s^{-1}, $\epsilon = 0.015$).

(see fig. 1). The mismatch in predicted describing function magnitudes is due to the mismatch in predicted $|\hat{\zeta}'_{tip}|$ from the two approaches as Figure 3b shows.

The key mechanism causing the above mismatch is the well known Darrieus-Landau (DL) instability which occurs due to preferential acceleration of the flow along the flame normal direction due to gas expansion across the flame surface (see e.g. ref. [33]). Truffaut and Searby [34] have shown experimentally, for a flame configuration similar to the present work, that the presence of a flow velocity component tangential to the flame surface (u_p), causes the nature of the DL instability to change from being absolutely unstable to being convectively unstable. For the present detailed computations, $u_p \approx 0.96$ ms^{-1}, suggesting that the flame in the present detailed computations is convectively unstable [35], resulting in the amplification of $|\hat{\zeta}'^{Det}_{tip}|$ which the ROM cannot capture.

Conclusions

Present results show that in the small excitation amplitude (linear response) limit, the present ROM reliably predicts the variation of the phase of describing functions across the range of excitation Strouhal numbers (St). The poor agreement in predicted describing function magnitudes are seen for intermediate St values because of the amplification of flame surface perturbations as they propagate through the flame, due to the influence of convective DL instability. At these St values, the DL instability also causes poor agreement between ROM predictions and corresponding detailed computations of both magnitude and phase characteristics of describing functions at large forcing amplitudes. As such, this suggests that the present ROM can predict flame response at large forcing amplitudes as long as DL instability has a minimal influence on the evolution of flame surface perturbations. Next, good agreement between the ROM and detailed computations for the predicted phase of the flame describing functions in the present weakly curved 2D computations, is due to the fact that the latter depend only on the characteristics of flame tip perturbations. Hence, for highly curved or axi-symmetric flames, this agreement is anticipated in cases where flame surface motions are minimally influenced by DL instability. Finally, the present paper studies the response of flames that are attached such

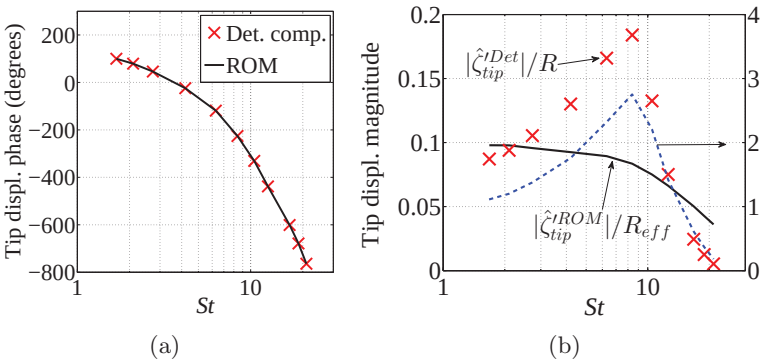

Figure 3: Comparison of the characteristics of flame tip displacement prdicted by the ROM (curve) and detailed computations (crosses) - (a) Phase (relative ϕ_b) and (b) Magnitude (left axis) and ratio of tip fluctuation magnitudes predicted from detailed computations and the ROM (left axis) ($v_o = 1$ m s^{-1}, $\phi_o = 0.85$, $\epsilon = 0.015$).

that the flame base remains fixed at all times. However, this is in general not always case and can have a significant influence on predicted flame response characteristics. Hence, the ROM formulation must be extended in order to include the influence of DL instability and flame attachment point dynamics within its framework in order to improve the quantitative reliability of its predictions.

Acknowledgment

This author's work was supported by the collaborative research center, SFB 686, funded by the Deutsche Forschungsgemeinschaft (DFG). The support is gratefully acknowledged. The author would like to thank Kittisak Chawalitwong for running the simulations used to re-validate the kinetics and Heinz Pitsch for the FlameMaster program.

References

[1] R. I. Sujith. An experimental investigation of interaction of sprays with acoustic fields. *Expts. in. Fluids*, 38:576–587, 2005.

[2] C. Wark, K. Eickmann, and C. Richards. The structure of an acoustically forced reacting two phase jet. *Combust. Flame*, 120:pp. 539–548, 2000.

[3] T. Lieuwen, H. Torres, C. Johnson, and B. T.. Zinn. A mechanism of combustion instability in lean premixed gas turbine combustors. *J. of Eng. in Gas Turb. and Power*, 123(1):182–189, 2001.

[4] T. Lieuwen and B. T.. Zinn. The role of equivalence ratio oscillations in driving combustion instabilities in low nox gas turbines. *Proc. Combust. Inst.*, 27:1809–1816, 1998.

[5] R. Mongia, R. Dibble, and J. Lovett. Meaurement of air-fuel ratio fluctuations caused by combustor driven oscillations. *ASME Turbo. Expo.*, ASME#98–GT–304, 1998.

[6] D. S. Lee and T. J. Anderson. Measurements of fuel/air acoustic coupling in lean premixed combustion systems. 37th *AIAA Aerospace Sciences Meeting and Exhibit, Reno, NV, USA*, AIAA# 99-0450, 1999.

[7] J. G. Lee and D. Santavicca. Experimental diagnostics for the study of combustion instabilities in lean premixed combustors. *J. Propul. Power*, 19(5):pp. 735–750, 2003.

[8] H. M. Altay, R. L. Speth, D. E. Hudgins, and A. F. Ghoneim. The impact of equivalence ratio oscillation on combustion dynamics in a backward-facing step combustor. *Combust. Flame*, 156:2106–2116, 2009.

[9] J. C. Broda, S. Seo, R. J. Santoro, G. Shirhattikar, and V. Yang. Experimental study of combustion dynamics of a premixed swirl injector. *Proc. Combust. Inst.*, 27:1849–1856, 1998.

[10] T. Schuller, D. Durox, and S. Candel. Dynamics of noise radiated by a perturbed impinging premixed jet flame. *Combust. Flame*, 128:88–110, 2002.

[11] G. A. Richards and D. L. Straub. Effect of fuel nozzle configuration on premix combustion dynamics. *ASME Turbo Expo.*, ASME# 98-GT-492, 1998.

[12] K. T. Kim, J. G. Lee, B. D. Quay, and D. Santavicca. Experimental investigation of the non-linear response of swirl stabilized flames to equivalence ratio oscillations. *J. of Eng. in Gas Turb. and Power*, 133:021502 (8 pages), 2011.

[13] C. Paschereit, E. J. Gutmark, and W. Weisenstein. Structure and control of thermoacoustic instabilities in a gas turbine combustor. *Combust. Sci. and Tech.*, 138:213–232, 1998.

[14] A. Peracchio and W. M. Proscia. Nonlinear heat-release/acoustic model for thermoacoustic instability in lean premixed combustors. *J. of Eng. in Gas Turb. and Power*, 121:415–421, 1999.

[15] K. Schildmacher, R. Koch, and H. Bauer. Experimental characterisation of premixed flame instabilities in a model gas turbine burner. *Flow Turb. and Combust.*, 76:177–197, 2006.

[16] J. G. Lee, K. Kim, and D. Santavicca. Measurement of equivalence ratio fluctuation and its effects on heat release during unstable combustion. *Proc. Combust. Inst.*, 28:415–421, 2000.

[17] K. K. Venkataraman, L. H. Preston, D. W. Simons, B. J. Lee, and D. Santavicca. Mechanism of combustion instability in a lean premixed dump combustor. *J. Propul. Power*, 15:909–918, 1999.

[18] H. Schwarz, L. Zimmer, D. Durox, and S. Candel. Detailed measurements of equivalence ratio modulation in premixed flames using laser rayleigh scattering and absorption spectroscopy. *Expts. in. Fluids*, 49:809–821, 2010.

[19] P. Flohr, C. Paschereit, B. Van Roon, and B. Schuermans. Using cfd for time-delay modelling of premixed flames. *ASME Turbo Expo*, ASME#2001–GT–376, 2001.

[20] B. Schuermans, V. Belluci, F. Guethe, F. Meili, and P. Flohr. A detailed analysis of thermoacoustic interaction mechanisms in a turbulent premixed flame. *ASME Turbo Expo*, ASME# GT2004–53831, 2004.

[21] C. Angelberger, D. Veynante, and F. N. Egolfopoulous. Les of chemical and acoustic forcing of a premixed dump combustor. *Flow Turb. and Combust.*, 65:205–222, 2001.

[22] W. Polifke, J. Kopitz, and A. Serbanovic. Impact of the fuel time lag distribution in elliptical premix nozzles on combustion instability. *7th AIAA/CEAS Aeroacoustics Conference*, AIAA# 2001-2104, 2001.

[23] A. Birbaud, S. Ducruix, D. Durox, and S. Candel. The nonlinear response of inverted "v"-flames to equivalence ratio non-uniformities. *Combust. Flame*, 154:356–367, 2008.

[24] J. Jarosinski and B. Veyssiere. *Combustion Phenomena*. CRC Press, Boca Raton, FL, USA, p. 91, 2009.

[25] A. Birbaud. *Dynamique d'interactions sources des instabilités de combustion*. PhD thesis, Ecole centrale, Paris, Chatenay-Malabry, 2006.

[26] J. H. Cho and T. Lieuwen. Laminar premixed flame respone to equivalence ratio oscillations. *Combust. Flame*, 140:116–129, 2005.

[27] Shreekrishna, S. Hemchandra, and T. Lieuwen. Premixed flame respone to equivalence ratio perturbations. *Combust. Theor. and Modelling*, 14:681–714, 2010.

[28] N. Peters. *Turbulent combustion*. Cambridge University Press, UK, 2000.

[29] M. Fleifil, A. M. Annaswamy, Z. A. Ghoneim, and A. F. Ghoneim. Response of a laminar premixed flame to flow oscillations: A kinematic model and thermoacoustic instability results. *Combust. Flame*, 106(4):487–510, 1996.

[30] T. Schuller, D. Durox, and S. Candel. A unified model for the prediction of laminar flame transfer functions: comparisons between conical and v-flame dynamics. *Combust. Flame*, 134(1-2):765–774, 2003.

[31] Preetham, Santosh H., and T. C. Lieuwen. Dynamics of laminar premixed flames forced by harmonic velocity disturbances. *J. Propul. Power*, 394:51–72, 2008.

[32] S. Hemchandra. Direct numerical simulation study of premixed flame response to fuel-air ratio oscillations. *ASME Turbo Expo.*, ASME# GT2011-45590, 2011.

[33] C.K. Law and C.J. Sung. Structure, aerodynamics, and geometry of premixed flamelets. *Prog. Energy Combust. Sci.*, 26:459–505, 2000.

[34] J.-M. Truffaut and G. Searby. Experimental study of the darrieus-landau instability on an inverted-'v' flame, and measurement of the markstein number. *Combust. Sci. and Tech.*, 149:35–52, 1999.

[35] G. Searby, J.-M. Truffaut, and G. Joulin. Comparison of experiments and a nonlinear model equation for spatially developing flame instability. *Phys. of. Fluids*, 13(11):3270–3276, 2000.

Multiphase Flow Modeling and Simulation

S. Subramaniam*
Department of Mechanical Engineering
Iowa State University
Ames, IA 50011 USA

Abstract

This talk attempts to summarize the state-of-the-art in modeling and simulation of multiphase flows. Modeling multiphase flows is challenging because they are characterized by nonlinearities (arising from inertia and polydispersity of the dispersed phase), multiscale interactions and nonequilibrium effects that lead to phenomena such as preferential concentration and clustering, which have a significant impact on multiphase flow applications. Multiphase flow models can be classified on the basis of three critiera: (i) whether each phase is represented using a *random field* or *stochastic point process* description, (ii) whether each phase is represented in an Eulerian or Lagrangian reference frame, and (iii) the level of closure in the statistical theory. This classification allows us to compare the relative merits of many modeling approaches. Multiphase flow simulations are classified according to the length and time scales that they are capable of representing. Accordingly, we have simulation approaches ranging from molecular dynamics of single droplets through Fully–Resolved DNS (FR–DNS), point–particle DNS (PP–DNS), LES and RANS. Such a classification allows comparison of trade-offs between accuracy, problem complexity and computational cost that each of these simulation approaches represents. This classification of multiphase flow models and simulation techniques is intended to provide a framework for stimulating discussions at the workshop.

Multiphase Flow Models

As shown in Fig. 1, the two principal approaches are: (i) the *random field* approach in which both dispersed and carrier phases are represented as random fields in the Eulerian frame, and (ii) the *point process* approach in which the dispersed phase is represented as a stochastic point process in the Lagrangian frame and the carrier phase represented as a random field in the Eulerian frame. The random field approach at the closure level of moments leads to the Eulerian–Eulerian (EE) two–fluid theory in its ensemble–averaged [1, 2] and volume–averaged variants [3]. The Lagrangian–Eulerian (or Euler-Lagrange) approach corresponds to a closure of the point process approach at the level of the droplet distribution function (ddf) or number density function (NDF), with the carrier phase being represented in an Eulerian frame through a Reynolds–averaged Navier–Stokes (RANS) closure, Large Eddy Simulation (LES) or Direct Numerical Simulation (DNS).

*Email: shankar@iastate.edu

Random–field description

In statistical theories of turbulent single-phase flow, the Eulerian velocity field is represented as a random vector field [4]. A similar approach can be adopted for two–phase flows, but in addition to the velocity (and pressure) field it is also necessary to specify the location and shape of the dispersed-phase elements. The velocity field $\mathbf{U}(\mathbf{x}, t; \omega)$, which is defined in both thermodynamic phases, is a vector field that is defined at each point $\mathbf{x}$ in the flow domain in physical space, on the ωth realization. The dispersed–phase elements in that same realization are similarly described by a dispersed–phase indicator *field* $I_d(\mathbf{x}, t; \omega)$, which is unity for all points inside the dispersed–phase elements that are contained in the flow domain, and zero outside. Statistical theories based on random–field representations require the consideration of multipoint joint probability density functions, and these have not resulted in tractable engineering models even for single–phase turbulent flow [4, 5, 6].

The simplest multipoint theory based on the random–field representation that is useful to modelers is a two–point representation. A comprehensive *two–point* statistical description of two–phase

flows based on the random-field representation can be found in Sundaram and Collins [7]. Even in the homogeneous case the resulting two–point equations lead to many unclosed terms that need closure models. Therefore, most engineering models currently rely on a simpler single–point theory.

Two–fluid theory

If statistical information at only a single space–time location $(\mathbf{x}, t)$ of the random–field representation is considered, this results in a single–point Eulerian–Eulerian two–fluid theory. In this case the statistics of the velocity field $\mathbf{U}(\mathbf{x}, t; \omega)$, and the dispersed–phase indicator field $I_d(\mathbf{x}, t; \omega)$, are considered at a single space–time location, i.e., the indicator *field* reduces to an indicator *function*. The velocity and indicator function can be treated as random variables (or random vector in the case of velocity) *parametrized* by space and time variables. The averaged equations resulting from this approach are described in Drew [1], and Drew and Passman [2]. The single–point Eulerian–Eulerian theory can be developed at the more fundamental level of probability density functions also, and this theory is described in Pai and Subramaniam [8].

Lagrangian representation of the dispersed phase

An alternative approach is to describe the dispersed–phase consisting of N_s solid particles or spray droplets using Lagrangian coordinates $\{\mathbf{X}^{(i)}(t), \mathbf{V}^{(i)}(t), R^{(i)}(t), i = 1, \ldots, N_s(t)\}$, where $\mathbf{X}^{(i)}(t)$ denotes the ith dispersed–phase element's position at time t, $\mathbf{V}^{(i)}(t)$ represents its velocity, and $R^{(i)}(t)$ its radius. The rigorous development of a statistical theory of multiphase flows [9] using the Lagrangian approach relies on the *theory of stochastic point processes* [10], which is considerably different from the *theory of random fields* [4, 11, 12] that forms the basis for the Eulerian-Eulerian approach. Starting from the definition of the ddf one can derive [13] the following collisionless form of the ddf evolution equation (also referred to as the spray equation) that corresponds to the droplet evolution equations:

$$\frac{\partial f}{\partial t} + \frac{\partial}{\partial x_k}[v_k f] + \frac{\partial}{\partial v_k}\left[\langle A_k | \mathbf{x}, \mathbf{v}, r; t\rangle f\right] + \frac{\partial}{\partial r}\left[\langle \Theta | \mathbf{x}, \mathbf{v}, r; t\rangle f\right] = 0. \quad (1)$$

In the above equation $\langle A_k | \mathbf{x}, \mathbf{v}, r; t\rangle$ represents the expected acceleration conditional on the location $[\mathbf{x}, \mathbf{v}, r]$ in phase space. Similarly $\langle \Theta | \mathbf{x}, \mathbf{v}, r; t\rangle$ represents the expected rate of change of radius (hereafter referred to as the expected vaporization rate) conditional on the location $[\mathbf{x}, \mathbf{v}, r]$ in phase space.

Multiphase Flow Simulations

Figure 2 shows simulation approaches ranging from molecular dynamics of single droplets through Fully–Resolved DNS (FR–DNS), point–particle DNS (PP–DNS), LES and RANS. Frequently LE methods couple Lagrangian tracking of computational particles to a carrier flow description based on Reynolds–averaged Navier–Stokes (RANS) equations. However, it is possible to use the LE approach to couple a Lagrangian description of the dispersed phase with large eddy simulations (LES) or direct numerical simulation (DNS) of the carrier gas phase, resulting in the following principal categories of LE methods:

1. Fully–resolved DNS (FR-DNS) of droplet or particle-laden flow where the exact Navier-Stokes equations are solved by fully resolving the droplet or particle by imposing boundary conditions at each particle or droplet's surface [14, 15, 16, 17, 18, 19, 20, 21, 22, 23]
2. Point-particle DNS (PP-DNS) with physical droplets or particles [24, 25, 26, 27, 28, 29, 30]
3. PP-DNS with stochastic particles [31]
4. Point particle LES with physical droplets [32, 33]
5. Point particle LES with stochastic particless [34, 35, 36]
6. Averaged equations: RANS CFD

The principal difference between the FR-DNS and PP-DNS is that while the former can be used to quantify the interphase models, the PP-DNS involve assumed models for interphase transfer terms such as particle acceleration and droplet vaporization. The treatment of collisions can also be used to categorize LE methods as those that employ a statistical treatment of collisions [37, 38, 39] in contrast to direct calculation of collisions between particles using either hard–sphere collisions [40] for low volume fraction or soft–sphere discrete element method (DEM) collision models [41, 42, 43] for high volume fraction [44]. The classification shown in Fig 2 allows a comparison of trade-offs between accuracy, problem complexity and computational cost that each of these simulation approaches represents.

References

[1] D. A. Drew. Mathematical modeling of two–phase flow. *Annu. Rev. Fluid Mech.*, 15:261–291, 1983.

[2] D. A. Drew and S. L. Passman. *Theory of Multicomponent Fluids*. Applied Mathematical Sciences. Springer, New York, 1998.

[3] M. Ishii. *Thermo–fluid dynamic theory of two–phase flow*. Eyrolles, Paris, France, 1975.

[4] S. B. Pope. *Turbulent Flows*. Cambridge University Press, Port Chester, NY, 2000.

[5] A. S. Monin and A. M. Yaglom. *Statistical Fluid Mechanics II*. MIT Press, 1975.

[6] E. Hopf. Statistical hydromechanics and functional calculus. *Journal of Rational Mechanics and Analysis*, 1:87–123, 1952.

[7] Shivshankar Sundaram and Lance R. Collins. A numerical study of the modulation of isotropic turbulence by suspended particles. *J. Fluid Mech.*, 379:105–143, 1999.

[8] M. G. Pai and S. Subramaniam. A comprehensive probability density function formalism for multiphase flows. *J. Fluid Mech.*, 628:181–228, 2009.

[9] S. Subramaniam. Statistical representation of a spray as a point process. *Phys. Fluids*, 12(10):2413–2431, 2000.

[10] D. J. Daley and D. Vere-Jones. *An Introduction to the Theory of Point Processes*. Springer–Verlag, New York, 1988.

[11] S. Panchev. *Random functions and turbulence*. Pergamon Press, New York, 1971.

[12] R. J. Adler. *The geometry of random fields*. SIAM, Chichester, NY, 1981.

[13] S. Subramaniam. Statistical modeling of sprays using the droplet distribution function. *Phys. Fluids*, 13(3):624–642, 2001.

[14] Ying Xu and Shankar Subramaniam. Effect of Particle Clusters on Carrier Flow Turbulence: A Direct Numerical Simulation Study. *Flow, Turbulence and Combustion*, 85(3-4):735–761, September 2010.

[15] P. Bagchi and S. Balachandar. Effect of turbulence on the drag and lift of a particle. *Physics of Fluids*, 15(11):3496, 2003.

[16] Markus Uhlmann. An immersed boundary method with direct forcing for the simulation of particulate flows. *Journal of Computational Physics*, 209(2):448–476, November 2005.

[17] S. E. Elghobashi and G. C. Truesdell. Direct simulation of particle dispersion in a decaying isotropic turbulence. *J. Fluid Mech.*, 242:655–700, 1992.

[18] Z Zhang and a Prosperetti. A second-order method for three-dimensional particle simulation. *Journal of Computational Physics*, 210(1):292–324, November 2005.

[19] Shaoping Quan, David P. Schmidt, Jinsong Hua, and Jing Lou. A numerical study of the relaxation and breakup of an elongated drop in a viscous liquid. *Journal of Fluid Mechanics*, 640:235, October 2009.

[20] Mikhael Gorokhovski and Marcus Herrmann. Modeling Primary Atomization. *Annual Review of Fluid Mechanics*, 40(1):343–366, January 2008.

[21] M Herrmann. A balanced force refined level set grid method for two-phase flows on unstructured flow solver grids. *Journal of Computational Physics*, 227(4):2674–2706, February 2008.

[22] A. Esmaeeli and G. Tryggvason. Direct numerical simulation of bubbly flows. Part 1. Low Reynolds number arrays. *J. Fluid Mech.*, 377:313–345, 1998.

[23] S. Tenneti, R. Garg, and S. Subramaniam. Drag law for monodisperse gas–solid systems using particle-resolved direct numerical simulation of flow past fixed assemblies of spheres. *International Journal of Multiphase Flow*, 37(9):1072–1092, November 2011.

[24] K. D. Squires and J. K. Eaton. Measurements of particle dispersion obtained from direct numerical simulations of isotropic turbulence. *J. Fluid Mech.*, 226:1–35, 1991.

[25] Kyle D Squires and John K Eaton. Lagrangian and Eulerian statistics obtained from direct numerical simulations of homogeneous turbulence. *Physics of Fluids*, 3(1):130–143, 1991.

[26] Lian-Ping Wang, Bogdan Rosa, Hui Gao, Guowei He, and Guodong Jin. Turbulent collision of inertial particles: Point-particle based, hybrid simulations and beyond. *International*

Journal of Multiphase Flow, 35(9):854–867, September 2009.

[27] F. Mashayek. Direct numerical simulations of evaporating droplet dispersion in forced low Mach number turbulence. *Intl. J. Heat Mass Transfer*, 41(17):2601–2617, 1998.

[28] F. Mashayek and F. A. Jaberi. Particle dispersion in forced isotropic low–Mach–number turbulence. *Intl. J. Heat Mass Transfer*, 42(15):2823–2836, 1999.

[29] Shivshankar Sundaram and Lance R. Collins. Collision statistics in an isotropic particle–laden turbulent suspension. part i. direct numerical simulations. *J. Fluid Mech.*, 379:75–109, 1997.

[30] R. S. Miller and J. Bellan. Direct numerical simulation of a confined three-dimensional gas mixing layer with one evaporating hydrocarbon-droplet-laden stream. *Journal of Fluid Mechanics*, 384:293–338, April 1999.

[31] Boivin, M. and Simonin, O. and Squires, K.D. Direct numerical simulation of turbulence modulation by particles in isotropic turbulence. *Journal of Fluid Mechanics*, 375:235–263, November 1998.

[32] Okong'o ; Josette Bellan Nora. A priori subgrid analysis of temporal mixing layers with evaporating droplets. *Physics of Fluids*, 12(6):1573–1591, June 2000.

[33] S V. Apte, K. Mahesh, P. Moin, and J.C. Oefelein. Large-eddy simulation of swirling particle-laden flows in a coaxial-jet combustor. *International Journal of Multiphase Flow*, 29(8):1311–1331, August 2003.

[34] T Almeida and F Jaberi. Large-eddy simulation of a dispersed particle-laden turbulent round jet. *International Journal of Heat and Mass Transfer*, 51(3-4):683–695, February 2008.

[35] Nora a. Okong'o and Josette Bellan. Consistent large-eddy simulation of a temporal mixing layer laden with evaporating drops. Part 1. Direct numerical simulation, formulation and a priori analysis. *Journal of Fluid Mechanics*, 499:1–47, January 2004.

[36] Sourabh V. Apte, Krishnan Mahesh, Michael Gorokhovski, and Parviz Moin. Stochastic modeling of atomizing spray in a complex swirl injector using large eddy simulation. *Proceedings of the Combustion Institute*, 32(2):2257–2266, 2009.

[37] P. J. O'Rourke. *Collective Drop Effects on Vaporizing Liquid Sprays*. PhD thesis, Princeton University, 1981.

[38] D. P. Schmidt and C. J. Rutland. A new droplet collision algorithm. *J. Comput. Phys.*, 164(1):62–80, 2000.

[39] P. J. O'Rourke, Paul (Pinghua) Zhao, and Dale Snider. A model for collisional exchange in gas/liquid/solid fluidized beds. *Chemical Engineering Science*, 64(8):1784–1797, April 2009.

[40] M. P. Allen and D. J. Tildesley. *Computer Simulation of Liquids*. Oxford University Press, Oxford, United Kingdom, 1989.

[41] H G Matuttis, S Luding, and H J Herrmann. Discrete element simulations of dense packings and heaps made of spherical and non-spherical particles. *Powder Technology*, 109(1-3):278–292, 2000.

[42] M. Alam and S. Luding. Rheology of bidisperse granular mixtures via event-driven simulations. *J. Fluid Mech.*, 476:69–103, 2003.

[43] P. A. Cundall and O. D. L. Strack. A discrete numerical model for granular assemblies. *Geotechnique*, 29:47–65, 1979.

[44] Jin Sun, Francine Battaglia, and Shankar Subramaniam. Hybrid Two-Fluid DEM Simulation of Gas-Solid Fluidized Beds. *Journal of Fluids Engineering*, 129(11):1394, 2007.

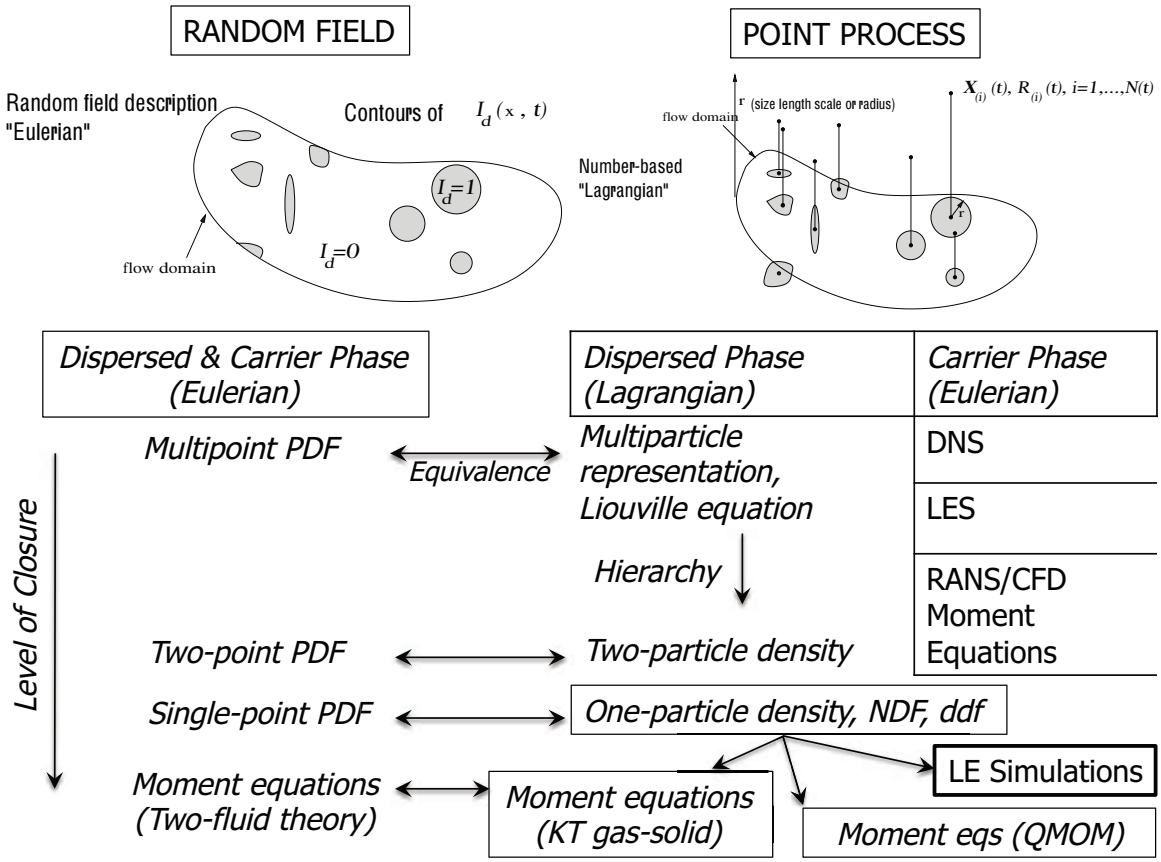

Figure 1: Representations of multiphase flow as random fields or a point process embedded in a random field, leading to the EE and LE approaches, respectively. Both approaches can be used at different levels of closure, and their equivalence is indicated.

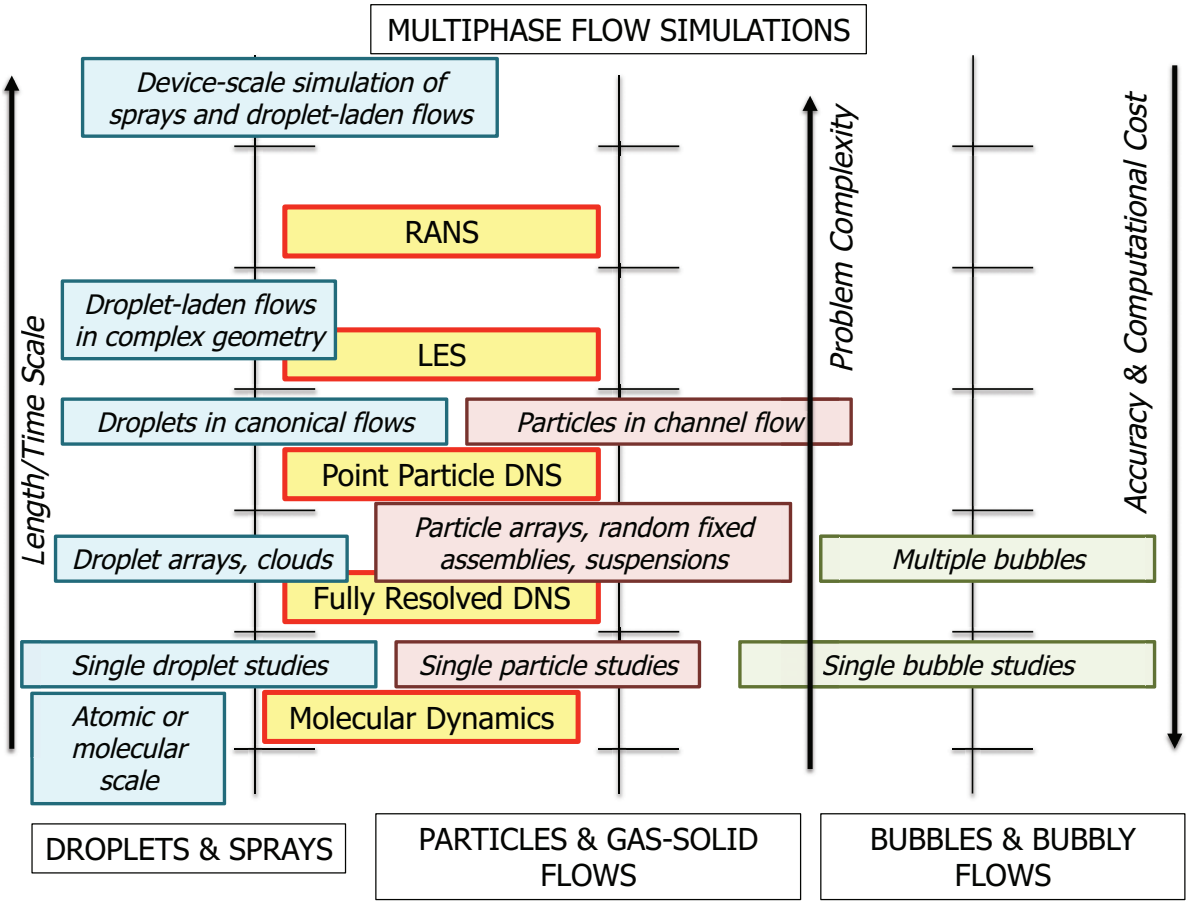

Figure 2: Classification of multiphase flow simulation approaches by scale, accuracy, computational cost, and problem complexity.

Prediction of drop size and velocity distributions in a spray for the simulation of liquid fuel combustion

Amitava Datta
Department of Power Engineering, Jadavpur University
Salt Lake Campus, Kolkata 700 098, India.

Motivation

The atomization of liquid fuel and subsequent vaporization and mixing of fuel spray with air in the combustor play a key role in the process of combustion and formation of pollutants. Odgers et al. [1] reported, from their experimental studies, a marginal increase in combustion efficiency with larger droplets and attributed the fact to droplet penetration as a probable cause. Datta and Som [2] performed a numerical study of spray combustion in a gas turbine can combustor to study the effect of initial spray characteristics. They reported that the combustion efficiency becomes the maximum at an optimum mean diameter (SMD) of the droplets in the spray. Droplet diameter and exhaust composition measurements in gas turbine combustors confirm that the initial droplet size is also a key factor in emission levels from the combustor [3]. Stochastic separated flow approach (SSF) is widely considered to be suitable for modeling liquid fuel combustion in gas turbine combustor. The separated flow analysis employs the Particle-Source-In-Cell (PSIC) approach and divides the spray into a finite number of representative droplet classes considering the poly-dispersity of the spray. The motion and transport of each droplet class through the flow field are determined using a Lagrangian formulation; while an Eulerian formulation is used to solve the conservation equations in the gas phase. The initial size and velocity of the droplets in the spray serve as the initial condition in the tracking of the droplet trajectories.

Empirical Distribution Functions for Drop Size Distribution

The empirical relation of Rosin and Rammler [4] is widely applied for droplet size distribution in a liquid spray for its mathematical simplicity and possibility of extrapolating it to very fine droplet sizes. Nukiyama and Tanasawa [5] developed an exponential function with four parameters to represent a drop size distribution in sprays from a pneumatic atomizer. Later on, Mugele and Evans [6] developed the upper limit function as a modified expression of log normal distribution function by specifying a maximum droplet size. Rizk and Lefebvre [7] introduced a modification to the Rosin-Rammler formula to provide a better data fit for larger droplet sizes. Bhatia et al. [8] applied the log hyperbolic distribution with four parameters to predict a size distribution function of droplets in sprays, which gives good fit to a wide range of experimental data. However, the drawback of the model lies in the difficulty of computing mathematically stable fitting parameters for the distribution. The three parameter log- hyperbolic distribution proposed by Xu et al. [9] solved the problem of numerical instability during the parameter determination at the cost of slightly inferior fit. The empirical distribution functions can be used for the initial prediction of the spray in the simulation of liquid fuel combustion.

Analytical Methods for drop size prediction

The empirical distribution functions have limited use as none of them has the universal predictive capability for different atomizers and different ambient conditions. In order to overcome these limitations, two different analytical methods had been prescribed [10] for modeling the drop size and velocity distributions in a spray, viz. the discrete probability function (DPF) method and the maximum entropy formulation (MEF) method.

The DPF model divides the atomization process into a deterministic and a non-deterministic part. First, the model deterministically predicts a specific mean diameter of the spray for a given set of flow conditions. Then the non-deterministic part of the model describes the influence of fluctuating initial and flow conditions on the resulting droplet size distribution through suitable probability distribution functions. The fluctuations can be due to the vibrations in the nozzles, variations in the liquid flow rate, liquid sheet velocity at the nozzle exit and fluid physical properties. Tharakan and Ramamurthi [11] have applied the discrete probability distribution function method to the breakup of planar liquid sheets, while Sovani et al. [12] used it to investigate the effervescent atomization of a Newtonian liquid. The main drawback of the process lies in considering the correct probability distribution functions for each of the fluctuating conditions.

The maximum entropy formulation (MEF) method, which is based on the information entropy theory, is the more established method for predicting droplet size and velocity distributions. Information theory defines a term called information entropy or Shannon's entropy [13], which takes a maximum value for the most probable distribution of a variable under the restrictions of constraint conditions describing the physical phenomena. The application of MEF principle to spray modeling was introduced by Li, Tankin and their co-workers [14, 15, 16] as also by Sellens, Brzustowski and their co-workers [17, 18, 19, 20]. These works as well as many other works for the prediction of spray size and velocity distributions using MEF models have been excellently reviewed by Dumouchel [21].

MEF based Spray Prediction Models

MEF method predicts the most likely droplet size and velocity distributions through the maximization of information entropy, under a set of constraint conditions expressing the available information about the disintegration process. The constraint equations can be formulated by conserving the mass, momentum and energy across the atomization process. The models proposed by Li *et al.* [14, 15, 16] and Sellens *et al.* [17, 18, 19] differ in the energy conservation aspect for describing the droplet distribution functions. Li and Tankin [15] considered the conservation of the sum of surface energy and kinetic energy across the zone of atomization. On the other hand, Sellens and Brzustowski [17] argued that the conservation of total energy may overlook some important information concerning irreversibility of certain energy transformations, e.g. translational kinetic energy can be readily transformed to surface energy but the reverse is not possible.

The other difference in the formulation of Sellens' group and Tankin's group is that while the former defined the droplets in terms of number based distribution the latter chose a volume based distribution for the purpose. The number based drop diameter distribution of Sellens and Brzustowski demonstrated an unrealistic situation near the smallest diameter, as the probability does not decrease to zero as the diameter reaches zero value. However, in Li and Tankin's solution the probability shows the expected trend at small diameter and reaches zero when the drop diameter becomes zero. To overcome this drawback, Sellens [19] used an additional constraint condition in the form of "partition of surface energy" in the formulation. The partition of surface energy refers to the surface to volume ratio for all the droplets in a spray, which is unknown a priori. As a result, the agreement with the experimental results necessitates repetitive trials by adjusting this quantity. Ahmadi and Sellens [20] developed a MEF based model for droplet size distribution considering conservation of mass, surface energy and partition of surface energy as the constraints. In their model, the droplet size distribution becomes independent of drop velocity as the velocity information is carried only in the momentum and kinetic energy terms. Cousin et al. [22] used the conclusion of Ahmadi and Sellens and formulated a MEF model for the prediction of droplet size distribution using a single mean drop diameter, termed as constraint diameter, to build the constraint equation. Some other attributes of MEF models for the predictions of droplet size distribution have been addressed in the work of Malot and Dumouchel

[23] and Dumouchel [24, 25, 26]. On the other hand, Van der Geld and Vermeer [27] investigated the effect of satellite drop formation on the droplet size distribution in their MEF model. Mondal et al. [28] predicted the droplet size distribution for a pressure swirl atomizer using the empirical characterizing parameters for the swirl spray nozzle, such as sheet thickness, spray cone angle and Sauter mean diameter (SMD), in their constraint equations. They later extended the model to predict the joint size and velocity distribution of the droplets in the spray from similar nozzles [29].

MEF theory has been applied on various types of atomizers, like plain jet atomizer [23], pressure swirl atomizer [22, 29], twin fluid atomizer [30] and ultrasonic atomizer [24], for predicting the resultant drop size distributions. Mitra and Li [31] coupled the breakup analysis of liquid sheet with the MEF model to predict the droplet size distribution in a spray. They used linear stability analysis to predict the mass mean diameter (d_m) and an empirical model for evaluating the breakup length. Boundary layer theory was used to evaluate the momentum and energy source terms and Shannon entropy was maximized to get the droplet size distribution. Later on Mitra [32] replaced Shannon entropy with another form of information entropy, called Bayesian entropy, in describing the MEF model for droplet size and velocity distributions in the liquid spray. However, this method requires the assumption of a size distribution in order to obtain the actual distribution of droplet diameters. Recently, Nath et al. [33] coupled a nonlinear break up analysis of a planar liquid sheet with the MEF based model to predict the droplet size and velocity distributions in a spray.

Summary and Conclusions

Though the MEF based modeling technique of droplet size prediction is almost three decades old, there are some issues which are yet to be resolved fully. The success of a MEF model lies in formulating the correct constraint equations which can supply all the necessary information regarding the event. Sirignano and Mehring [34], while analyzing the break up of a round jet, showed that a part of the liquid surface energy causes an oscillatory kinetic energy in the droplet, which dissipates into internal energy as a result of viscous action. Though the dissipation increases the internal energy only by a small amount, Sirignano and Mehring [34] hypothesized that internal energy could also be accounted in the conservation of energy equation for maximum entropy formulation for the prediction of droplet size and velocity distributions. However, the contribution of this consideration on the predicted results has not been shown explicitly in the literature and could be taken into consideration. Dumouchel [21] further questioned the use of total energy conservation for the prediction of spray characteristics citing that the energy source responsible for atomization is not the directed kinetic energy but the turbulent and circulatory kinetic energy. A final consensus to this effect has not yet been reached. Moreover, the conservation equations normally considered for formulating the constraint conditions in MEF results into the higher order moments in diameter and velocity, while one school of thought considers the lower order moments have the greatest influence on the shape of the PDF. The argument goes as the distribution with only the higher order moments may not be sufficiently reliable. Another critical observation is that most of the MEF prediction for different spray systems results in a mono-modal distribution of the droplet size, while in practice more complex distributions, like bi-modal, is also observed. Further studies in the subject with necessary experimental validations can overcome the prevailing doubts. Experiments on the variation of velocity of the droplets generated from a spray are sparse in the literature and therefore validation of droplet velocity distribution predicted by MEF model is hardly found. However, this is an important information for the simulation of the spray combustion process, as the variation in the initial velocity of the droplets can affect their trajectory in the combustion chamber. For a comprehensive prediction of spray characteristics it is also required to know the right break up mechanism of the sheet or jet issuing from the atomizer. This is another area on which further studies are to be conducted.

Acknowledgement
I gratefully acknowledge the contributions of my students, Sujit Nath and Dulal Mandal and my colleagues, Profs. Achintya Mukhopadhyay, Swarnendu Sen and Amitava Sarkar, with whom I have worked on the subject.

References

1. Odgers, J., Kretschmer, D., Pearce, G.F., *ASME J. of Engg. for Gas Turbine and Power*, 115, p. 522, 1993
2. Datta, A., Som, S.K., *Int. J. Energy Res*., 23, 217-228, 1999.
3. Colby, J.A., Menon, S., Jagoda, J., Paper no. GT2006-90974, pp. 753-762, ASME Turbo Expo 2006.
4. Rosin, P., Rammler, E., *J. Inst. Fuel*, 31, 29-36, 1933.
5. Nukiyama, S., Tanasawa, Y., *Trans. Soc. Mech. Eng. Jan.*, 5, 62-67, 1939.
6. Mugele, R.A., Evans, H.D., *J.Ind.Eng.Chem.*,43,pp. 1317-1324, 1951.
7. Rizk, N.K., Lefebvre, A.H., *AIAA J. Propul. Power*, 1, pp. 16-22, 1985.
8. Bhatia, J.C., Dominick, J., Drust, F., Tropea, C., *Part. Part. Syst. Charact*., 5, 153-164, 1988.
9. Xu, T.H., Durst, F., Tropea, C., *Proc.Int.Conf.Liquid Atomization Spray Systems*, pp. 316-331, 1991.
10. Babinsky, E., Sojka, P.E., *Prog. Energy Combust. Sci.*, 28, 303-329, 2002.
11. Tharakan, T.J., Ramamurthi, K., *Atomisation and Sprays*, 15, 181-200, 2005.
12. Sovani, S.D., Sojka, P.E., Shivathanu, Y.R. , *Atomization and Sprays*, 9, 133-152, 1999.
13. Shannon, C. E., *Bell System Tech. J*., 379-623, 1948.
14. Li., X., Tankin, R.S., *Combust. Sci. Technol.*, 60, 345-357, 1988.
15. Li , X., Tankin, R.S., *Combust.Sci.Technol.*, 68, 147-155, 1989.
16. Li, X., Tankin, R.S., *Part.Part.Syst. Charact.*, 9, 195-201, 1992.
17. Sellens, R.W., Brzustowski, T.A., *Atomization Spray Technol.*, 1, 195-201, 1985.
18. Sellens, R.W., Brzustowski, T.A., *Combust. Flame*, 65, 273-279, 1986.
19. Sellens, R.W., *Part.Part.Syst. Charact.*, 6, 17-27, 1989.
20. Ahmadi, M., Sellens, R.W., *Atomization and Sprays*, 3, 291-310, 1993.
21. Dumouchel, C., *Entropy*, 11, 713-747 , 2009.
22. Cousin, J., Yoon, S.J., Dumouchel, C., *Atomization Sprays*, 6, 601-622, 1996.
23. Malot, H. and Dumouchel, C., H., *In Proceedings of ILASS–Europe 2001, Zürich*, 2001.
24. Dumouchel, C., Sindayihebura, D., Bolle, L., *Part. Part. Syst. Charact*., 20, 150-161, 2003.
25. Dumouchel, C., *Part. Part. Syst. Charact*., 23, 468-479, 2006.
26. Dumouchel, C., Boyaval, S., *Part. Part. Syst. Charact*., 16, 177-184, 1999.
27. VanDer Geld, C.W.M., Vermeer, H., *Int. J. Multiphase Flow*, 20, 363-381, 1994.
28. Mondal, D., Datta, A., Sarkar, A., *Proc. Instn Mech. Engrs, Part: C* , 217(C7), 831-838, 2003.
29. Mondal, D., Datta, A., Sarkar, A., *Proc. Instn Mech. Engrs, Part:C*, 218(C7), 737-749, 2004.
30. Lecompte, M., Dumouchel, C., *Part. Part. Syst. Charact*., 25, 154-167, 2008.
31. Mitra, S.K., Li, X., *Atomization and Sprays*, 9, 29-50, 1999.
32. Mitra, S. K., *PhD. thesis*, University of Waterloo, Waterloo, Ontario, Canada, 2001.
33. Nath, S., Mukhopadhyay, A., Datta, A., Sen, S. and Tharakan, T.J., Prediction of size and velocity distributions in sprays formed by the break up of planar liquid sheets using maximum entropy formalism Atomization Sprays, 20, under review, 2011.
34. Sirignano, W.A. and Mehring, C., Prog. Energy Combust. Sci., 26, 609–655, 2000.

Spray impingement studies for biofuels

Anand T N C and Shamit Bakshi

Biofuels are becoming more important and relevant than ever before in the Indian context, both as a potential fuel for use in India, and also from an energy security point of view. Whereas the use of straight vegetable oils (SVOs) in engine is more challenging, the esterified version of non-edible vegetable oils is already being used directly or more frequently as blends with conventional fuels. One well known problem as we move from fossil fuel to bio-fuels is the decreasing volatility of the fuel. This makes the process of spray impingement unavoidable for direct injection engines where the use of the fuel is envisaged. Studies on spray impingement in general are not abundant in literature and the same for bio-fuels are very few. The efficient use of bio-fuels in engines requires extensive study of these fuels in terms of spray characterization, evaporation and spray/droplet wall interaction. These studies are of direct relevance in developing technologies which can enable the efficient utilization of biofuels in engines, and also to develop and validate models which can enable engine optimization using computational fluid dynamics (CFD). Taken together, these studies are even more relevant now when researchers in other parts of the world are working towards a ‘designer’s bio-fuel’. As rapid strides in fuel processing and synthesis takes place, it is important for the scientific community to identify the effect of fuel properties keeping in mind the various processes which take place. This will help identify the properties desired of a dream fuel, the synthesis of which is likely to become possible in the near future.

The spray characteristics are important parameters for all direct injection engines. In this regard, it is important to characterize a bio-fuel spray and compare it with that of a conventional fuel. Additionally, it is important to look at spray impingement for biofuels as it is apparent from earlier studies that the slow evaporation of biofuels will definitely lead to impingement of the spray onto the piston surface. Although a number of studies exist in the literature pertaining to the impact of single droplet onto a dry and wet surface, the literature on spray impact onto a

surface is very limited. A recent review on the spray impact and how single droplet studies are important in understanding spray impact is given by Moreira et al. [1]. Spray impact as compared to a single drop impact is influenced by more parameters like the influence of the neighbouring and/or previous drops, the film surface fluctuation, film height, film velocities, crown-crown interactions etc. Sivakumar et al. [2] present one of the first studies on the extent of these effects in a spray wall interaction process. It is concluded from their study that the spray impingement cannot be explained as a superposition of individual drop impacts, or even by accounting for drop-drop or drop-crown interaction. Liquid film velocities and film heights can strongly influence the secondary breakup. An experimentally obtained threshold limit for splash in case of a single droplet impact onto a dry or wet surface is given by Cossali et al. [3]. This is given as, $K=We*Oh^{-0.4}$, where K is the discriminating variable for splash, which depends on the surface conditions (roughness for a dry surface and the thickness of the film for a wet surface), We is the Weber number and Oh is the Ohnsorge number. The impact of film thickness on the formation and time evolution of the traversing rim was studied by Cossali et al [4]. They studied the drop formation by secondary atomization after drop impact onto a film and found that for the configuration and parameter range used by them, the impact of film thickness is only limited. Panao et al. [5] studied the impingement characteristics of a pulsating gasoline spray which is used for manifold injection with a hollow-cone PFI injector. They used PDA systems to characterize the free spray (spray without the target) and the spray impinging onto a small disc. The comparison of droplet size distribution and drop velocities throws light into the mechanism of secondary atomization. Their study suggests that splash is the primary mechanism of secondary atomization. A large fraction of the droplets in the stagnation region are seen to adhere to the surface which feeds momentum into the film for crown formation. It is apparent from their study that it is important to include the spread and dynamics of the liquid film in impingement modelling. The outer spray is influenced by the entrainment from the convective vortex which can cause reimpingement of the entrained droplets. In a later paper, Panao et al. [6] extended this work and suggested that the effect of the film dynamics can be captured in a model possibly by modelling the fractions of mass, momentum and energy transfer between the spray, liquid film and the outgoing droplets. This way, the effect of film dynamics can be captured without going into the details of the local variations in the film. Roisman et al. [7] studied the spray impaction

process onto a target both theoretically and experimentally. They proposed an empirical model for the secondary spray based on the experimental data by using phase Doppler anemometry. In this model, the secondary spray is described as an average using integral parameters of the primary spray. Kalantari et al. [8] also studied the spray impact onto a target by using phase Doppler technique and high-speed photography. They studied the development of crown height with time for impact of individual droplets in a spray. The mismatch between these results and the single droplet impact results observed, and the differences are attributed to the local film velocity fluctuations. Randy et al. [9] studied single droplet impact onto a film with variable film heights. They observed that thin films can promote splashing whereas larger film thickness can inhibit it. Even in absence of strong film dynamics induced by the spray, the film height can substantially change the splash thresholds and the secondary atomization.

From the literature presented, one thing is very clear: the spray impingement onto a surface cannot be explained as the superposition of several single drop impacts. Particularly, the film dynamics introduced by the impingement process itself strongly influences the secondary atomization process. As pointed out in the recent review article [1], the effect of surface properties on secondary atomization is not available in the literature. The literature on spray impact onto heated surface is also very sparse. These effects can possibly be studied for bio fuel sprays, as it is apparent that such a spray will definitely impinge onto the piston surface. Measures to tailor the piston surface and its temperature can help in improving secondary atomization (post impingement) characteristics.

References:

1. Moreira, A.L.N., Moita, A.S., Panao, M.R., ‘Advances and challenges in explaining fuel spray impingement: How much of single droplet impact research is useful?’, Progress in Energy and Combustion Science, 36 (2010) 554–580.
2. Sivakumar D, Tropea C., ‘Splashing impact of a spray onto a liquid film’, Phys Fluids, 14 (2002) L85–L88.

3. Cossali G.E., Coghe A., Marengo M., ‘The impact of a single drop on a wetted solid surface’, Exp Fluids, 22 (1997) 463–72.
4. Cossali G.E., Marengo M., Coghe A., Zhdanov S., ‘The role of time in single droplet splash on thin film’, Exp Fluids, 36 (2004) 888–900.
5. Panao, M.R.O., Moreira A.L.N., ‘Experimental study of the flow regimes resulting from the impact of an intermittent gasoline spray’, Exp Fluids, 37 (2004) 834–55.
6. Panao, M.R.O., Moreira A.L.N., ‘Flow characteristics of spray impingement in PFI injection systems’, Exp Fluids, 39 (2005) 364–74.
7. Roisman I.V., Horvat K., Tropea C., ‘Spray impact: rim transverse instability initiating fingering and splash: description of a secondary spray’, Phys Fluids, 18 (2006) 102104.
8. Kalantari D., Tropea C., ‘Phase Doppler measurements of spray impact onto rigid walls’, Exp Fluids, 43 (2007) 285–296.
9. Randy L., VanderWal G., Berger M., Mozes S.D., ‘Droplets splashing upon films of the same fluid of various depths’, Exp Fluids, 40 (2006) 33–52.

Studies on Atomization and Sprays of Plant Oil Biofuels

Devendra Deshmukh and R. V. Ravikrishna
Department of Mechanical Engineering
Indian Institute of Science, Bangalore

Introduction

With depleting petroleum resources, the world needs to find safe, sustainable and cost effective alternative fuel for automotive engines. Non-edible plant oils such as Pongamia and Jatropha are being considered as important partial or complete substitutes for diesel to reduce dependence on fossil fuels. The use of plant oils (also called as Straight Vegetable Oil or SVO) have significance over biodiesel as they do not require any processing after crushing hence keeping the cost of production lower. The performance of diesel engine and its emissions are significantly affected by the spray characteristics and sub- sequent mixture formation. While considering these oils as replacement fuels in diesel engines, it is important to study the spray behaviour of these fuels. The physical properties such as viscosity, density and surface tension are the main properties affecting spray atomization. These properties, mainly viscosity and surface tension are known to have adverse impact on atomization of the spray.

The literature on sprays of plant oils shows that there is a need for fundamental studies in terms of spray formation (atomization and evaporation) and combustion of these oils to improve the engine efficiency and emission performance. Furthermore, there is no study on detailed spray characterization of non-edible plant oils such as Jatropha and Pongamia. There is also a need for spray tip penetration correlation for such fuels. In the present work, a detailed spray characterization of Pongamia oil and its blends with diesel at various injection pressures and gas pressures is studied for the first time. The spray characteristics, tip penetration, cone angle, SMD and liquid volume fraction distribution are measured for Pongamia oil, P20 blend (20% Pongamia + 80% diesel by volume), P50 blend (50% Pongamia + 50% diesel by volume) and diesel. The spray tip correlation for diesel is modified to take into account the different liquid viscosity. The modified correlation is verified for the Pongamia oil and its blends.

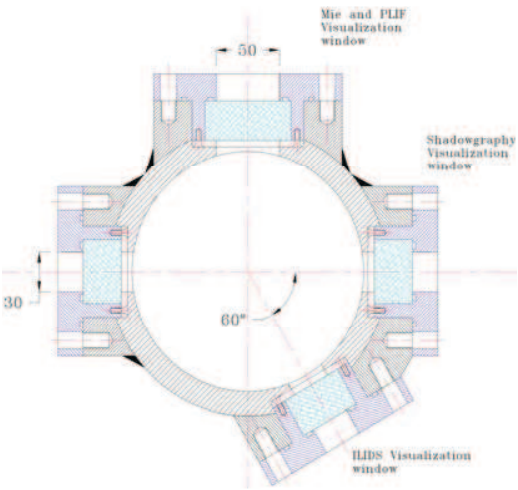

(a) Visualization window arrangement

(b) High pressure chamber

Figure 1: The high pressure spray visualization chamber.

High pressure spray visualization facility

A spray visualization facility is designed and developed to characterize the high pressure spray. A high pressure, constant volume chamber is designed for spray visualization up to gas pressures of 60 bar and gas temperatures of 600 K. The chamber is fabricated using a stainless steel (SS-304) cylinder with inner diameter of 182 mm, height of 300 mm and wall thickness of 20 mm. A solenoid injector and temperature and pressure sensors are mounted on the top plate. The optical access inside the chamber is provided using four, 30-mm thick quartz windows placed along the periphery of the chamber (Fig. 1). Two windows placed diametrically opposite are used for the shadowgraphy and PDIA (Particle/Droplet Image Analysis) techniques to obtain spray tip penetration, cone angle, droplet size and shape. The visualization window used for spray characterization is 50 mm high and 30 mm wide. The window placed at 90° is used for fluorescence and Mie imaging.

Droplet size measurement

The PDIA technique is used for droplet size measurement. The droplet size distribution for the diesel spray is shown in Fig. 2a. The SMD obtained for diesel at an injection pressure of 1000 bar and gas pressure of 30 bar is 18 μm. There are very few droplets with diameter above 30 μm. Only droplets with diameter above 8 μm are shown as the accuracy of determining diameter of droplets smaller than 8 μm was poor. The droplet size distribution for Pongamia oil is shown in Figure 2b. A large number of droplets above 30 μm are detected resulting in an SMD of 43 μm. The presence of larger droplets in the range

of 60 μm possibly represents the larger droplets undergoing secondary breakup. The SMD measured for the different fuels is compared in Fig. 3. The larger SMD in case of Pongamia SVO and its blends in comparison with diesel indicates a reduced level of atomization. The SMD for the Pongamia spray is more than 200% higher compared to that of diesel. From the SMD values of Pongamia oil, the trend observed in the tip penetration can now be explained. Pongamia and blends have shown higher SMD signifying presence of larger droplets as compared to that of diesel. Due to presence of the larger droplets, the Pongamia spray carries more mass and momentum. However, in case of diesel, improved atomization leads to smaller droplets with less mass and momentum. Hence, although initial penetration in case of diesel, Pongamia oil and blends is similar, diesel droplets loose momentum early, whereas the Pongamia oil spray with higher momentum continues to penetrate further.

Planar measurement of SMD and liquid volume fraction

A novel methodology utilizing the Planar Laser Induced Fluorescence (PLIF) and Mie images along with PDIA point measurements is developed to get quantitative liquid volume fraction and SMD measurement. The PLIF images of natural fluorescence from diesel and Pongamia oil are obtained using the 355-nm excitation wavelength. The Mie images are obtained using the 532-nm laser wavelength to isolate images from the absorption loss of the laser sheet.

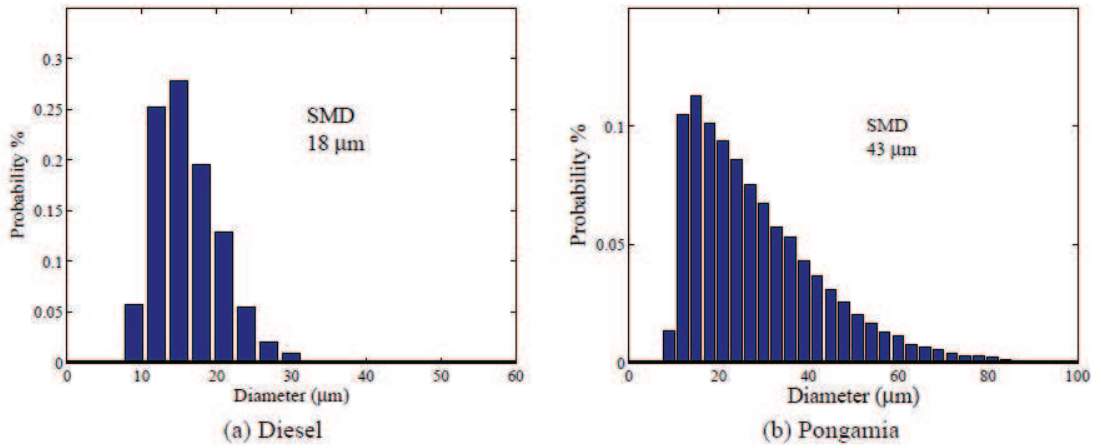

Figure 2: Droplet distribution of diesel and Pongamia spray at 25 mm below nozzle tip, 2.5 ms from start of the injection pulse, injection pressure 1000 bar, chamber pressure 30 bar.

The diesel and Pongamia sprays are studied at an injection pressure of 1000 bar and a gas pressure of 30 bar under non-evaporating condition. The methodology is used to obtain the

liquid volume fraction distribution in diesel and Pongamia spray at various time instants (Fig. 4). The diesel spray showed uniform distribution of fuel compared to that of Pongamia. The Pongamia spray showed more liquid volume fraction at the center of the spray and there was less spread of the liquid radially with time. The SMD distribution is obtained using the LSD technique with corrected Mie and PLIF images. The SMD images (not shown here) indicate a relatively uniform distribution in the diesel spray, whereas higher values are observed in the center of the Pongamia oil spray.

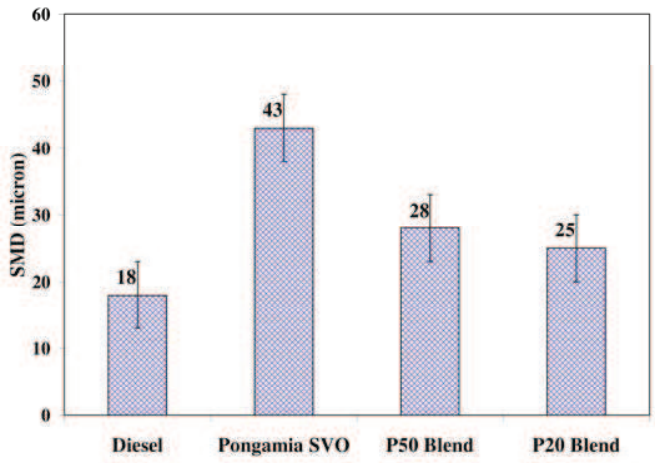

Figure 3: SMD for different fuels. Injection pressure of 1000 bar, gas pressure of 30 bar, 25 mm below the nozzle tip, 2.5 ms after start of the injection pulse.

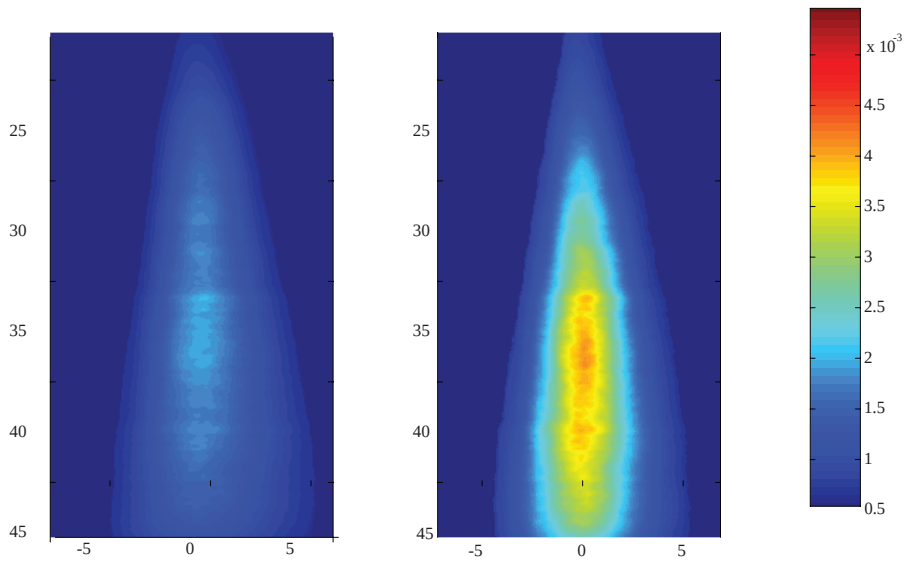

(a) Diesel (b) Pongamia oil

Figure 4: Liquid volume fraction distribution for Pongamia oil and diesel at injection pressure of 1000 bar and gas pressure of 30 bar, 2 ms from start of the injection pulse.

The State of the Art in Biomedical Sprays

Prof. Guillermo Aguilar[1]
Department of Mechanical Engineering
University of California Riverside
Riverside CA, 92521
gaguilar@engr.ucr.edu

Sprays have found varied uses within biomedical fields, particularly in applications where flexibility, precision, and control are essential. In delivering drugs to the lungs, nose, or eyes, sprays provide accurate dosing and placement, while avoiding first-pass metabolism that plagues oral pharmaceuticals. Spray delivery to mucous membranes has near-instant absorption, and thus much more rapid effect. Sprays applied directly to the skin can directly treat fungus and other ailments, as well as deliver treatments to subsurface layers. A less known use of spray sin biomedicine relates to its cooling capacity. Laser treatment of sub-dermal problems, such as port wine stain (PWS) birthmarks, is enabled through the use of refrigerant sprays to prevent skin from burning, while many other skin disorders can be treated by precision through cryogenic spray freezing.

Drug delivery is the most widespread use of biomedical sprays; the well-known asthma inhaler is an aerosol spray to get drugs to the lungs and throat. The goal of all spray research in lung-delivery drugs is to optimize and control deposition within the lungs while minimizing deposition prior to the target. The spray characteristics, such as droplet size range and distribution, have a tremendous impact on the performance of the spray as a delivery vehicle. Studies have statistically analyzed the optimal drop size related to the lung morphometry, leading to correlations for ideal drop size based on patient's age, size, and gender [1]. These correlations are especially useful in light of recent findings that the traditional asthma inhaler provides reduced dosing due to inadequate use and optimization, especially in school-age children [2]. Sprays also provide useful and easily adaption of drug delivery to intubated patients, although a new host of challenges for optimizing sprays for drug delivery is under current investigation. In state-of-the-art macromolecule-based drugs, sprays have shown promise in delivering these fragile particles to their targets, although the high shear stress and cavitation commonly encountered in spray flows needs to be addressed.

In counterpoint to lung-targeted drugs, sprays are also useful to deliver drugs to the nasal cavity. Whereas sprays targeting the lungs must have minimal deposition until they reach the alveolar branches, nasal cavity delivery requires very short air-time and quickly need to deposit on the membranes within the nose. By controlling the angle and plume of the spray, up to 90% of a dose can be deposited on the targeted region of the nose, as illustrated in Fig. 1 [3]. The interplay of droplet aerodynamic diameter, spray velocity, and patient inhalation controls the deposition rates [4]. Sprays have the potential to restrict drug delivery to targeted diseased regions within the nose, avoiding collateral dosing of healthy tissue.

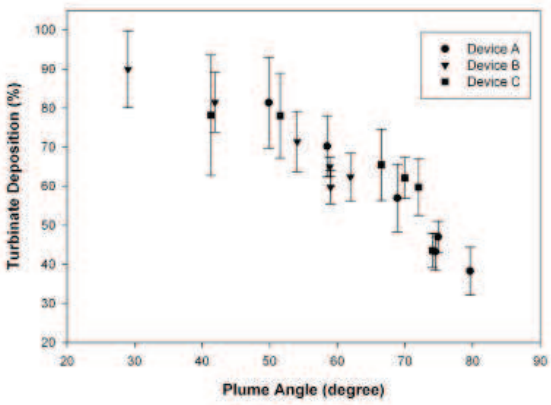

Figure 1. Deposition of spray within turbinate region of nasal cavity at varying spray plume angles. From Foo et al. 2007.

Delivering drugs to the eyes is a novel potential application of sprays, where traditional

[1] Portions of this extended abstract have been taken from a 2011 Review: C.S. Lengsfeld and G. Aguilar, "Targeted medical sprays stimulating therapeutic effects", Atomization and Sprays, 21 (4), 327-348, 2011.

methods have significant obstacles to overcome: the layering of the eye restricts mass transfer, and using needles to bypass these layers causes discomfort to the patient and requires highly specialized personnel. Topical drugs for treatment of the eye (eye drops and washes) are imprecise, requiring the therapeutic dose to be delivered many times due to volume loss, which can lead to overdose and severe side effects. Sprays can replace topical drug delivery easily, while providing the therapeutic dose more efficiently [5].

Sprays applied directly to the skin are flexible, powerful, and as-yet unresearched tools that could fulfill numerous requirements within the biomedical field. As direct treatment methods, sprays are already in use in fungal remedies, being at least as effective as topical methods [6]. Delivering replacement skin cells to injured or diseased regions using a spray is under investigation [7]. Spray sunscreen and insect repellant is of widespread, although recent studies are examining further their effectiveness and absorption into the skin [8].

Transdermal drug delivery is another potent use of sprays. If a drug can be delivered via a spray, instead of a dermal patch, the patient does not have to deal with the discomfort associated with wearing patches for prolonged times. Through absorption [9] or ballistic sprays [10], drug particles can be moved through the skin. This method is still very much under development and faces some challenges. For example, it has been shown that spray delivery of testosterone is very difficult to accomplish, as the drug is affected by the atomization process [11]. Comparable results to standard administration of heparin have been achieved with sprays [12]. Recently, two novel methods of creating micro-incisions through the stratum corneum layer of the skin have been proposed and investigated by our group: first, through superficial skin freezing followed by mechanical stretching to create micro-cracks that serve as channels for drug delivery: *cryopneumatic* approach [13]; second, through continuous wave lasers aimed at highly-absorbing liquid films which induce optical thermocavitation previously applied to the skin surface [14]. The end result of both procedures is that by permeating the stratum corneum, absorption of drugs by the skin is greatly enhanced.

Cryogenic cooling of skin is a well-established use of biomedical sprays. In the last 17 years, the research on this type of sprays has exploded, developing refrigerant sprays into a controlled, safe, and repeatable method of skin cooling. Thermal management of skin using sprays has two primary applications. First, spray cooling is used as a protective measure during sub-dermal targeted laser surgery. By rapidly removing heat from the skin, thermal damage and, thus, scarring can be avoided on the outer layers of skin, while blood vessels and other subcutaneous tissues can be thermally damaged selectively by a laser. Port wine stain (PWS) birthmarks are treated through this method—capillaries below the skin are photocoagulated while an R134a spray provides thermal protection to the skin from unintended laser heating. This method is in use for the treatment of PWS, hemangiomas and many other vascular and pigmented lesions as well as cosmetic procedures. The second purpose for cryogen spray cooling of the skin is to intentionally damage a select region, referred to as cryosurgery. Both protective cooling and cryosurgery are dependent on controlled heat flux removal from the skin. Research on spray cooling has focused on enhancing or predicting the heat flux induced by the spray. The effects of spray characteristics, such as mean droplet diameter, spray velocity, density, and evaporative properties have been studied primarily experimentally using sophisticated non-intrusive laser Doppler (LDV and PDPA) techniques [15]. The temperature variation

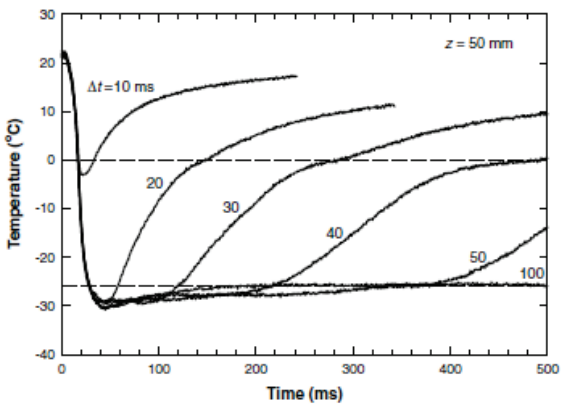

Figure 2. Skin temperature history for several spray durations. Δt is the time duration of the spurt of cryogen. From Aguilar et al, 2003 [16].

related to spray duration (Δt) and distance from target have accompanied these studies [16]. En example is shown in Fig. 2.

Predictive modeling and experiments for various surface conditions, such as skin indentation and roughness, also occurred in the early 2000s [17]. An example is illustrated in Fig. 3. After modeling factors controlling heat flux, the goal of the cryogen cooling studies became to maximize the cooling heat flux to enable higher laser fluence to be used during therapy. Preheating of the skin to increase net heat flux [18], using ambient humidity to alter the optical absorption of skin [19], and measurement of the deposition of rapidly-evaporating sprays [20], among other topics, were explored to improve heat transfer. Further, the safety and side effects of the cryogen sprays on human skin were evaluated, especially with concern over long-duration exposures to CSC [21]. Side effects of CSC upon human skin include transient hyperpigmentation, which can become permanent if the spray duration is extended but is unlikely for the short pulse sprays [22].

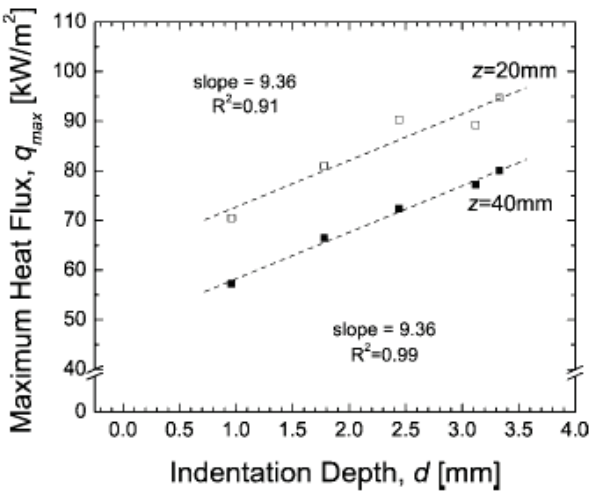

Figure 3. Maximum heat flux of CSC vs skin indentation. From Basinger et al, 2004 [17].

The rise of the use of CSC in subcutaneous treatments spread to several other laser skin therapies. For example, CSC became useful in conjunction with laser hair removal [23]. Further, the process of sutureless tissue welding has been enhanced by spray cooling the skin [24]. Many additional biomedical applications of CSC have developed, such as in treatment of scars [25], acne [26], and cartilage reshaping [27].

Optical thermocavitation is a recent idea in spray control and enhancement. Using a highly focused laser, with a wavelength tuned to the absorption spectrum of the liquid, cavitation bubbles can be induced in a liquid flow as the laser superheats the liquid. The subsequent collapse of the bubble produces a shockwave of tremendous pressure. As mentioned previously, this process has already been harnessed to puncture the stratum corneum [14]. Cavitation can be induced by pulsed lasers or with a steady frequency using continuous wave lasers. The laser power controls the frequency of cavitation. Preliminary work included use of an infrared continuous wave laser to induce cavitation in a quiescent droplet, creating high-velocity microjets, using the configuration shown (see Fig. 4). An example of a jet induced by thermocavitation using the experimental arrangement illustrated above is shown in Fig. 5.

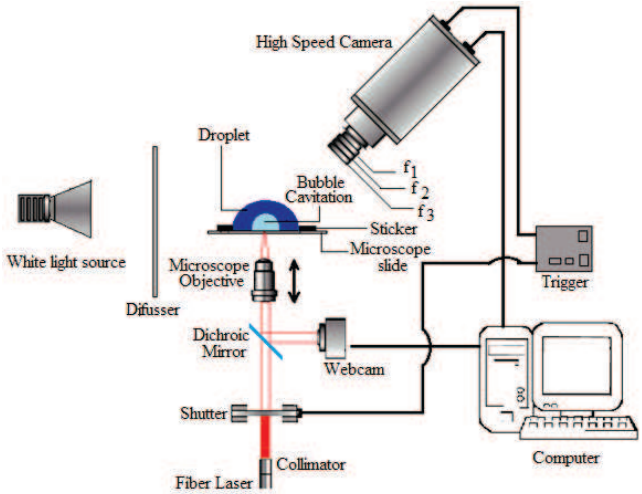

Figure 2. Experimental setup to examine thermocavitation within a quiescent droplet.

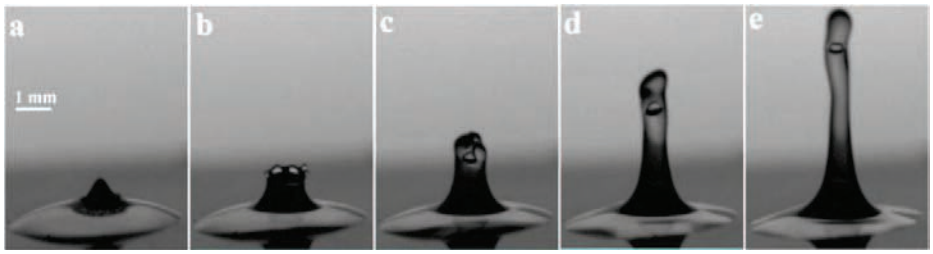

Figure 5. Liquid jet formed by thermocavitation bubble collapse. a) bubble collapse, b) 497, c) 1082, d) 2135 and e) 3451 µs after the collapse.

Notice that after 3.5 ms, a droplet is prone to be formed at the tip of the liggament that was ejected the the shock wave. The liggament size and frequency of formation can be controlled well with laser power, suggesting that droplet formsation and atomization may be optimized.

Our ultimate goal is to use this method of inducing controlled thermocavitation with inexpensive sources like the CW lasers to control atomization. Cavitation within a nozzle has been shown to affect the ultimate atomization [28, 29]. Cavitation induced outside of the nozzle, *e.g.*, within the liquid jet, may now be used to induce atomization and control spray characteristics. For example, by moving the cavitation point farther downstream from the nozzle, the spray coverage area can be reduced as the spray plume has less distance to widen; in the same configuration, turning off the laser completely will result in a jet instead of a spray. Optical thermocavitation can provide flexible spray control in situations where precision is needed.

Finally, thermocavitation may also be a potentially useful tool that helps agitate a deposited liquid on the surface, promoting mixing within a thin liquid layer. Most of the energy provided in optical thermocavitation is dispersed acoustically, with much less sustained heating than anticipated. Inducing cavitation in a thin film can thin the thermal boundary layer, increasing net heat flux. It may also enhance an evaporative process of a refrigerant or cryogenic spray, further enhancing the cooling efficiency [18]. The rapid velocity fluctuations caused by cavitation will disperse deposited liquid, helping make way for fresh coolant to impinge upon the substrate. Through these mechanisms, optical thermocavitation has the potential to enhance spray and other liquid cooling methods for high heat flux applications. This is a topic of current investigation in my group, which will be reported shortly.

REFERENCES

1. Weber, L., Lengsfeld, C. *Spray Nebulizer Deposition Efficiency as a Function of Age*. in *ILASS-Americas.* 2011. Ventura, California
2. Pedersen, S., Dubus, J. C., Crompton, G., *ADMIT series - Issues in Inhalation Therapy. Inhaler selection in children with asthma.* Respiratory Care Journal, 2010. **19**.
3. Foo, M.Y., et al., *The influence of spray properties on intranasal deposition.* Journal of Aerosol Medicine, 2007. **20**(4): p. 495-508.
4. Kimbell, J.S., et al., *Characterization of Deposition from Nasa Spray Devices using a computational fluid dynamics model of hte human nasal passages.* Journal of Aerosol Medicine, 2007. **20**(1): p. 59-74.
5. Akman, A.A., *Comparison of mydriatic efficacy of spray application and drop instillation of tropicamide 1%.* eye. **13**: p. 653-655.
6. Pierard, G.E., R. Wallace, and P. DeDoncker, *Biometrological assessment of the preventive effect of a miconazole spray powder on athlete's foot.* Clinical and Experimental Dermatology, 1996. **21**(5): p. 344-346.
7. Schlabe, J., et al., *Isolation and culture of different epidermal and dermal cell types from human scalp suitable for the development of a therapeutical cell spray.* Burns, 2008. **34**(3): p. 376-384.

8. Wang, T. and X.C. Gu, *In vitro percutaneous permeation of the repellent DEET and the sunscreen oxybenzone across human skin.* Journal of Pharmacy and Pharmaceutical Sciences, 2007. **10**(1): p. 17-25.
9. Morgan, T.M., B.L. Reed, and B.C. Finnin, *Enhanced skin permeation of sex hormones with novel topical spray vehicles.* Journal of Pharmaceutical Sciences, 1998. **87**(10): p. 1213-1218.
10. Lahm, K. and G. Lee, *Penetration of crystalline powder particles into excised human skin membranes and model gels from a supersonic powder injector.* Journal of Pharmaceutical Sciences, 2006. **95**(7): p. 1511-1526.
11. Leichtnam, M.L., et al., *Impact of antinucleants on transdermal delivery of testosterone from a spray.* Journal of Pharmaceutical Sciences, 2007. **96**(1): p. 84-92.
12. Gorski, G., et al., *Liposomal heparin spray: A new formula in adjunctive treatment of superficial venous thrombosis.* Angiology, 2005. **56**(1): p. 9-17.
13. Sun, F., R. Anderson, and G. Aguilar, *Stratum Corneum Permeation and Percutaneous Drug Delivery of Hydrophilic Molecules Enhanced by Cryopneumatic and Photopneumatic Technologies.* Journal of Drugs in Dermatology, 2010. **9**(12): p. 1528-1530.
14. Padilla-Martinez, J.P., et al. *Thermocavitation as a tool for stratum corneum permeation*. in *ILASS-Americas*. 2011. Ventura, CA.
15. Aguilar, G., et al., *Theoretical and experimental analysis of droplet diameter, temperature, and evaporation rate evolution in cryogenic sprays.* International Journal of Heat and Mass Transfer, 2001. **44**(17): p. 3201-3211.
16. Aguilar, G., G.X. Wang, and J.S. Nelson, *Effect of spurt duration on the heat transfer dynamics during cryogen spray cooling.* Phys Med Biol, 2003. **48**(14): p. 2169-81.
17. Basinger, B., G. Aguilar, and J.S. Nelson, *Effect of skin indentation on heat transfer during cryogen spray cooling.* Lasers Surg Med, 2004. **34**(2): p. 155-63.
18. Jia, W., et al., *Improvement of port wine stain laser therapy by skin preheating prior to cryogen spray cooling: a numerical simulation.* Lasers Surg Med, 2006. **38**(2): p. 155-62.
19. Ramirez-San-Juan, J.C., et al., *Effect of ambient humidity on light transmittance through skin phantoms during cryogen spray cooling.* Phys Med Biol, 2006. **51**(1): p. 113-20.
20. Vu, H., G. Aguilar, and J. Stuart Nelson, *Passive mass deposition control of cryogen sprays through the use of wire meshes.* Lasers Surg Med, 2004. **34**(4): p. 329-34.
21. Kao, B., et al., *Evaluation of cryogen spray cooling exposure on in vitro model human skin.* Lasers Surg Med, 2004. **34**(2): p. 146-54.
22. Lee, S.J., et al., *Cryogen-induced arcuate shaped hyperpigmentation by dynamic cooling device.* J Eur Acad Dermatol Venereol, 2008. **22**(7): p. 883-4.
23. Tuqan, A.T., et al., *Clinical and reflectance measurement comparison of tissue culture skin substitutes formed using melanocytes from dark-skinned versus light-skinned donors.* Journal of Investigative Medicine, 2004. **52**(1): p. S79-S80.
24. Fried, N.M. and J.T. Walsh, Jr., *Cryogen spray cooling during laser tissue welding.* Phys Med Biol, 2000. **45**(3): p. 753-63.
25. Alam, M., et al., *Clinical effect of a single pulsed dye laser treatment of fresh surgical scars: randomized controlled trial.* Dermatol Surg, 2006. **32**(1): p. 21-5.
26. Glaich, A.S., et al., *Treatment of inflammatory facial acne vulgaris with combination 595-nm pulsed-dye laser with dynamic-cooling-device and 1,450-nm diode laser.* Lasers Surg Med, 2006. **38**(3): p. 177-80.
27. Karamzadeh, A.M., et al., *Laser-mediated cartilage reshaping with feedback-controlled cryogen spray cooling: biophysical properties and viability.* Lasers Surg Med, 2001. **28**(1): p. 1-10.
28. Sou, A., S. Hosokawa, and A. Tomiyama, *Effects of cavitation in a nozzle on liquid jet atomization.* International Journal of Heat and Mass Transfer, 2007. **50**(17-18): p. 3575-3582.
29. Vu, H., O. Garcia-Valladares, and G. Aguilar, *Vapor/liquid phase interaction in flare flashing sprays used in dermatologic cooling.* International Journal of Heat and Mass Transfer, 2008. **51**(23-24): p. 5721-5731.

Water Mist based Suppression of Flow Opposed Flame Spread over Thin Solid Fuels in Space and Earth Environments

K Chenthil Kumar and Amit Kumar
Department of Aerospace Engineering
IIT Madras, Chennai

Introduction

The flame spread phenomenon is described as a diffusion flame propagating in an oxidizer environment, parallel to a condensed fuel surface by pyrolysis of fuel ahead of the flame. The interest in this class of problems is specifically driven by the need to have better fire safety. Extinction of flame is an aspect that is important to fire safety. For various reasons water mist has been considered a good fire extinguishing agent. The literature shows that there is an optimal size of water mist droplet (20-30μm) at which mass consumption of water is minimum. However, in certain flames ultra fine mist (1-10μm) is found to be more effective. The effectiveness of water mist in suppressing spreading flame has not been investigated. Spreading flame suppression in normal gravity and zero gravity could be different because of the different predominant transport processes.

Here in this work we investigate numerically the suppression of opposed flow spreading flame in space environment by water mist specifically to answer questions raised above. The results are also compared and contrasted with down flame spread in normal gravity.

Theoretical Formulation and Numerical Method

The flame suppression by water mist required development of a 2D liquid phase model which was coupled with the flame spread model.

Figure 1 shows the schematic of computational configuration for the opposed flame spread over thin solid fuel. The gas-phase consists of 2D governing equations of full Navier-Stokes equations for laminar flow along with the conservation equations of mass, energy and species. The specie equations are for fuel vapor, oxygen, carbon dioxide and water vapor. A one-step, second-order finite rate Arrhenius reaction between fuel vapor and oxygen is assumed. The system of coupled elliptic partial differential equations for the flow and combustion in the gas phase is solved numerically by SIMPLER/PISO algorithm with multigrid technique. The thin solid fuel model comprises of equations of continuity and energy in 1D/2D along with a zeroth order solid fuel pyrolysis law. The solid fuel considered here is an aerodynamically and thermally thin cellulosic material. The solid is assumed to burn

ideally *i.e.* it vaporizes to form fuel vapors without melting or charring. The solid-phase equations are solved by the finite-difference technique. The non-dimensional governing equations are solved in flame fixed coordinates. The liquid-phase is modeled in Eulerian frame following the approach of Beck (2000). The main assumptions in water mist modeling include spherical water droplets, no collisions, no coalescence, no droplet break-up and no surface wetting.

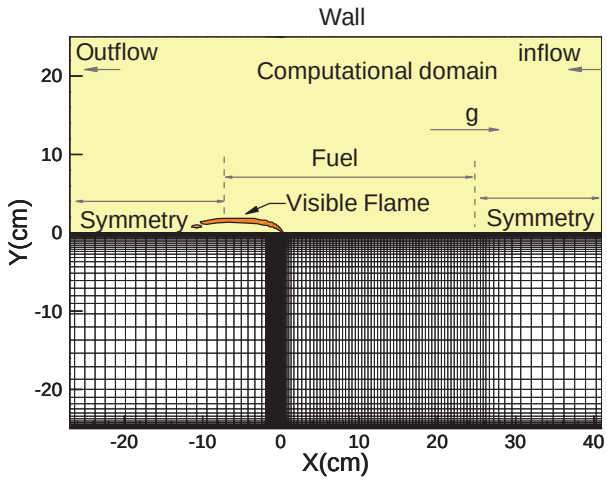

Fig. 1 Schematic of the 2D computational domain with geometrical details and a typical mesh. The fuel is located at *y=0*.

Result and Discussion

The 2D liquid phase model based on work of Beck(2000) was developed and validated against experimental work of Ndubizu *et al.*(1998) where water mist was used to suppress co-flow Methane-Air diffusion flame. Figure 2 shows this configuration and comparison of numerical prediction of flame temperature at various axial locations with the experimental data.

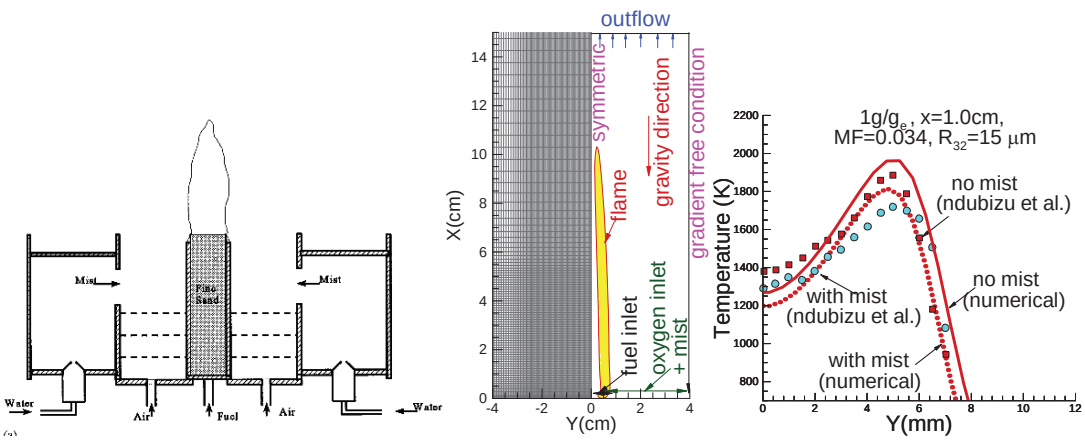

(a) (b) (c)

Fig. 2(a) Schematic of experimental setup of Ndubizu *et al.*, (b) schematic of present numerical study (c) temperature profiles with and without water mist suppression.

The two phase model was integrated with the flame spread code to examine spreading flame suppression characteristics of water mist. The present model does not include gas radiation. Computations were carried out for zero-gravity spreading flame and normal gravity downward spreading flame. The effect of droplet size, water mass fraction, free stream velocity have been investigated. The oxygen level in all the simulation was maintained at 50%. Figure 2 presents a summary of the effect of droplet size and liquid mass fraction on flame suppression of downward spreading flame (Fig 2a) and a zero gravity opposed flow flame (Fig. 2b). The flame length may increase or decrease or increase and decrease with increase in droplet size or water mass fraction. This results from two competing effects; one, the evaporating water droplets inhibits lateral diffusion of fuel and oxidizer there by increases flame length and the other is flame size reduction by cooling. One can also see that there is a critical water mass fraction, only above which can the flame be extinguished by the application of water mist. There may exist for certain water mass fraction an optimal droplet size range only within which flame can be extinguished. At higher water mass fraction there exists a maximum droplet diameter above which the flame cannot be extinguished. This critical diameter increases with increase in water mass fraction (here computed up to water mass fraction of 0.8) in the gas-water mixture. At certain higher mass fraction this trend is expected to reverse but is out of the scope of this study as model assumptions of no collision and no droplet break-up will not hold true.

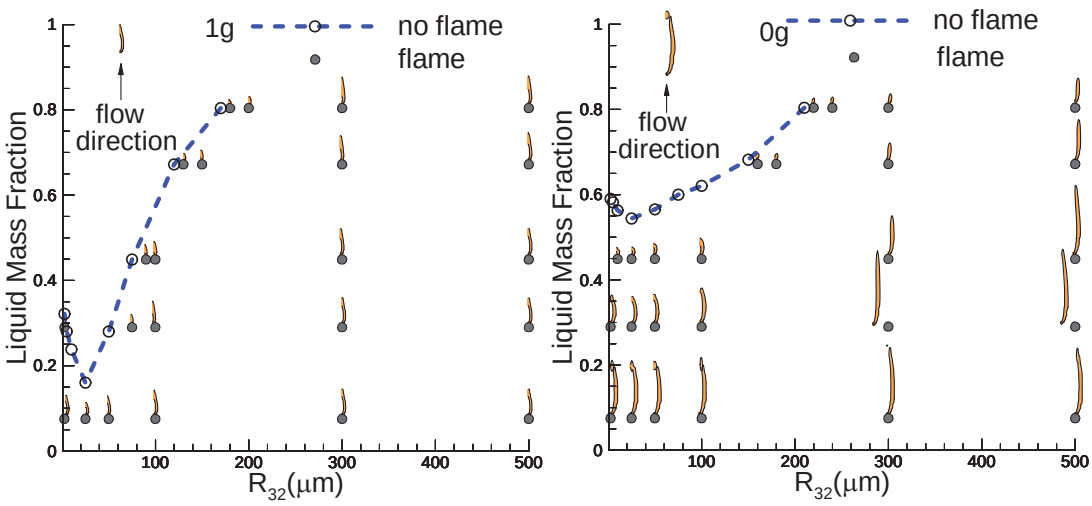

(a) (b)

Fig. 3 Effect of droplet diameter and water mass fraction on suppression of opposed flow spreading flame. (a) Downward spreading flame (b) zero-gravity flame.

A comparison of normal gravity flame suppression and zero gravity flame suppression here shows that there is a crossover of extinction boundary. While the critical water mass fraction is higher for zero gravity flame it can be extinguished more easily (i.e. at larger droplet size) than normal gravity flame at higher mass fraction.

Conclusions

1. The computations showed existence of critical water mass fraction, maximum critical droplet diameter and for some water mass fraction an optimal droplet size range for suppression of opposed flow spreading flame.

2. The zero gravity and normal gravity opposed flow spreading flame may show a reversal in trend for flame extinction by water mist. Present computations showed that while the critical water mass fraction is higher for zero gravity flame it can be extinguished more easily (i.e. at larger droplet size) than normal gravity flame at higher water mass fraction.

References

1. Beck, J.C. (2000) Computational modelling of polydisperse sprays without segregation into droplet size classes. *Ph.D.Thesis, University of Manchester Institute of Science and Technology,* Manchester, U.K.

2. Ndubizu, C.C., R.Ananth, and P.A.Tatem (1998) On Water Mist Fire Suppression Mechanisms in a Gaseous Diffusion Flame. *Fire Safety Journal,* 31, pp. 253-276.

From Williams spray equation to multiphase population balance: a viable route to modeling dense sprays

Mahesh V. Panchagnula
Department of Applied Mechanics, Indian Institute of Technology Madras, Chennai – 600036 INDIA

Introduction

Dense sprays are important to a wide range of engineering systems. The primary challenge in studying the structure of these sprays lies in the multiphysics nature of the interactions in this spatial region. Two specific challenges are more daunting than others. Firstly, droplet-droplet interaction resulting in secondary breakup or coalescence is a modeling challenge especially when the presence of the continuous phase is included as a causal effect. Secondly, this spatial region in the spray is associated with the steepest size-velocity correlation. To further complicate matters, the liquid entities are known to be highly aspherical resulting in a very complicated nature of the interaction between the continuous and dispersed phases. Employing exact physical models which capture all the physics is currently not feasible, especially in real engineering situations. As we will show, the best modeling choice lies in a statistical modeling approach coupled to a phenomenological treatment of the physical processes.

Williams spray equation and population balance models

The statistically *exact* approach to modeling this problem is through the Williams spray equation [1] which is an evolution equation for the evolution of a probability density function, $f(\mathbf{x},\mathbf{y},\mathbf{v},t)$. Here $\mathbf{x}=[x_1,x_2,x_3]$ denotes spatial (or external) co-ordinate vector and $\mathbf{y}=[y_1,y_2\ldots y_k]$ represents a k-dimensional internal co-ordinate (or state) vector. Examples of internal states are size, sphericity, composition and other properties that can be associated with the drops. In addition, $\mathbf{v}=[v_1,v_2,v_3]$ is the velocity vector co-ordinate (treated as an independent variable). In general, this treatment allows for drops at the same internal state and external co-ordinate location to exhibit variations in velocity. This is quite unlike a classical Eulerian velocity field and is referred to as a polykinetic treatment and will be discussed in some detail later. The evolution of f in this $k+6$ dimensional space and time is given by the Williams spray equation:

$$\frac{\partial f}{\partial t}+\nabla_{\mathbf{x}}\cdot(\mathbf{v}f)+\nabla_{\mathbf{y}}\cdot(\mathbf{g}f)+\nabla_{\mathbf{v}}\cdot(\mathbf{F}f)=S_C(f)+S_D(f) \qquad (1)$$

Here $\mathbf{g}=[g_1,g_2\ldots g_k]$ represents a velocity associated with the *motion* of the *pdf* in the internal co-ordinate space. In the simplest case where $k=1$, $\mathbf{g}$ represents a rate of growth of drops. $\mathbf{F}=[F_1,F_2,F_3]$ represents a force vector which causes the *pdf* to evolve in the velocity co-ordinate space. $\nabla_{\mathbf{x}}$, $\nabla_{\mathbf{y}}$ and $\nabla_{\mathbf{v}}$ are divergence operators defined on the appropriate spaces. S_D is a nucleation operator involving nucleation of drops (due to say, condensation) and will not be discussed herein. S_C is a collision operator which models the evolution of f due to droplet-droplet interaction. Both these terms represent sources in the equation and will influence the evolution of f. Therefore, developing models for these terms which capture the essential microscale physics of droplet-droplet interaction is important. Population balance modeling provides a phenomenological framework for such a treatment of these source terms.

Phenomenological modeling attempts to capture the essential higher order behavior through lower order constitutive input parameters or functions. These constitutive input functions are usually obtained or validated through experiments. Population balance modeling is one such approach where the collision and growth terms are modeled in a thermodynamically and physically consistent framework. In

this approach, droplet collisions are thought to result in four possibilities - birth or death of drops either due to agglomeration or atomization. The result is given by [2],

$$S_C(f) = -\underbrace{\Gamma(f,\mathbf{y})f(\mathbf{x},\mathbf{y},\mathbf{v},t)}_{Death\ of\ \mathbf{y}-drops\ by\ breakage} + \underbrace{\int_{\mathbf{y}}^{\infty}\beta(\mathbf{y}|\mathbf{y}')\Gamma(\mathbf{y}')f(\mathbf{x},\mathbf{y}',\mathbf{v},t)d\mathbf{y}'}_{Birth\ of\ \mathbf{y}-drops\ from\ breakage\ of\ large\ drops} - \underbrace{f(\mathbf{x},\mathbf{y},\mathbf{v},t)\int_{\mathbf{y}}^{\infty}\alpha(\mathbf{y}|\mathbf{y}')f(\mathbf{x},\mathbf{y}',\mathbf{v},t)d\mathbf{y}'}_{Death\ of\ \mathbf{y}-drops\ by\ agglomeration} + \underbrace{\frac{1}{2}\int_{\mathbf{y}}^{\infty}\alpha(\mathbf{y}-\mathbf{y}'|\mathbf{y}')f(\mathbf{x},\mathbf{y}-\mathbf{y}',\mathbf{v},t)f(\mathbf{x},\mathbf{y}',\mathbf{v},t)d\mathbf{y}'}_{Birth\ of\ \mathbf{y}-drops\ by\ agglomeration} \quad (2)$$

Here the term "$\mathbf{y} - drops$" is used to indicate drops of state (or size), $\mathbf{y}$. $\alpha(\mathbf{y}|\mathbf{y}')$ represents the probability kernel of coalescence between a drop at state $\mathbf{y}$ with a drop at state $\mathbf{y}'$; $\beta(\mathbf{y}|\mathbf{y}')$ represents the probability kernel of formation of a drop at state $\mathbf{y}$ from a drop at state $\mathbf{y}'$ and $\Gamma(f,\mathbf{y})$ represents the breakage frequency of drops of state $\mathbf{y}$. In general, these functions can admit all internal state variables and dependent variables as arguments, but not external co-ordinates or time. The set of these four terms give rise to balance of mass for drops in the internal state space, $\mathbf{y}$ to $\mathbf{y} + d\mathbf{y}$. These three functions can be constitutively determined from experiments. For example, the liquid-liquid dispersion literature has evolved systematic experimental approaches to develop these functions from first principles. [2] This approach to modeling the source terms coupled with multiphase continuum mechanical description of the transport processes will complete a mathematical description of the dense spray region.

Eulerian multiphase models

Multiphase continuum mechanics allows the modeling of fragmentation, agglomeration, nucleation and growth of particles, bubble in an Eulerian transport framework. These models are sometimes referred to as population balance models in the Chemical Engineering literature. In this approach, it is customary to start with the balance of mass equation with the above- mentioned physical phenomenon modeled as either advection or source terms associated with the Eulerian balance equation. [3, 4] In all previous studies with population balance models, the multiple particulate phases are assumed to all be moving with the same velocity in an isothermal environment which precludes the need for presenting additional balances of momentum and energy. In several situations however, it is likely that the particles of varying sizes are moving with different velocities at the same physical point in space. An example to illustrate the case in point occurs with polydisperse sprays, especially in the near nozzle region. This requires that an explicit balance of momentum and energy be stated to accompany the balance of mass equation. We herein present these equations to complete the set of balance equations that describe the evolution of a multidimensional particle size/velocity distribution in a continuous polydisperse multi-velocity formulation.

Multiphase continuum mechanical models are employed in situations where a finite number of interpenetrating continua with each continuum is characterized by its own constitutive law and set of internal co-ordinates (for example, drop size in the case of a spray). For this case, mass, momentum and energy balance can be written with source terms similar to equation (2). The main hurdle to harnessing the vast body of Eulerian continuum mechanics knowledge for this cause is to consistently incorporate polykinetic physics.

Polykinetic droplet motion suggests that drops at a given external co-ordinate location, $\mathbf{x}$ and at a given internal state, $\mathbf{y}$ can manifest a velocity *pdf* that can be measured in time. This possibility is not

completely exclusive of multiphase continuum mechanical treatment. For the case where a mean velocity of such droplet motion can be identified, the process is akin to a turbulent flow. Therefore, polykinetic physics can be handled using modeling techniques based on Reynolds averaging similar to those employed to study turbulent flow. The velocity would be dependent on size but *variations* in such velocity would then be associated with the stress field. Under this assumption, equation (1) would represent a Direct Numerical Simulation of a *polykinetic* droplet flow. The averaging process when employed rigorously (upon defining an appropriate mean velocity field) yields a Navier-Stokes like equation with source terms given by equation (2). These equations will be referred to as Eulerian Population Balance equations (EPBM).

As mentioned before, sprays form the perfect case study for the need for such a formulation. Previous attempts to pose such a complete set of equations have resulted from modifying the Williams spray equation. [5, 6] The Williams spray equation attempts to treat the spray akin to a monatomic ideal gas where momentum transfer between particles is modeled through a collision operator as is customary in the Boltzmann equation. However, in adapting the Boltzmann equation into the Williams spray equation, the collision operator is usually left out. This leads to the assumption that the particle phase is so dilute as to be approaching a stress free medium. Further, this assumption renders the Knudsen number, so large that Eulerian continuum models are rigorously invalid. We propose an alternate approach wherein the stress tensor which causes momentum and energy diffusion in the particulate medium is retained in the balance laws. If the drops are allowed to interact with each other, drop phase continuum stresses are to be considered and consistently incorporated into a balance of momentum and energy. This implies that the mass balance terms arising out of the population balance modeling (equation 2) need to be coupled with accompanying momentum balance terms.

Numerical solution of Eulerian population balance equations

The simplest and most direct numerical technique that has been employed to solve the EPBM equations is the classes method (CM). [7] In this method the internal state space, $\mathbf{y}$ is divided into a finite number of classes. The EPBM equations can then be integrated similar to a finite volume technique to yield a balance law for the discrete probability of each class, f_i. This set of equations can be solved using a standard Navier-Stokes solver. This method, while being simple to implement, is computationally intensive owing to the large number of such classes required for convergence.

A second method that has been employed is called the quadrature method of moments (QMOM). [8, 9] In this method, the EPBM equations can be integrated in the internal co-ordinate to yield a transport equation for the moments of the *pdf*, f. However, there are two problems associated with implementing this method numerically. For the case where droplets in different internal states move with different kinetic velocities, the moment transport equations are not closed. So, other postulates are required to bring in the size-velocity correlation information and close the system of equations. Recent extensions of this method called the Discrete Quadrature Method of Moments (DQMOM) [10] have attempted to overcome this problem, but still require validation against a CM solution. This is still an active area of research. If a solution can be found to this problem, DQMOM solution of EPBM offers a viable modeling route to studying transport in dense sprays.

REFERENCES

1. Williams, F.A., *Spray combustion and atomization.* Physics of Fluids, 1958. **1**: p. 541-545.
2. Ramkrishna, D., *Population Balances*. 2000, New York: Academic Press.
3. Rayapati, N.P., et al., *Analytical solutions for convective fragmentation.* Mechanics Research Communications, 2010. **37**(8): p. 712-716.

4. Rayapati, N.P., et al., *Analytical solutions for particulate pipe flows with fragmentation, evaporation, and diffusion.* Mechanics Research Communications, 2010. **37**(6): p. 604-610.
5. Fox, R.O., F. Laurent, and M. Massot, *Numerical simulation of spray coalescence in an Eulerian framework: Direct quadrature method of moments and multi-fluid method.* Journal of Computational Physics, 2008. **227**(6): p. 3058-3088.
6. Kah, D., et al., *Eulerian Quadrature-Based Moment Models for Dilute Polydisperse Evaporating Sprays.* Flow Turbulence and Combustion, 2010. **85**(3-4): p. 649-676.
7. Rayapati, N.P., et al., *Eulerian multiphase population balance model of atomizing, swirling flows.* International Journal of Spray and Combustion Dynamics, 2010. **3**(2): p. 111-136.
8. Marchisio, D.L., R.D. Vigil, and R.O. Fox, *Quadrature method of moments for aggregation-breakage processes.* Journal of Colloid and Interface Science, 2003. **258**(2): p. 322-334.
9. Marchisio, D.L., et al., *Quadrature method of moments for population-balance equations.* AIChE Journal, 2003. **49**(5): p. 1266-1276.
10. Fan, R., D.L. Marchisio, and R.O. Fox, *Application of the direct quadrature method of moments to polydisperse gas-solid fluidized beds.* Powder Technology, 2004. **139**(1): p. 7-20.

VOF-Lagrangian Particle Tracking Coupling to Simulate Multiscale Primary Atomization

Gaurav Tomar[1], Daniel Fuster[2], Stephane Popinet[3], Stephane Zaleski[2]
[1]Department of Mechanical Engineering
Indian Institute of Science Bangalore, India
[2]Institute Jean Le Rond D'Alembert
University Perrie et Marie Curie, Paris, France
[3]National Institute for Water and Atmospheric Research
Wellington, Newzealand

***Correspondence address: gtom@mecheng.iisc.ernet.in**

Extended Abstract

A high speed liquid jet atomizes into small droplets with broken off droplets being orders of magnitude smaller than the jet diameter. Numerical simulations of the primary atomization process have been performed using different interface tracking algorithms, namely, Volume-of-Fluid method by Zaleski et al. [1-3], Level-set method by Hermann et al. [4,5] and Front-Tracking algorithm by Tauber et al [6]. Grid resolution required to accurately capture the smallest drop is orders of magnitude smaller and computational cost increases with an increase in the number of droplets formed during atomization. Computational cost can be reduced by artificially removing the small droplets that are moving away from the liquid jet core. This, however, leads to loss of physics as secondary effects of the droplets interacting with the liquid-core downstream are ignored. Also, the prediction of the probability density function of the size of droplets in different parts of the computational domain downstream of the liquid jet cannot be computed. Figure 1 shows an schematic of a 3D drop resolved using an adaptive mesh refinement. The uniform grid size in the absence of the droplet is 2^4 larger. Thus, the extra computational effort in the presence of hundreds of such droplets would be enormous.

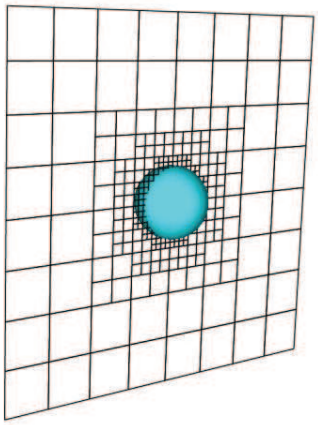

Figure 1. *Schematic shows a 3D drop resolved with a very fine grid.*

We present here simulations using volume-of-fluid method coupled with a Lagrangian particle tracking (VOF-LPT) algorithm [7]. A similar algorithm coupling level-set with Lagrangian spray model has been given by Hermann [8]. The smallest droplets are removed from the VOF description [9] and modeled as point particles using a two-way coupling. The motion of the particles is tracked using the following equations:

$$\frac{dx}{dt} = v \tag{1}$$

$$m_p \frac{dv}{dt} = F_A + F_I + F_D + F_L + F_{ext} \tag{2}$$

The drag force on the particle, F_D, is given by,

$$F_D = -3/(4d)C_D(\mathrm{Re}_p)\rho V(v-u)|v-u| \tag{3}$$

Here, d is the diameter of the particle, C_D is the drag coefficient and is a function of the Reynolds number based on particle diameter. The velocity of the particle is represented by v, volume of the particle is V and the density and local fluid velocity is given by ρ and u, respectively. The inertia force, F_I, on the particle is given by,

$$F_I = \rho V\left[\frac{\partial u}{\partial t} + (u \cdot \nabla)u\right]. \tag{4}$$

The added mass force, F_A, on the particle is given by,

$$F_A = \rho V C_M\left[\frac{\partial u}{\partial t} + (u \cdot \nabla)u - \frac{dv}{dt}\right]. \tag{5}$$

Here, C_M is the added mass coefficient which has value 0.5 for spherical particles. The lift force, F_L, is given by,

$$F_L = -\rho V C_L(v-u)\times\omega, \tag{6}$$

where $\omega = \nabla \times u$ is the local vorticity of the fluid at the particle location and C_L = 0.5. In the simulations presented here, the Basset history force on the particles due to history of the wake behind the particle has been ignored.

For two-way coupling a momentum source term is added in the Navier-Stokes equation governing the flow of the underlying fluid. The momentum source term is given by,

$$\Phi = \lim_{V_f \to 0} \sum_{i=1}^{N} \frac{V^i}{V_f}\left[\rho_p^i\left(g - \frac{dv^i}{dt}\right) + \rho\left(\frac{Du}{Dt} - g\right)\right] \tag{7}$$

To model interaction between the particles and the VOF resolved interface, particles are transformed back into the VOF description based on a proximity algorithm. Figure 2 shows a sequence of drops splashing on a liquid surface. Initially the drops are modeled as particles which transform into VOF description near the liquid surface (Figure 2b). Drops splash into the surface (Figure 2c) generating thousands of small size droplets (Figure 2d).

Figure 3 shows the simulation of gas assisted atomization of a liquid jet. The density ratio in the simulation is 100. The liquid-gas momentum ratio is 16. The gas Reynolds number is 2060 and liquid Reynolds number is 5000. The thickness of the liquid jet is 1mm and the smallest grid size resolving the VOF interface is 5 μm. The droplets near the nozzle are of the order of 10-50 μm whereas drops in downstream are of the order of a 50-100 μm.

Number of droplets which couldn't be modeled in the fully resolved simulation due to impractical computational requirements can be accounted for in the VOF-LPT algorithm. This model can be extended further to account for turbulence dispersion effect by including a fluctuating term in the momentum equation of particles. Also, if the particle densities are higher one needs to account for collision and four-way hydrodynamic interactions between particles.

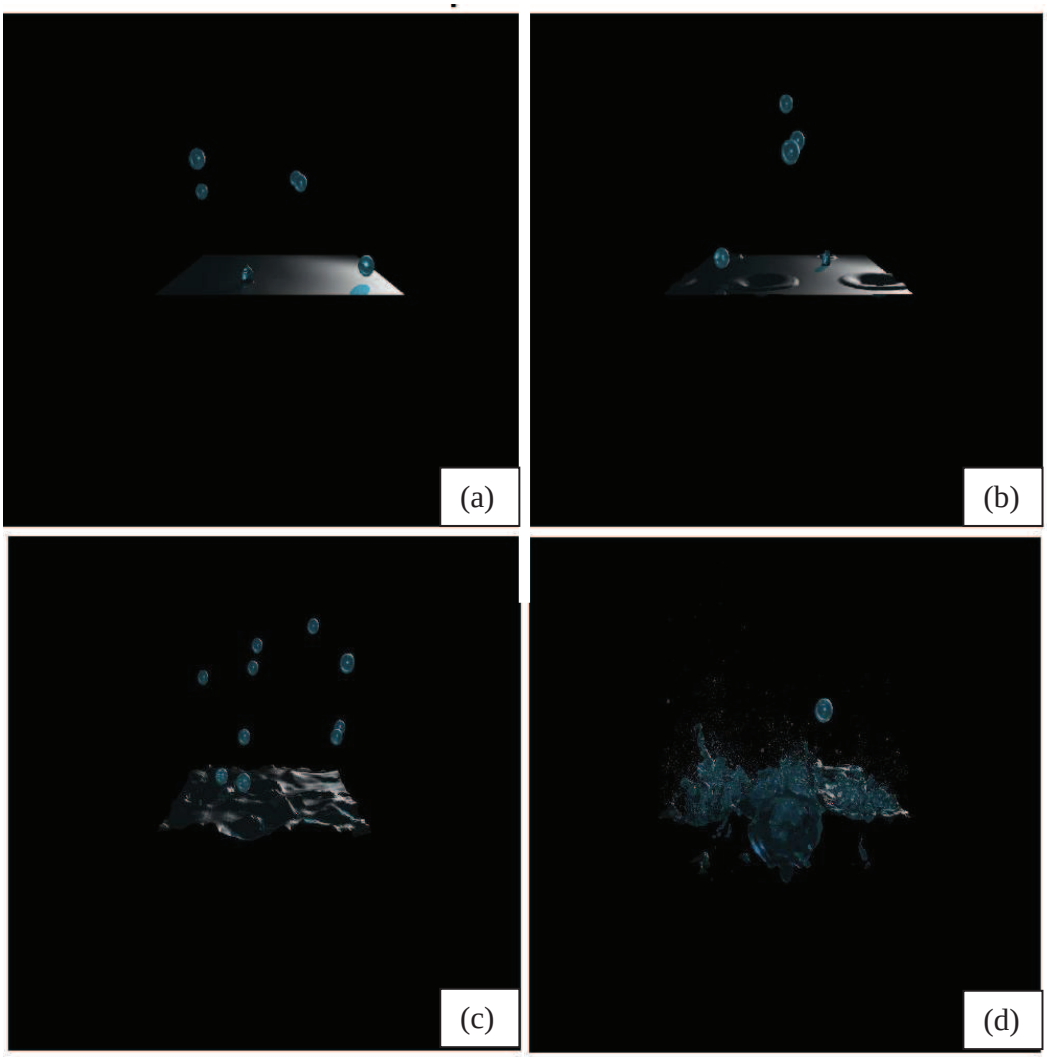

Figure 2 (a) Drops injected into the computational domain as particles (b) Drops transforming from Lagrangian description into VOF-description. (c) Splashes created due to multiple drop collisions (d) Thousands of small droplets formed due to splashes caused by the impact of multiple drops at the liquid surface.

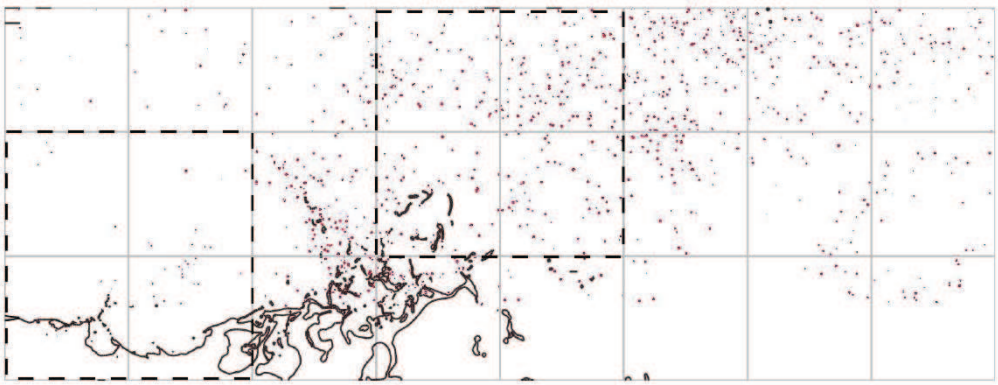

Figure 3. Liquid jet fragments into droplets assisted by a high-speed gas. Droplets modeled as particles are marked in red [7].

References:

[1] D. Fuster, A. Bague, T. Boeck, L. Moyne, A. Leboissetier, S. Popinet, P. Ray, R. Scardovelli, S. Zaleski, Simulation of primary atomization with an octree adaptative mesh refinement and vof method, Int. J. Multiphase Flow 35 (2009) 550–565.

[2] S. Zaleski, T. Boeck, Direct numerical simulation of high speed jet atomization, in: International Conference on Liquid and Spray Systems 17 (ICLASS) 2003, Sorrento, Italy, 2003.

[3] F. K. Keller, J. Li, A. Vallet, D. Vandromme, S. Zaleski, Direct numerical simulation of interface breakup and atomization, in: Proc. Sixth Int. Conf. on Liquid Atomization and Spray Systems, Rouen, 1994, pp. 56–62.

[4] D. Kim, M. Herrmann, P. Moin, The breakup of a round liquid jet by a coaxial flow of gas using the refined level set grid method, in: American Physical Society, 59th Annual Meeting of the APS Division of Fluid Dynamics, November 19-21, 2006, p. FB.010.

[5] Detailed Numerical Simulations of the Primary Atomization of a Turbulent Liquid Jet in Crossflow, J. Eng. Gas Turbines and Power, 132 (2010), 061506.

[6] W. Tauber, G. Tryggvason, Direct numerical simulation of primary breakup, Comput. Fluid Dynamics J. 9 (2000) 594.

[7] G. Tomar, D. Fuster, S. Zaleski, S. Popinet, Multiscale simulations of primary atomization using Gerris, Computers and Fluids 39(10) (2010)1864.

[8] M. Herrmann, A Parallel Eulerian Interface Tracking/Lagrangian Point Particle Multi-Scale Coupling Procedure, J. Comput. Phys., 229, (2010) 745.

[9]S. Popinet, Gerris: a tree-based adaptive solver for the incompressible Euler equations in complex geometries, J. Comput. Phys. 190 (2003) 572.